

Engineering-Scale DC Arc Furnace Testing Summary

R. W. Goles G. A. Whyatt
R. A. Merrill D. K. Seiler
C. J. Freeman D. A. Lamar
G. B. Josephson

Mixed Waste Focus Area
TTP No. RL3-6-MW-51

September 1998



Prepared for the U.S. Department of Energy
under Contract DE-AC06-76RL0 1830

DISCLAIMER

This report was prepared as an account of work sponsored by an agency of the United States Government. Neither the United States Government nor any agency thereof, nor Battelle Memorial Institute, nor any of their employees, makes **any warranty, express or implied, or assumes any legal liability or responsibility for the accuracy, completeness, or usefulness of any information, apparatus, product, or process disclosed, or represents that its use would not infringe privately owned rights.** Reference herein to any specific commercial product, process, or service by trade name, trademark, manufacturer, or otherwise does not necessarily constitute or imply its endorsement, recommendation, or favoring by the United States Government or any agency thereof, or Battelle Memorial Institute. The views and opinions of authors expressed herein do not necessarily state or reflect those of the United States Government or any agency thereof.

This effort is based on the continuation of work initiated under a collaborative “National Laboratory-University-industrial Three-party Program” namely: Pacific Northwest National Laboratory (PNNL), Massachusetts Institute of Technology (MIT) and Electro-Pyrolysis, Inc. (EPI). Those three organizations pooled their efforts in order to demonstrate the technology using the graphite electrode DC arc furnace for treatment hazardous waste. Electro-Pyrolysis, Inc., the industrial participant, currently provides the DC arc technology on a commercial basis, in connection with its licensee Svedala Industries, Inc. through its Pyro-Systems Division.

PACIFIC NORTHWEST NATIONAL LABORATORY

operated by

BATTELLE

for the

UNITED STATES DEPARTMENT OF ENERGY

under Contract DE-AC06-76RLO 1830



This document was printed on recycled paper.

Engineering-Scale DC Arc Furnace Testing Summary

R. W. Goles G. A. Whyatt
R. A. Merrill D. K. Seiler
C. J. Freeman D. A. Lamar
G. B. Josephson

Mixed Waste Focus Area
TTP NO. RL3-6-MW-51

September 1998

Prepared for
the U.S. Department of Energy
under Contract DE-AC06-76RLO 1830

Pacific Northwest National Laboratory
Richland, Washington 99352

Summary

This report gives a summary of all engineering-scale direct current (DC) arc furnace testing activities conducted in support of Technology Task Plan (TTP) RL3-6-MW-51 for DOE Project 18689 during FY 1997 and FY 1998. The work is being performed by the Pacific Northwest National Laboratory (PNNL) and managed by the Department of Energy's (DOE) Mixed Waste Focus Area (MWFA). The purpose of this work is to evaluate the ability of this thermal treatment technology to convert a wide variety of chemically and/or radiologically hazardous materials present in the DOE complex to compact, stable, durable waste forms that can be disposed of in a cost-effective, environmentally friendly manner. The specific waste disposal issues addressed by the current Project are fully discussed in the introduction of this report. Descriptions of the specific tests supporting the TTP are documented in formal Test Plans issued to the MWFA Program Office at the beginning of each fiscal year.

Two engineering-scale furnace (ESF) tests were conducted at PNNL during FY 1997. The first test campaign was successfully completed using a soil/lime feed material. This was the first extended operation of the furnace, and served as a final check of the system and the sampling and analytical procedures to be used in subsequent testing on surrogate debris wastes. Approximately 320 kg of feed material was processed over an 86 hour period, producing 275 kg of vitrified product. The feed rate over the duration of the test was about 5 kg/hr, and was as high as 10 kg/hr during the actual test segments of the run.

The system performed as designed, with a few minor problems encountered. The failure of an overflow heater required feeding to be stopped while the repair was made, but the furnace was able to be maintained in an idling condition while the repair was made. Additionally, the can feeder ram failed due to the overheating of rubbers seals, resulting in the postponement of the can feeding test segment. The existing ram was replaced with a different model, having higher temperature seals. This new design was evaluated during FY 1998 testing.

Post-test inspection of the hearth busing revealed significant attack on the graphite in that area. The attack was the result of residual water vaporizing from the castable refractories and reacting with the hot graphite as it was drawn into the melter plenum. The corroded regions were repaired and design changes were implemented in FY 1998 that successfully controlled this corrosion based problem.

The vacuum assisted overflow drain performed well throughout the test, once the repair to the heaters was made. Some wandering of the pour stream occurred, which eventually resulted in a glass plug that had to be broken out of the overflow section outlet. Modification of the pouring procedure and better sealing of the overflow container to the overflow section minimized this problem.

The electrode feeder provided excellent control of the arc, especially during the exposed arc segments when the position of the electrode was critical to maintaining the arc. In several instances when the arc was extinguished, it was readily restarted by simply lowering the electrode into the melt pool and raising the electrode again above the melt surface. Electrode consumption rates were low, as only one additional segment of electrode was required during the weeklong test.

A primary focus of the initial FY 1997 melter test was to investigate the effect of process operating conditions on the partitioning of hazardous metals and plutonium surrogates. The feed was spiked with heavy metals and plutonium surrogates, and the partitioning of the species to the glass and off-gas was determined for several test conditions. The operating conditions varied in this testing included the degree of cold-cap coverage (unmelted, cool material floating on the surface of the melt) and the position of the electrode (submerged in the glass, or above the surface).

These operating conditions were found to have significant impact on the partitioning of the metals to the off-gas. Both overall bulk solids and individual elemental partitioning followed similar trends. A decrease in the cold-cap coverage increased the carryover of solids into the off-gas during submerged arc operation. When the arc was exposed, solids carryover was high regardless of the cold-cap coverage. Minimum solids carryover was obtained with a high cold-cap coverage and submerged arc operation.

Volatilization of hazardous, semi-volatile metals to the off-gas was found to be significant, especially for cadmium and lead. Partitioning followed the same trends as described above for bulk solids; however, low total recovery in the mass balance for these elements weakens these conclusions. Nevertheless, submerged-arc / high-cold-cap operating conditions were found to be important factors in reducing overall process losses of semi-volatiles.

The effect of particle size on entrainment was investigated by adding three different elements, which form non-volatile, stable oxides in particle sizes ranging from <1 micron to 4 mm in diameter. A measurable partitioning increase relative to bulk entrainment was found for these additives, as well as the lime flux. However, the maximum partitioning to the off-gas observed for any of these additives was 4 wt%, or about two times the bulk entrainment value. This data indicates that the off-gas partitioning of even sub-micron particulate remains near the bulk entrainment value in this system operating at the conditions of this test.

The glass product obtained from the initial FY 1998 test was visually uniform and homogeneous. The vitrified product achieved a 52% reduction in volume compared to the initial soil material. Samples of the vitrified product were subjected to the toxicity characteristic leach procedure (TCLP), and leachate concentrations were well below the regulatory limits for all hazardous metals in the samples. The overall leach rate, determined from the concentration of all elements in the TCLP leachate, shows the leaching of the glass to be very low, comparable to that of natural basalt, a material of similar composition. No apparent impact of the test operating conditions on the leachability of the glass product was noted. TCLP leachate concentrations from the baghouse solids were found to exceed regulatory standards for lead and chromium, as expected.

The second FY 1997 test campaign was initiated several months after the first test campaign. The furnace was shut down in the interim. The objective of the second test campaign was to process a non-radioactive surrogate of Savannah River Site (SRS) debris and assess its performance. This surrogate was tested in the bench-scale DC arc furnace, where glass forming additives and amounts were identified. Operational evidence during the furnace restart indicated that current had fired through a crack or fissure in the furnace's Monofrax K-3 sidewall instead of the exposed graphite on the bottom of the furnace. Approximately 110 pounds of soil-lime feed, the same material used in the first campaign, was fed to the

furnace until glass pouring was reestablished through the overflow. Next, SRS debris surrogate was fed to the furnace. After 120 pounds of this material had been fed to the furnace, with batch pours of glass every half hour, pouring ceased from the furnace overflow. All attempts to resume pouring from the overflow were unsuccessful; therefore, the system was shut down. Inspection of the furnace during and after the test and analysis of the glass provided indication that the Monofrax K-3 glass contact refractory corroded at higher-than-expected rates, primarily due the furnace restart and the high organic content of the SRS debris surrogate. Visual inspections revealed that part of one Monofrax K-3 sidewall (approximately 3 in. by 4 in.) was entirely missing. The corrosion products appear to have increased the alumina and chromia levels in the slag during operation resulting in a viscous, unpourable material. Another possibility is that a piece of the refractory dislodged from the sidewall and physically obstructed the overflow channel. The actual cause or causes of the pour stream failure, however, could not be conclusively established by the existing analytical data.

The failure of the DC arc furnace (melter) during the second FY 1997 melter test necessitated a major repair before waste processing tests could commence. Since numerous bench-scale DC arc furnace tests had previously established that off-gas partitioning for transuranic waste components was dominated by scale-independent entrainment losses, it was generally accepted that additional engineering-scale testing of plutonium bearing soils would provide little additional information regarding the technology deficiencies identified in the MWFA's Technology Development Requirement Document for plasma and DC arc melters (MWFA 1997b). Consequently, application of the DC Arc Melter Project was redirected to evaluate this technology's capability of converting classified hardware containing both hazardous and radioactive materials (Pantex ferroelectric neutron generators) into unclassified (demilitarized), durable waste forms that could be disposed of conventionally in a commercial waste repository.

Since the repair of the DC arc melter required replacement of most furnace internals, several design changes were made to avoid or minimize operational difficulties encountered during previous FY 1997 testing. These changes included the procurement of a commercial bottom drain induction heating system, eliminating the refractory hearth liner, using a graphite overflow block, minimizing the use of water-bearing castable refractories, and protecting the melter's graphite bus bars with ceramic sheaths.

During the FY 1998 ESF repair, bench-scale furnace scoping tests were carried out to define the chemical additives required to produce a well-behaved baseline waste composition when combined with the neutron generator feed stream. Although the Pantex neutron generators previously described, could be melted and/or sintered alone, this material would not be readily removable from the furnace. In order to create a melt which could be easily transferred from the furnace, the feed stream had to be blended with chemical additives designed to reduce the viscosity of the melted material. On the basis of these melter scoping tests, a $\text{CaO-Al}_2\text{O}_3\text{-SiO}_2$ waste product with ~20% waste loading was chosen that satisfied the requirements for both low viscosity characteristics (<100 poise at 1300 °C) and high dissolution kinetics for high density alumina.

The FY 1998 ESF test demonstrating the demilitarization of Pantex neutron generators commenced at the conclusion of melter repairs and the subsequent refractory bakeout campaign. After the furnace's arc was struck and a 400°C plenum operating temperature was achieved, glass forming chemicals were fed to the melter (using the ESF's large object, or can, feeder) in order to prepare a molten bath into which the

neutron generators and their components would be melted and/or dissolved. After 300 lbs of target glass was produced, processing of the neutron generators commenced. Radioactive processing continued until all 200 neutron generators were successfully demilitarized by the plasma arc furnace.

Several sub-system operational problems were encountered during the test that slowed the overall progress of the demonstration. The reliability of the melter's large object, or can feeder, was a major source of operational delays. A significant improvement in processing efficiency was achieved when the automatic can feeder was abandoned in favor of a manual, gravity-fed backup system. Also, the inability to develop a pressure differential between the main melt chamber and the melter's overflow section eliminated the ability to batch-transfer glass from the melter. Consequently, the melter was operated in a continuous overflow mode, which created glass collection problems in the melter's overflow section, and glass receipt canisters. In addition, inadequate temperatures existing below the melter's hearth precluded bottom drain tapping of the ESF's melt chamber.

In spite of these operational difficulties, the processing of neutron generators continued in more or less continuous manner. During a 21-hour period, 150 neutron generators were successfully processed. At the maximum feeding conditions achieved during this period, a neutron generator was being processed every 6 minutes. This corresponds to a maximum hourly feed rate (generator + glass-formers) of 36 lbs/hr. The average feeding rate over the 21-hour period when 75% of the neutron generators were processed was 27 lbs/hr. The project plan for the demonstration was based on a 25 lbs/hr processing rate.

The fate and behavior of the elemental constituents of neutron generators were of particular interest during this demonstration. Based on the unclassified bounding value, approximately 85% of the available tritium present in the neutron generators was released to the environment through the process stack. The unreleased tritium was primarily collected as tritiated water in the process quench scrubber which accounted for 15% of the cumulative bounding value. Particulate matter collected by the bag house filter (0.3% of the bounded total) and the melter's glass product (0.2% of the bounded total) accounted for the remaining unreleased tritium.

Lead, the major hazardous constituent present in neutron generators, partitioned primarily to the off-gas system. Approximately 75% of the available Pb was accounted for in the off-gas system's bag house solids. The semivolatile Zn, which was an unidentified neutron generator constituent, was also a dominant component of these solids. Since the lead content of the glass was quite low (500 ppm), this waste form easily passed TCLP testing. Process operating conditions, driven by glass pour rate concerns, were most likely responsible for the high partitioning of semivolatile feed constituents to the off-gas system during the Pantex processing campaign. Previous FY 1997 ESF testing (see Section 4.8.3.3) has shown that Pb partitioning to the glass can be strongly enhanced by operating with high cold-cap coverage and a submerged electrode.

The suitability of applying the DC plasma arc technology for the treatment of a wide range of materials containing hazardous and radioactive constituents, including soil-based waste and military hardware, has been successfully demonstrated using both engineering- and bench-scale furnaces. Highly durable waste forms generated by this process have successfully immobilized chemically and/or radiologically hazardous feed stream constituent, while the high-temperature melting capabilities of this plasma arc

technology has been shown to be more than sufficient to satisfy demilitarization requirements. Although only first-generation, developmental equipment was used in the present tests, all major technology-based objectives were, nevertheless, successfully demonstrated. Significant design improvements incorporated in 2nd generation, commercially-available, plasma-arc equipment have, however, significantly improved operational reliability of this technology. One such improvement, that of providing Joule heating capabilities, has eliminated the need for, and associated risk of, cold melter restarts by allowing for low-temperature melter idling operations.

Contents

Summary	iii
1.0 Introduction.....	1.1
2.0 Conclusions.....	2.1
2.1 FY 1997 Representative Mixed Waste Simulation Testing	2.1
2.2 FY 1998 Pantex Neutron Generator Demonstration Test	2.2
3.0 Equipment Description	3.1
3.1 Furnace System	3.1
3.1.1 Vessel and Refractories	3.1
3.1.2 Overflow Section	3.6
3.1.3 Furnace Cooling.....	3.6
3.1.4 Bottom Drain	3.7
3.2 Power System.....	3.8
3.2.1 Power Supply	3.8
3.2.2 Electrode Feed System	3.8
3.3 Feed Systems.....	3.9
3.3.1 Bulk Solids Feeder	3.9
3.3.2 Ram Feeder.....	3.9
3.4 Off-Gas System	3.10
3.4.1 Film Cooler.....	3.10
3.4.2 Baghouse Filter	3.11
3.4.3 Ejector Venturi Scrubber.....	3.11

3.4.4	High Efficiency Mist Eliminator.....	3.12
3.4.5	High Efficiency Particulate Air Filter	3.14
3.5	Furnace Restart Equipment	3.14
3.6	Data Acquisition and Control System.....	3.15
3.7	Off-Gas Particulate Sampler	3.15
4.0	Testing Campaign #1: Melter Performance Using Idaho National Engineering and Environmental Laboratory Soil.....	4.1
4.1	Objectives.....	4.1
4.2	Test Approach	4.2
4.3	Experimental	4.5
4.3.1	Feed Preparation and Furnace Operation	4.5
4.3.2	Data Collection	4.5
4.3.3	Sample Collection	4.6
4.3.4	Analytical	4.6
4.4	Operating Performance	4.7
4.4.1	Furnace Restart	4.7
4.4.2	Operational Overview	4.7
4.4.3	Test Segment Descriptions	4.13
4.4.4	Post-Test Furnace Inspection.....	4.17
4.5	Energy Balance.....	4.18
4.6	Off-Gas Analyses	4.19
4.7	Slag Analyses	4.20

4.8	Mass Balances and Partitioning.....	4.26
4.8.1	Overall Mass Balance.....	4.26
4.8.2	Individual Test Segment Mass Balances.....	4.27
4.8.3	Metals Partitioning.....	4.31
5.0	FY 1997 Testing Campaign #2: SRS Debris Testing.....	5.1
5.1	Test Objectives.....	5.1
5.2	Flowsheet.....	5.1
5.3	Operations.....	5.2
5.4	Post-Test Furnace Inspection.....	5.3
6.0	FY 1998 Pantex Demonstration.....	6.1
6.1	Test Objectives.....	6.1
6.2	Test Approach.....	6.3
6.3	Experimental.....	6.4
6.3.1	Flowsheet Development.....	6.4
6.3.2	Feed Preparation.....	6.6
6.3.3	Furnace Operations.....	6.6
6.3.4	Data Collection.....	6.7
6.3.5	Sample Collection.....	6.7
6.3.6	Analytical.....	6.8
6.4	Operating Performance.....	6.9
6.4.1	Test Segment 1.....	6.9
6.4.2	Test Segment 2.....	6.10

6.4.3	Test Segment 3.....	6.10
6.4.4	Post Test Melter Examination and Evaluation.....	6.12
6.5	Off-Gas Analyses	6.12
6.5.1	Baghouse Solids.....	6.13
6.5.2	Ejector Venturi Scrubber.....	6.16
6.5.3	HEME and HEPA Filter.....	6.18
6.5.4	Melter Exhaust Gas Composition	6.19
6.6	Slag Analysis.....	6.20
6.7	Mass Balance and Partitioning	6.25
6.7.1	Overall Mass Balance.....	6.25
6.7.2	Partitioning of Flowsheet Constituents	6.26
7.0	Economic Analysis of the DC Plasma Arc Melter	7.1
8.0	References	8.0
	Appendix A – Data Point Listing	
	Appendix B – Analytical Data	

Figures

1.1 Schematic View of the DC, Plasma-Arc Melter.....	1.1
3.1 Engineering-Scale DC Arc Furnace Flowsheet	3.2
3.2 Engineering-Scale Furnace Equipment Layout.....	3.3
3.3 Furnace Vessel	3.4
3.4 Furnace Section Showing Refractory Layers (Side View).....	3.4
3.5 Furnace Section Showing Refractory Layers (Top View).....	3.5
3.6 Overflow Block Cooling Coils.....	3.7
3.7 Bottom Drain Assembly.....	3.8
3.8 Electrode Positioner System.....	3.9
3.9 Ram Feeder Mechanism	3.10
3.10 Film Cooler	3.11
3.11 Baghouse and Dust Collection System	3.12
3.12 Ejector Venturi Scrubber	3.13
3.13 High Efficiency Mist Eliminator	3.13
3.14 Furnace Restart Equipment.....	3.14
3.15 Isokinetic Sampler	3.15
3.16 Typical Off-Gas Particulate Sampling System.....	3.16
4.1 Campaign #1 Event Summary.....	4.8
4.2 Main Furnace Plenum Temperature and DC Arc Power Data	4.9
4.3 Measured Off-Gas Temperatures During Campaign #1	4.9
4.4 Overflow Section Temperature and Power Data.....	4.10

4.5	DC Arc Potential and Current Data with Metal Addition	4.11
4.6	Measured Feed Rates During Campaign #1	4.12
4.7	Glass Pour from Furnace Overflow During Campaign #1	4.13
4.8	Photographs of Glass Surface Conditions During Testing	4.14
4.9	Glass Versus Feed Production for Each Test Segment	4.16
4.10	Observed Side Bus Oxidation	4.18
4.11	Energy Balance Summary	4.19
4.12	Overall Mass Balance for the Engineering-Scale Furnace Test Campaign #1	4.27
4.13	Total Off-Gas Solids Carryover Versus Plenum Temperature	4.31
4.14	Partitioning of Primary Feed Constituents and Plutonium Surrogates at the Various Test Conditions	4.32
4.15	Partitioning of Plutonium Surrogates Compared to Aluminum	4.33
4.16	Partitioning of Hazardous Metals to the Off-Gas Solids at the Various Test Conditions	4.35
5.1	Monofrax K-3 Corrosion Rate Estimates for the Engineering-Scale Furnace	5.3
6.1	Unclassified Photo of a Ferroelectric Neutron Generator Tube	6.2
6.2	DC Arc Melter Operational and Processing Data	6.9
6.3	Steady-State Neutron Generator Processing Data	6.11
6.4	Temporal Compositional Changes in Pantex Slag	6.22
6.5	Temporal, Glass Compositional Changes of Ti and Zr	6.24
6.6	Pantex Demonstration Mass Balance Processing Data	6.26

Tables

4.1	Analyzed INEEL Soil Composition	4.3
4.2	Campaign #1 Feed Composition	4.4
4.3	Processing Information for Each Test Segment	4.15
4.4	Elemental Composition of Collected Baghouse Solids	4.20
4.5	Mass Spectrometer Analysis of Off-Gas Grab Samples	4.20
4.6	Normalized Composition of Slag Samples from the Engineering-Scale Furnace Test Campaign #1	4.21
4.7	Comparison of the Normalized Average Glass Composition to the Target Batch Composition	4.23
4.8	Mass in Feed Compared to Mass Dissolved from Refractory for Several Elements.....	4.24
4.9	TCLP Leachate Concentrations from Glass Product	4.24
4.10	TCLP Leachate Concentrations from Baghouse Solids.....	4.24
4.11	Overall Fractional Release of the ESF Glass Product.....	4.25
4.12	Elemental Mass Balance for Test Segments 1 Through 5	4.29
5.1	SRS Debris Waste Surrogate with Glass Forming Additives.....	5.1
6.1	Neutron Generator Composition	6.4
6.2	Trial Pantex Flowsheet Compositions	6.5
6.3	Pantex Demonstration Test Segments	6.6
6.4	Baghouse Solids Composition (2 nd segment)	6.14
6.5	Baghouse Solids Composition (3 rd segment).....	6.15
6.6	EVS Effluent Compositional Data	6.17
6.7	HEME/HEPA Effluent Compositional Data.....	6.19

6.8	Plenum Oxygen Content at Various Levels	6.20
6.9	Average Melter Exhaust Composition of Process Generated Gases	6.20
6.10	Pantex Waste Glass Compositional Data.....	6.21
6.11	TCLP Leachate Concentrations from Pantex Waste Glass	6.25
6.12	Flowsheet Partitioning Data.....	6.26
7.1	Estimated Capital Cost for a Graphite Electrode DC Arc Furnace System	7.1
7.2	Graphite Electrode DC Arc System Operating Costs	7.2
7.3	Waste Management Option Cost Comparison	7.3

1.0 Introduction

The DC arc plasma furnace, schematically illustrated in Figure 1.1, is a robust, high-temperature thermal treatment system that has been tested in support of the treatment of DOE mixed wastes under the MWFA. In this system, a stable DC arc is created by applying a potential between a graphite electrode and the graphite hearth of the furnace. The thermal energy produced by this arc creates and maintains a molten bath of material (glass/slag and/or metal) in the furnace hearth. Waste materials fed into the system are melted into the bath. Organics are pyrolyzed at the high operating temperatures and may be destroyed in the plenum or in a suitable afterburner. Oxide materials, including many hazardous and radioactive species, are immobilized in the durable glass/slag phase, while metals are converted to a second, more dense, molten-metal phase. The melter's inductively heated bottom drain and resistively heated overflow section are used to periodically transfer molten metal and glass waste products, respectively to waste receipt canisters. A great advantage of this technology is its potential application to waste streams containing a wide range of materials (debris, trash, metals, soil, etc.).

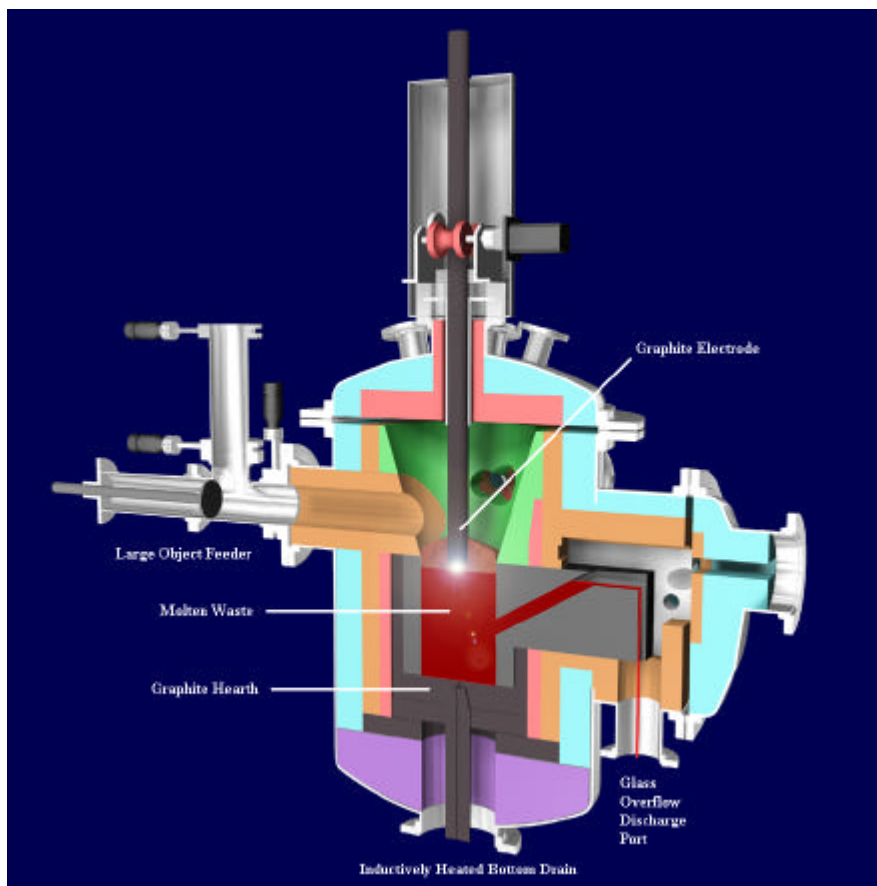


Figure 1.1. Schematic View of the DC, Plasma-Arc Melter

Although the DC arc plasma furnace exhibits great promise for treating the types of mixed waste that are commonly present at many of DOE sites, several data and technology deficiencies were identified by the MWFA regarding this thermal waste processing technique (MWFA 1997a). The technology deficiencies that have been addressed by the current studies include

- establishing the partitioning behavior of radionuclides, surrogates, and hazardous metals among the product streams (metal, slag, and off-gas) as a function of operating parameters, including melt temperature, plenum atmosphere, organic loading, chloride concentration, and particle size
- demonstrating the efficacy of product removal systems for slag and metal phases
- determining component durability through test runs of extended duration
- evaluating the effect of feed composition variations on process operating conditions and slag product performance
- collecting mass balance and operating data to support equipment and instrument design.

These issues were first addressed by a series of bench-scale plasma arc furnace tests (48 total, 5 radioactive) that were especially useful for evaluating the processibility of wide ranges of feeds and operating conditions prior to committing to large scale tests (Freeman and Seiler 1997). A series of engineering-scale furnace test campaigns followed in FY 1997.

The first of these engineering-scale test campaigns, which was successfully completed in April 1997, provided data regarding the effect of process operating conditions on partitioning behavior as well as the opportunity to shakedown the system and to validate sampling and operating procedures. The second test campaign, conducted in July 1997, was to investigate the effect of variation in feed composition and operating conditions on partitioning; however, damage sustained to the melter during startup operations caused the test to be terminated prematurely.

The actual damage to the DC arc furnace incurred during the second FY 1997 melter test was extensive enough to require major repairs before waste processing tests could resume. Since numerous bench-scale DC arc furnace tests had previously established that off-gas partitioning for transuranic waste components was dominated by scale-independent entrainment losses,^(a) it was reasoned that additional engineering-scale testing of plutonium bearing soils would provide little, if any, additional information regarding the technology deficiencies identified in the MWFA's Technology Development Requirement Document for plasma and DC arc melters. Consequently, application of the DC Arc Melter project was redirected to evaluate this technology's capability of converting classified hardware containing both hazardous and radioactive materials (Pantex ferroelectric neutron generators) into unclassified, durable waste forms that could be disposed of conventionally in a commercial waste repository.

(a) March 1988 draft report, Bench-Scale DC Arc Furnace Testing Using Simulated INEEL Sludge and SRS Debris Waste Feeds, Pacific Northwest National Laboratory, Richland, Washington.

The primary objective of the FY 1998 demilitarization demonstration of the DC arc melter was to evaluate how well this technology provides solutions to several needs identified by the Site Technology Coordination Groups (STCG) at the Pantex and Savannah River DOE sites. These specific needs identified include

- treatment of classified inorganic debris with TCLP metals, STCG Need #AL07-02-01-MW
- plasma-fired demilitarization and sanitization of classified weapon components and volume reduction of mixed wastes, STCG Need #AL07-06-03-MW.

This summary report provides a description and analysis of all of the engineering-scale DC arc melter tests conducted in support of the DOE's mixed waste disposal mission. Toward this end, a description of the technology and equipment will be provided first followed by a chronological description of the melter tests conducted and the analytical results obtained.

2.0 Conclusions

2.1 FY 1997 Representative Mixed Waste Simulation Testing

A primary purpose of the FY 1997 engineering-scale test campaign was to demonstrate and evaluate the operability of the engineering-scale DC arc furnace at PNNL. The objective of the second test campaign was to evaluate the processing performance of SRS debris surrogate, which had higher organic and metal contents than the soil-lime feed used in the first campaign. The following are a few specific conclusions regarding the system operations:

- The engineering-scale DC arc furnace operated successfully during the first engineering-scale test campaign. All major equipment functioned as designed and the system operated smoothly in either the submerged or exposed arc modes. The plugging of the overflow section during the second campaign caused that test effort to end prematurely.
- The feed rate was controlled by a mix of visual observation and monitoring of the plenum temperature. By the end of the campaign, the temperature of the plenum was determined to correlate well with cold-cap coverage and feed rate in the submerged arc operation.
- The processing rates during the submerged arc tests were comparable to those reported for solids feeding of joule-heated melters. No attempt was made to maximize these rates during exposed arc operation.
- The vacuum-assisted overflow drain, which has been proven in low-temperature, Inconel-based melters, can be designed and operated successfully at temperatures up to 1450°C.
- An electrical by-pass was demonstrated to provide an alternate conduction path when the hearth is covered with glass. Although this equipment was not used for restart during the first test campaign, it was used for the restart of the second test campaign. It is suspected, however, that this restart technique may have resulted in short circuiting through a crack or fissure in the furnace side wall. This may have subsequently caused preferential corrosion in that area of the furnace, contributing to the plugging of the furnace overflow section.
- Post test examination during both test campaigns found damage to the graphite rod buses and the hearth from attack by water vapor which was driven off from the incompletely baked-out refractory. Therefore, when constructing a similar system, care must be taken to fully bake out the refractory to remove all water prior to commencing operations. Complete immersion of the melter in an oven environment is recommended to assure that a uniform bake-out temperature is achieved throughout the entire melter.

The FY 1997 engineering campaign also provided data on the partitioning of hazardous metals and radionuclide surrogates. Following are a few specific conclusions regarding the product analyses:

- Overall bulk solids carryover and volatile element partitioning were both reduced by increasing the cold-cap coverage in the submerged arc mode of operation; both entrainment and volatility were high for exposed arc operation, regardless of the cold-cap coverage. Partitioning to the off-gas solids ranged from 0.4 wt% to 4 wt% for submerged arc operation, and 0.9 wt% to 3.8 wt% for exposed arc operation.
- Particle size appears to have some impact on partitioning to the off-gas; however, the effect appears to be minor. The partitioning of finer particle additives (including particles <1 micron) was measured to be within a factor of two of the bulk entrainment value at all test conditions, indicating that even sub-micron particulate entrainment is low in this system at the operating conditions of this test.
- Operating with a high cold-cap coverage of feed on the glass with a submerged arc reduced volatility of cadmium and lead to the off-gas by a factor of two to three compared to exposed arc, low cold-cap operating conditions.
- The engineering-scale furnace produces a uniform, durable product substantially reduced in volume relative to the starting material. Chemical analysis showed little variation in composition over the course of the run. Leach testing found the product to be comparable to natural basalt in durability and non-hazardous according to the TCLP.
- Lead is readily leached from the off-gas solids by the TCLP. All the off-gas solids are characteristically hazardous because of lead and in some samples, chrome.

2.2 FY 1998 Pantex Neutron Generator Demonstration Test

The primary purpose of the FY 1998 engineering-scale test campaign was to demonstrate the demilitarization and sanitization of classified weapons components containing radioactive and hazardous materials, and to evaluate the impact of this technology upon reducing the life cycle costs for managing these types of materials. Processing performance and the overall operability of the DC arc melter and its ancillary support systems were also of interest during the test. The following are results and conclusions drawn from the Pantex demonstration test.

Neutron Generator Processibility

- All (200) neutron generators were successfully processed and converted into glass and metallic waste forms. The prompt liberation of hydride isotopes accompanying the melting/desolution process accomplished the declassification (demilitarization/sanitization) objective of the demonstration.
- Stack discharge accounted for a major part of the tritium released by the processed neutron generators.
- The ejector venturi scrubber (EVS) quench scrubber operating at 40°C and a off-gas flow of 100 standard cubic feet per minute (SCFM) developed a tritiated water concentration of 2 µCi/cc.

- Baghouse solids collected at a ~250°C processing temperature and containing pyrolyzed organic matter and a residual moisture content, exhibited a specific activity of 2 μCi/g for tritium. A nanogram (10⁻⁹g) of tritiated water (HTO) per gram of solids would account for this observed activity.
- The residual water in the melter's waste glass is believed to be responsible for the measured tritium activity 0.05 μCi/g in the glass product. The maximum quantity of tritiated water (HTO vs T₂O) that would have to be present to account for this activity is 3.4 x 10⁻¹¹ wt%.
- Lead partitioned mainly to the off-gas system. Only ~4% of the flowsheet value of lead could be accounted for in the melter's slag, since submerged electrode melter-operations (see Section 4.8.3.3) could not be used during this demonstration. Based on mass balance considerations, up to 20% of the lead may have been incorporated within the melter's molten-metal phase.
- The lead content of the process glass was quite low (500 ppm). This durable waste form easily passed TCLP testing, thus, qualifying it as a nonhazardous waste.
- Containerized feeding appears to reduce physical entrainment of feed stream materials when compared to FY 1997 bulk feeding results. Overall, only 0.9% of the chemicals fed to the melter during target glass formation were lost to the off-gas system, despite non-ideal processing conditions.

System Operations

- The engineering-scale DC arc furnace operated successfully, with few exceptions, throughout the duration of the Pantex demonstration test. Three-quarters of the neutron generators to be treated during the demonstration were continuously processed at rates at or above the plan value (25 lbs/hr).
- The feed rates were controlled by cold-cap coverage. A 90% cold-cap condition was maintained at an average feeding rate of 27 lbs/hr. At 37 lbs/hr, the maximum feed rate used during the test, complete (100%) glass pool coverage was quickly attained with an average arc-power of 35 kW.
- The lack of vacuum isolation between the melt-chamber and the overflow section of the melter precluded the use of batch, glass-pouring techniques. The continuous glass overflow condition that resulted required maximizing processing rates and abandoning submerged-electrode operations. Meandering of the cold glass pour stream did create a non-critical blockage in the overflow section's spillway at the conclusion of the test.
- Although the containerized feed stream delivery technique appears to reduce gross physical entrainment, it adds substantial organic material to the process flowsheet and increases off-gas loadings of condensable debris. An afterburner used to oxidize organic material exiting the melter could significantly mitigate this off-gas system buildup of pyrolyzed material.

- Insufficient temperatures below the melt cavity prevented bottom drain tapping of the melter's molten metal phase. Although, pretest evaluations coupled with visual test observations suggest the bottom drain's induction heater was providing adequate heat to the melter's external freeze valve, the plasma arc's power density at the bottom of the unlined crucible was apparently insufficient to achieve expected temperature conditions at the bottom of the melter. Approximately 2 in. to 4 in. of metal is estimated to have accumulated within the graphite crucible during the Pantex test.
- Although minimizing the use of water-bearing castable refractories during the repair effort may have been responsible for the lack of vacuum isolation between melt and overflow chambers, no evidence for water-based corrosion of melter graphite components, which plagued earlier tests, was observed during the Pantex demonstration.

3.0 Equipment Description

The ESF system consists of the furnace, power control systems, feed systems, off-gas system, and a supervisory control and data acquisition system. Figure 3.1 shows the flowsheet for the ESF system. The furnace and most of the off-gas system are located within a walk-in enclosure/hood, while the remainder of the system is located outside this enclosure. Figure 3.2 shows the layout of the equipment in the room. The ESF was designed to deliver 50 to 100 kW of arcing power and to operate at bulk glass temperatures in excess of 1500°C. The off-gas system is designed to handle furnace outlet gas temperatures up to 1000°C laden with sub-micron particulate and acid gases. The following sections describe the primary components of the ESF system.

3.1 Furnace System

Special features in the ESF design include a bottom drain for both metals and glass, an overflow discharge section proven in many PNNL melters, and a graphite glass cavity capable, if ceramically lined, of operating in both oxidizing and reducing environments. A removable furnace roof, which is constructed of stainless steel, supports hangers for the insulating and refractory brick liner. There are eight openings through the furnace wall. Four of these penetrations are for the side busses to the graphite hearth. The other penetrations are present for a large object ram feeder, glass overflow discharge, furnace off-gas, and pyrometer access. Both a vacuum-assisted overflow and inductively-heated bottom drain permit molten glass and metal to be poured from the furnace.

The refractory design of PNNL's Engineering-Scale DC Arc Melter was modified somewhat during the FY 1998 furnace repair. The changes in materials were prompted both by FY 1998 projects flowsheet alterations and from lessons learned during FY 1997 testing. Since these modifications were slight, the original design will be discussed first followed by a description of FY 1998 alterations.

3.1.1 Vessel and Refractories

The ESF comprises a 3.5-ft diameter by 4-ft high stainless steel vessel which encloses the furnace hearth and contains a discharge section and penetrations for introducing feed, adding electrode, discharging off-gases, viewing, and emergency pressure relief. A diagram of the vessel with external connections is shown in, Figure 3.3. The distribution of refractories in the furnace are shown in Figures 3.4 and 3.5.

Electrical conductivity for the DC plasma arc is established between a graphite electrode introduced through the furnace lid and a graphite crucible which forms the hearth. Electrical contact is made to the hearth through four graphite rods, or busses, threaded into the crucible wall. These busses penetrate through 4-in. flanged penetrations in the shell and similar sized openings in the refractory (see Figure 3.5). The walls of the crucible are 2 in. thick and the bottom of the crucible is 4 in. thick. The

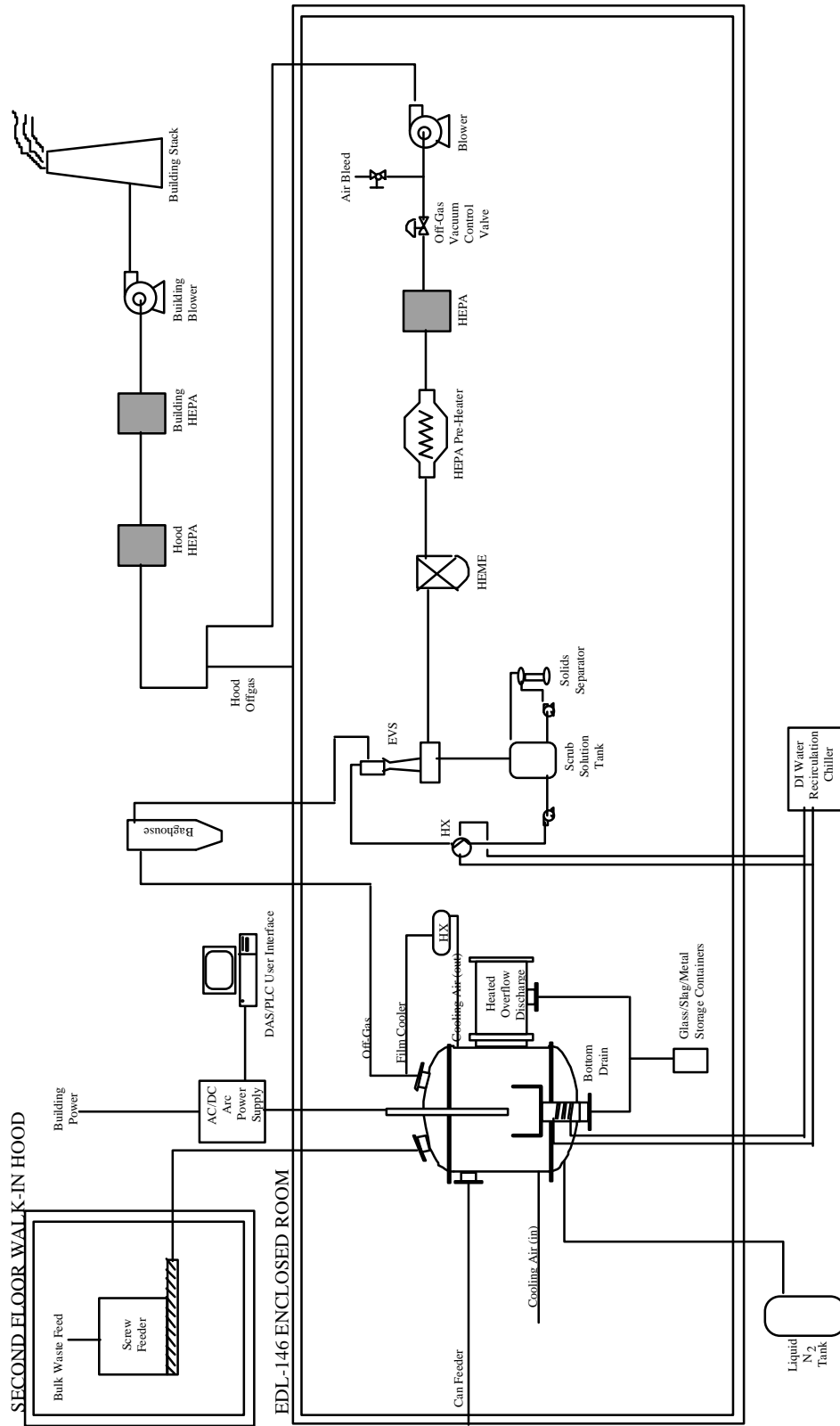


Figure 3.1. Engineering-Scale DC Arc Furnace Flowsheet

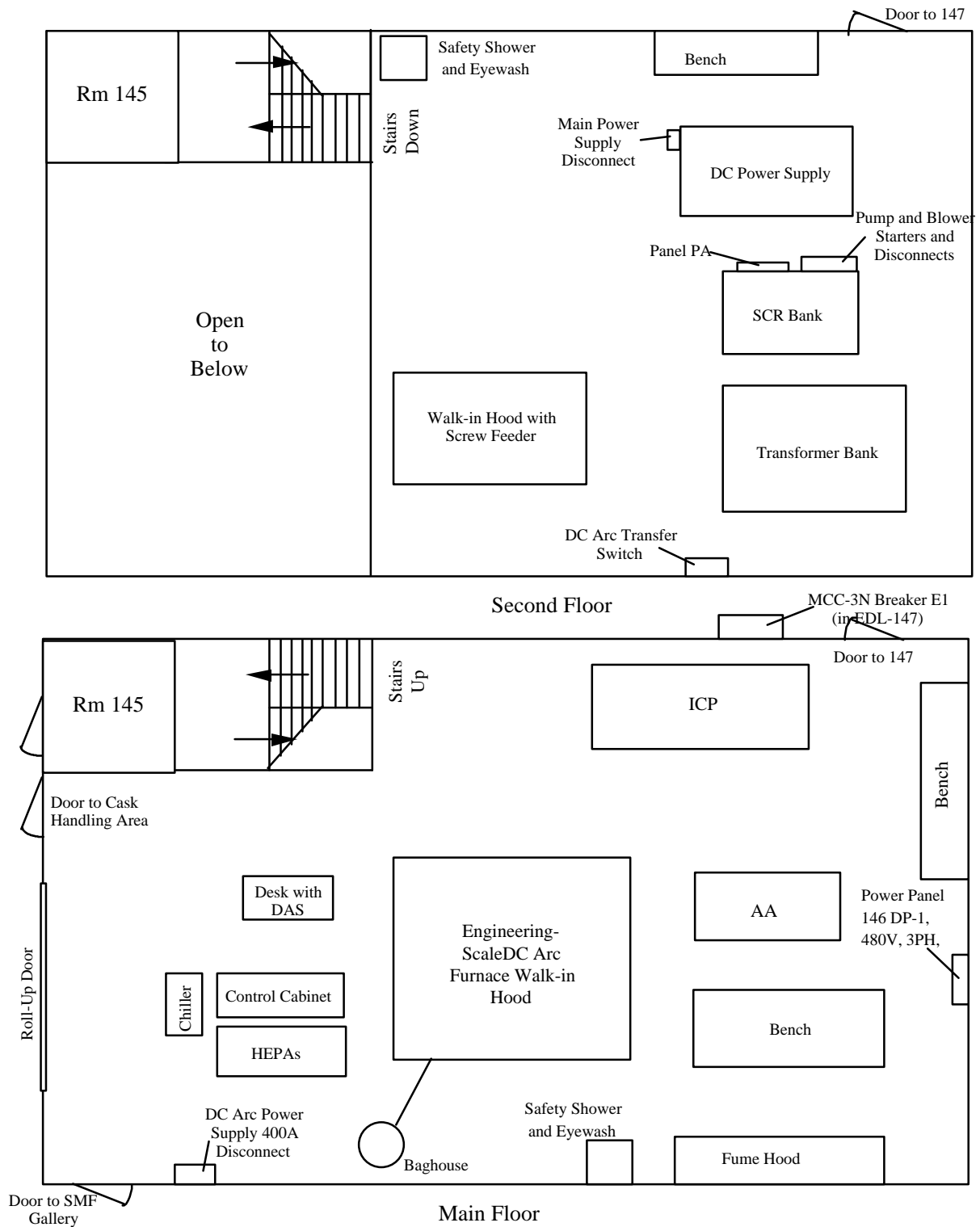


Figure 3.2. Engineering-Scale Furnace Equipment Layout

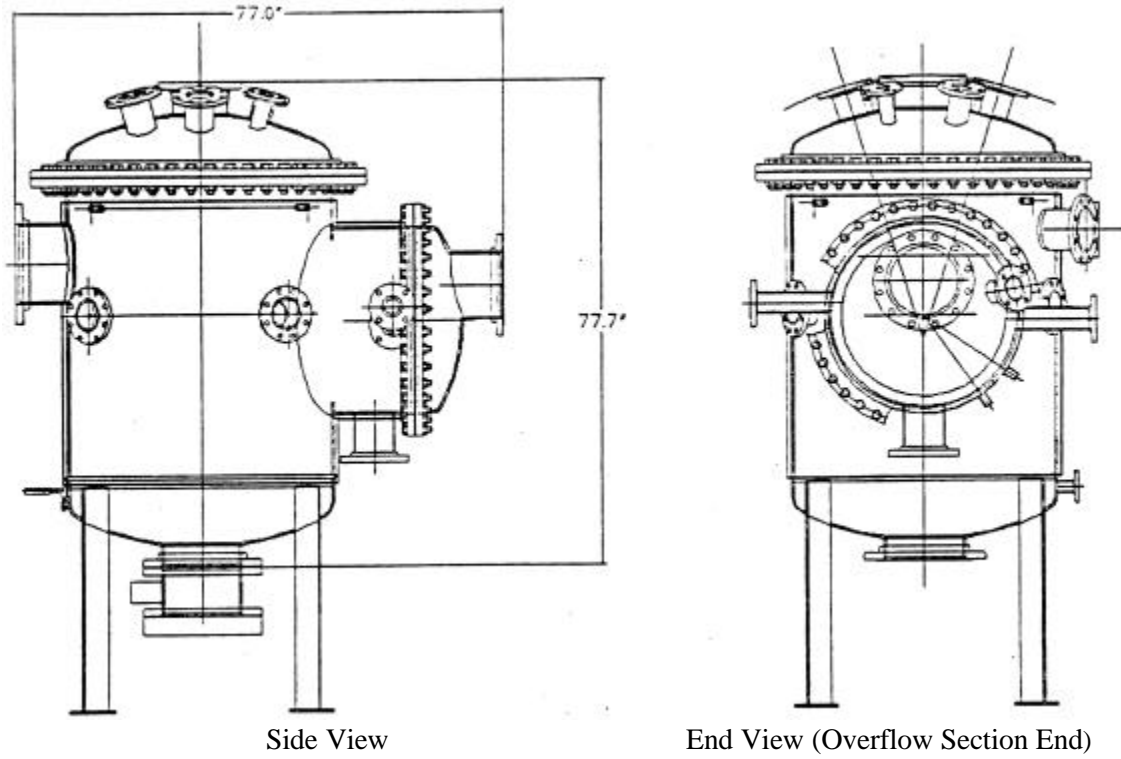


Figure 3.3. Furnace Vessel

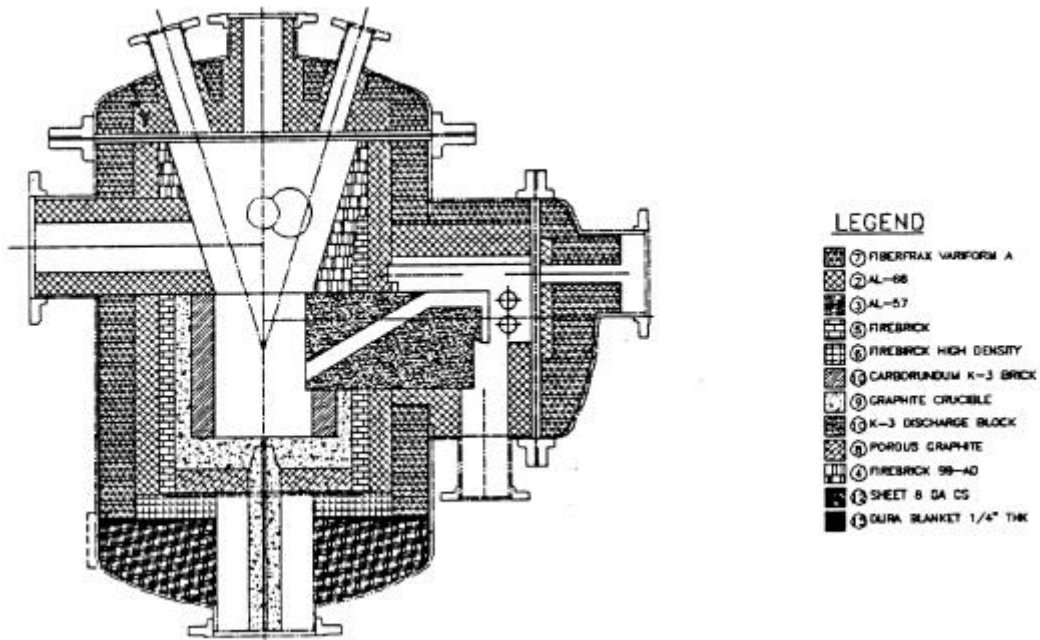


Figure 3.4. Furnace Section Showing Refractory Layers (Side View)

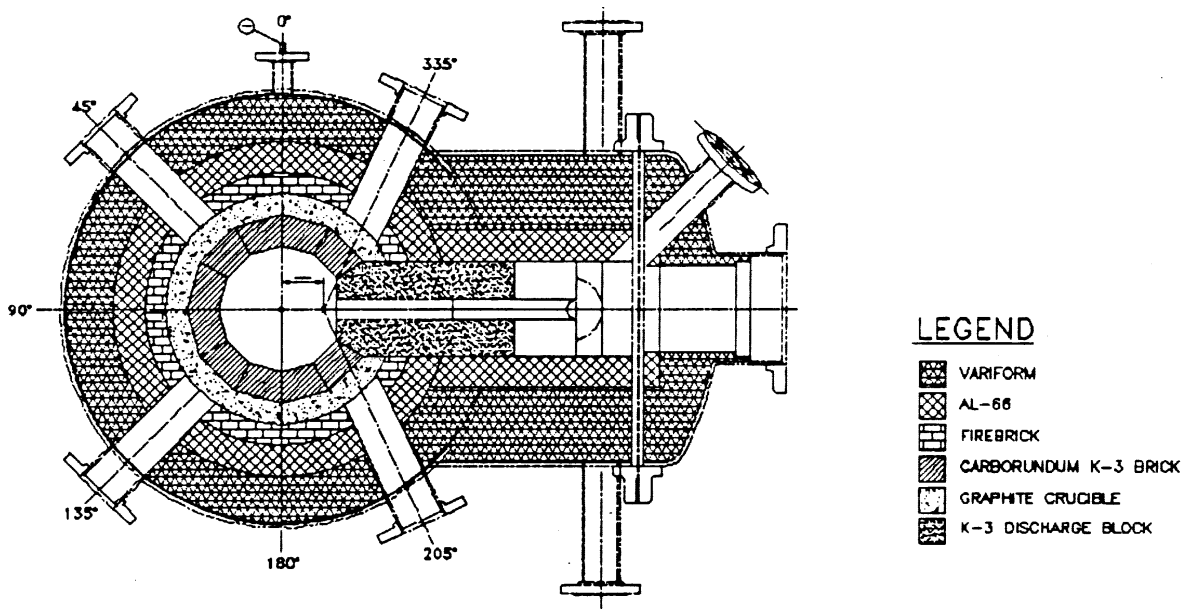


Figure 3.5. Furnace Section Showing Refractory Layers (Top View)

walls of the graphite crucible are lined with 3 in. of Monofrax K-3 refractory, manufactured by Carborundum, to protect the crucible from oxidizing conditions in the glass and gases above the melt. Immediately below the graphite crucible is a 3-in. layer of porous graphite on top of a 3-in. layer of high density firebrick. A 2-in. layer of Greenlite-28 firebrick surrounds the wall of the graphite crucible. This layer is, in turn, surrounded by a 3-in. layer of Alfrax-66. Both layers are supported on the dense firebrick, BN23000.

To prevent oxygen from attacking the graphite crucible, nitrogen is purged through a 24-in. diameter ring of stainless steel tubing embedded where the Greenlite and high-density firebrick join. The flow rate of nitrogen through this ring is nominally 1 to 2 SCFM. An additional nitrogen gas purge of 10-20 SCFM introduced around the top feeding electrode to reduce oxidation of the graphite.

The high density firebrick is supported on a layer of Alfrax-57 castable refractory which fills the domed bottom of the vessel. The outermost wall of refractory is formed by Fiberfrax Variform A cast refractory, nominally 4 5/8 in. thick. Firebrick 99-AD is used to line the plenum area of the melter above the K-3 refractory level. Outside of the firebrick are layers of cast Alfrax-66 and Variform A refractories, respectively.

The most significant change to the melter design during FY 1998 was the elimination of the graphite hearth's ceramic liner. This change was prompted by initial technical guidance (later proved to be false) that the neutron generators to be processed were primarily composed of metallic components that would require reducing process conditions with little formation of glass. Since the Monofrax K-3 refractory liner used during FY 1997 testing was shown to be unsuitable under reducing conditions and its corrosion was believed to be a contributory cause of the FY 1997 melter failure, a search for a more compatible liner refractory was made. However, a suitable substitute with a proven performance record could not be

identified for the processing conditions anticipated. Because unlined graphite crucibles are routinely used in electric melters used to smelt metals, and graphite, unlike K-3, cannot dissolve into and change the viscosity characteristics of any slag that might be generated in the projected process, the design of the FY 1998 melt cavity did not include a crucible liner.

To minimize the problems of water-based corrosion of graphite melter components that had destroyed the graphite bus-bars in both FY 1997 tests, alternatives for water-containing castable refractories were sought whenever possible. Specifically a dry Duraboard insulator was substituted for castable Fiberfrax Variform A originally used to form the melter's outer-wall refractory. In addition, to further reduce the rate or probability of bus-bar corrosion, each current carrying graphite rod was equipped with a protective ceramic sleeve with its own, independent nitrogen purge.

3.1.2 Overflow Section

Figures 3.4 and 3.5 also show cut-away views of the furnace overflow section. The molten slag or glass phase is withdrawn from the furnace through an overflow channel cut into a block of. The overflow tube is approximately 2 in. in diameter and is cut into the block at approximately a 30° upward slope, which seals the overflow section from the furnace hearth when the furnace is filled with molten glass. Glass pours from the overflow section as its level within the furnace increases above the pour spout. Additionally, a small vacuum can be pulled on the overflow section to provide better pouring control and flexibility. The side of the overflow block opposite from the furnace is centered over the discharge port so that glass which flows through and over the block falls down the middle of the 6 in. discharge nozzle into the receiving container. The receiving container is an 8-gallon drum that sits on a transfer dolly and is sealed to the overflow section with a steel bellows. Load cells are used to monitor the drum weight.

The overflow section is heated so that the glass remains molten while pouring. Temperatures as high as 1500°C are maintained with five silicon carbide bayonet heaters; two entering from opposite sides (face heaters) and three entering through the end of the overflow section (trough heaters). These heaters protrude over the overflow block to keep the glass heated as it is poured from the furnace. The total power rating of the overflow section heaters is 16 kW.

Because of the incompatibilities of the Carborundum K-3 refractory with the anticipated need for strong reducing conditions required by a metal smelting flowsheet, the original design was modified to include a graphite overflow block. The rationale for the choice was similar to that used for eliminating the hearth liner: graphite was compatible with reducing process conditions and would not materially contribute to any slag produced. For similar reasons the FY 1998 design also specified graphite material for the transfer channel linking the melt and overflow chambers. No other substantive changes were made to the overflow design.

3.1.3 Furnace Cooling

The outside walls of the furnace are cooled to provide unwanted glass migration throughout the refractories and insulation. Molten glass will flow through all of the crevices between the refractories until cooled to a temperature where the viscosity is high enough to prevent flow. The primary means of

cooling these regions is a cooling jacket surrounding the furnace. Air flows through this jacket at rates as high as 50 SCFM. This cooling also helps keep the outer jacket temperature below 200°C to minimize safety hazards to the system operators. Special cooling is also provided to prevent glass from flowing around the bottom and sides of the Monfrax K-3 pour block. Two cooling coils are embedded in the Alfrac-66 refractory on each side of and underneath the pour block. The coils are designed to maintain the temperature at the surface of the pour block below the liquidus temperature of the glass. The total designed air flow to these coils is approximately 16 SCFM. Figure 3.6 shows the shape and location of each of the cooling coils.

3.1.4 Bottom Drain

The ESF is equipped with an inductively-heated/freeze-valve bottom drain for the tapping of metals and/or slag from the bottom of the furnace. A schematic of this drain is shown in Figure 3.7. This drain consists of a 4 in. diameter x 24 in. long graphite rod, or udder, that is screwed into the bottom of the furnace hearth. Material is drained from the furnace through a 1/2 in. diameter hole in the center of the udder. A water-cooled induction coil powered by a 50 kW induction power supply surrounds the udder. The induction coil provides the energy to heat the graphite tube when under power, and also provides the cooling to stop the flow of molten material when the power is shut off. Nitrogen is purged into the bottom drain area to protect the graphite from oxidization.

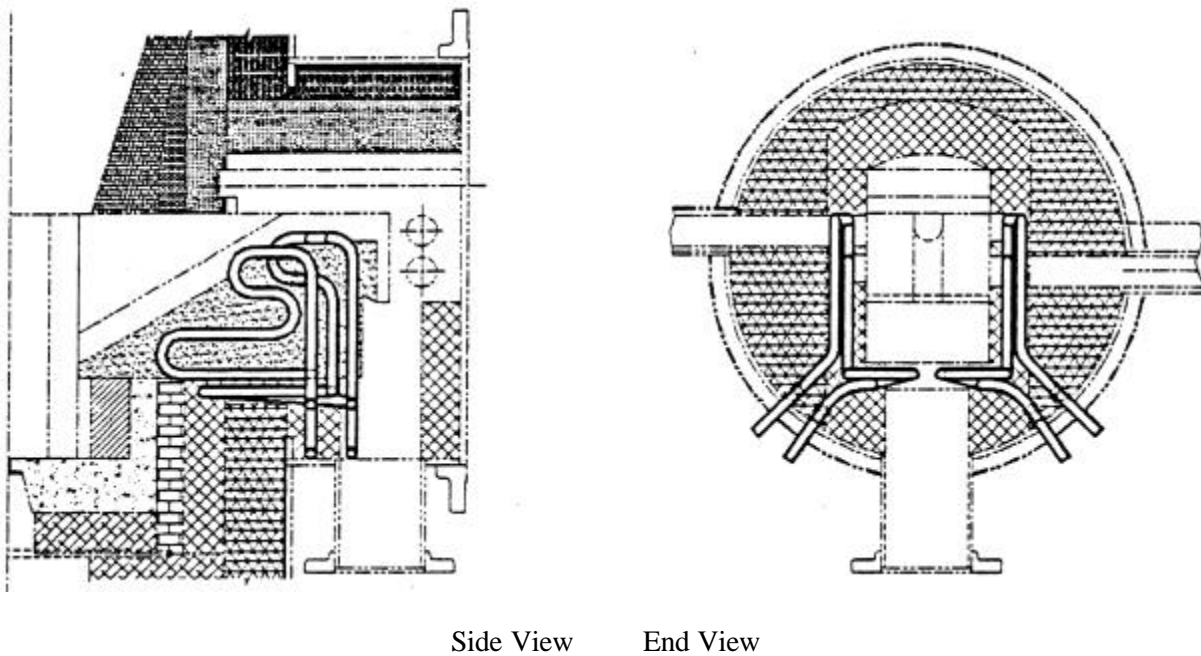


Figure 3.6. Overflow Block Cooling Coils

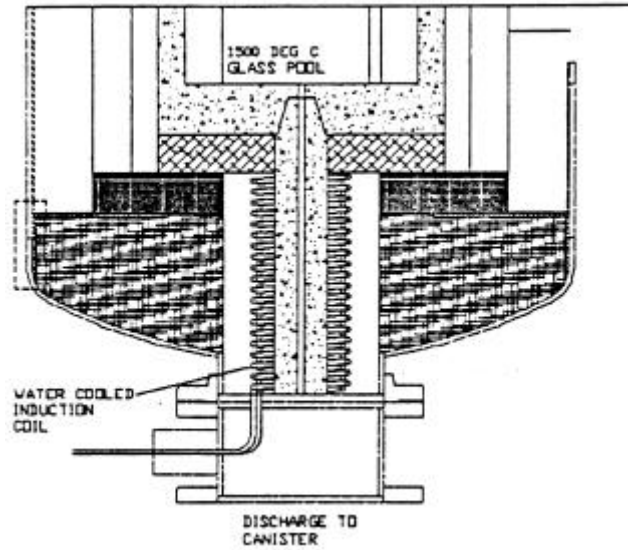


Figure 3.7. Bottom Drain Assembly

3.2 Power System

3.2.1 Power Supply

The furnace is designed to operate at DC power levels ranging as high as 100 kW. However currents and voltages used under steady-state processing conditions have been limited to 100 A to 400 A at 100 V to 150 V. The power to the furnace is controlled by adjusting either the arc voltage or arc current. The arc current is controlled using a thyristor-controlled rectifier. Generally the power supply is operated in a constant-current mode. The arc voltage is increased by raising the electrode and elongating the arc. The electrode is 3-in. diameter graphite rod and serves as a cathode in the DC circuit. Correspondingly, the graphite hearth acts as the anode in the circuit.

3.2.2 Electrode Feed System

During the course of operation, the graphite electrode is continuously consumed. Therefore, the vertical electrode position is critical to maintain steady operating potentials. This positioning is performed in the ESF using a specially-designed electrode feeding/positioning mechanism. A schematic of this mechanism is shown in Figure 3.8. Here two motor-driven rollers (made from copper/nickel alloy) vertically adjust the electrode in increments as small as 1/64 in. These rollers also provide the electrical contacts to the graphite electrode so that bulky clamping assemblies are not required. Electrical contact to the rollers is achieved using an electric brush assembly. The small size of the mechanism allows it to easily be contained in a high-pressure enclosure so that gases cannot escape to the atmosphere where the electrode penetrates the furnace. Additionally, the configuration of the mechanism allows new electrode

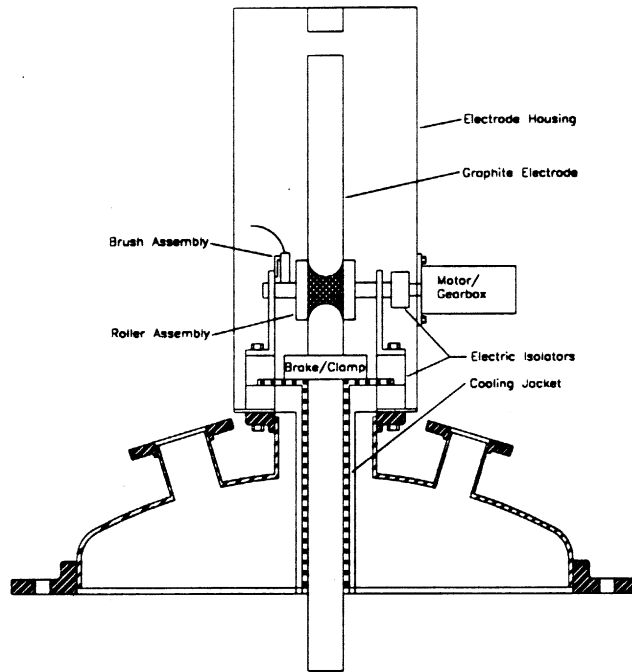


Figure 3.8. Electrode Positioner System

segments to be easily and quickly screwed onto the upper portion of the remaining electrode through a small access port. This configuration is also amenable to an automatic mechanism for adding additional electrode segments.

3.3 Feed Systems

The ESF can be fed with using an auger, or bulk solids, feeder or larger object ram feeder. The following sections provide descriptions of each.

3.3.1 Bulk Solids Feeder

Bulk solids may be added to the furnace through an auger feed system located on the second floor above the furnace, inside a walk in hood. An auger moves bulk materials such as soils and small particulate from the hopper into a feed pipe that conveys the feed material through the top of the hood in which the furnace is housed, and directly into the furnace through a 4-in. port on the furnace lid.

3.3.2 Ram Feeder

Large objects are fed to the furnace through ram feeder system. Figure 3.9 shows a schematic of this feeding system. An inclined shelf of adjustable width and pneumatically-controlled stops to allows cylindrical cans to be fed into the ramming mechanism. Cans individually fall into ram feeder via double gate valves to maintain a seal in the furnace.

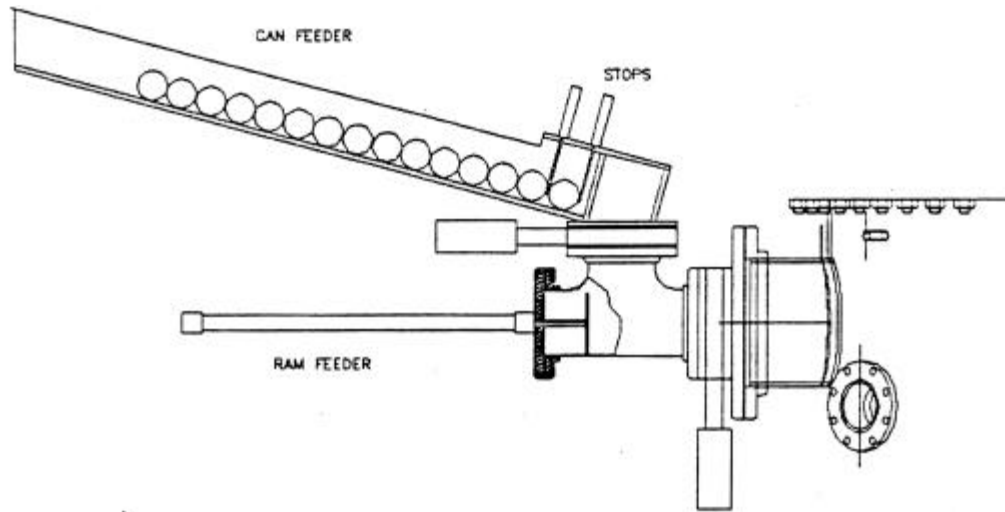


Figure 3.9. Ram Feeder Mechanism

3.4 Off-Gas System

During operation the ESF produces an off-gas which may contain particulate, gaseous, or mist contaminants. The ESF system includes an off-gas treatment system with several components to treat a variety of off-gas contaminants. The off-gas system draft is provided by a 250 CFM blower located just in front of the system HEPA filters. A control valve and air bleed at the blower inlet regulate the flow to maintain a negative pressure of 1 in.-5 in. water column (“wc) in the furnace plenum. The system discharges the cleaned off-gas to the hood ventilation duct, which includes a second HEPA filtration system. The hood duct conducts the off-gas to the building ventilation exhaust system, which includes a third bank of HEPA filters before the gases are discharged to atmosphere. The individual system components for the ESF off-gas system are described in the following sections.

3.4.1 Film Cooler

Gas temperatures leaving the furnace plenum may be as high as 1000°C, too hot for the subsequent processing equipment. The purpose of the film cooler is to cool these exhaust vapors and protect the down-line equipment. Additionally, the film cooler can condense fumes and increase the gas velocity to prevent them sticking and plugging the off-gas line. Figure 3.10 shows a schematic of the film cooler assembly. The film cooler is made from concentric pipes with the plenum gases passing through the inner pipe. Air is blown into the shell around the inner pipe. The wall of the inner pipe is made of louvers (or fins) so that air blows through the slots from the shell into the inner pipe and mixes with the plenum gases. The film cooler is designed for a quenching air flow of approximately 150 CFM to cool the furnace effluent to less than 300°C.

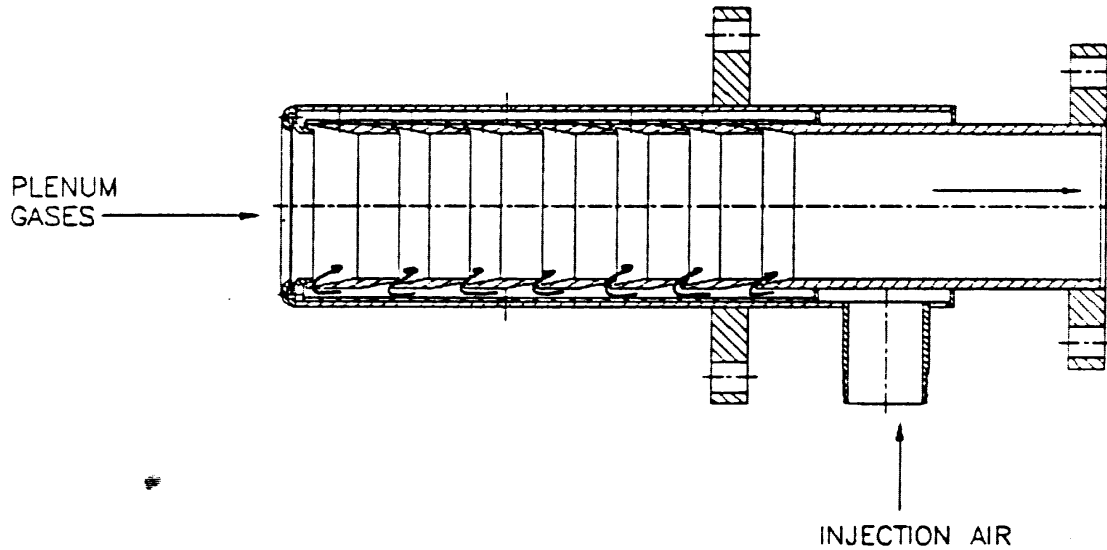


Figure 3.10. Film Cooler

3.4.2 Baghouse Filter

Most of the particulate generated in the furnace or condensed particulate created from the film cooler are collected with a Model 12-4-100 “C” Mikro-Pulsaire baghouse filter. The filter system is designed to remove up to 5 pounds per hour of particulate from 150 SCFM of air. The filter media is NEXTEL (manufactured by 3M), which can withstand operating temperatures in excess of 600°C. Dust is knocked off the filter bags with pulses of air and falls into a collection container underneath the baghouse. The dust collection container is fitted with a Plexiglas lid so that the character and quantity of the dust can be observed during operation. A photograph of the baghouse is shown in Figure 3.11.

3.4.3 Ejector Venturi Scrubber (EVS)

The EVS scrubber removes excess water vapor and a fraction of the soluble gas constituents. The venturi uses approximately 10 gpm of recirculated water at 60 psig to draw gases through a conical water spray. Figure 3.12 shows a schematic of the EVS. The water spray scrubs particulate and water-soluble vapors from the gas. Gas flow through the EVS is rated for 100 SCFM. Integral with the EVS is a liquid gas separator tank which serves as the reservoir for the water circulating pump. It also removes entrained water droplets from the gas stream. Fine water droplets (mist) are removed in the high efficiency mist eliminator (HEME). A heat exchanger is installed in the pump recirculation line to remove heat absorbed from the hot gases by the venturi scrubber.

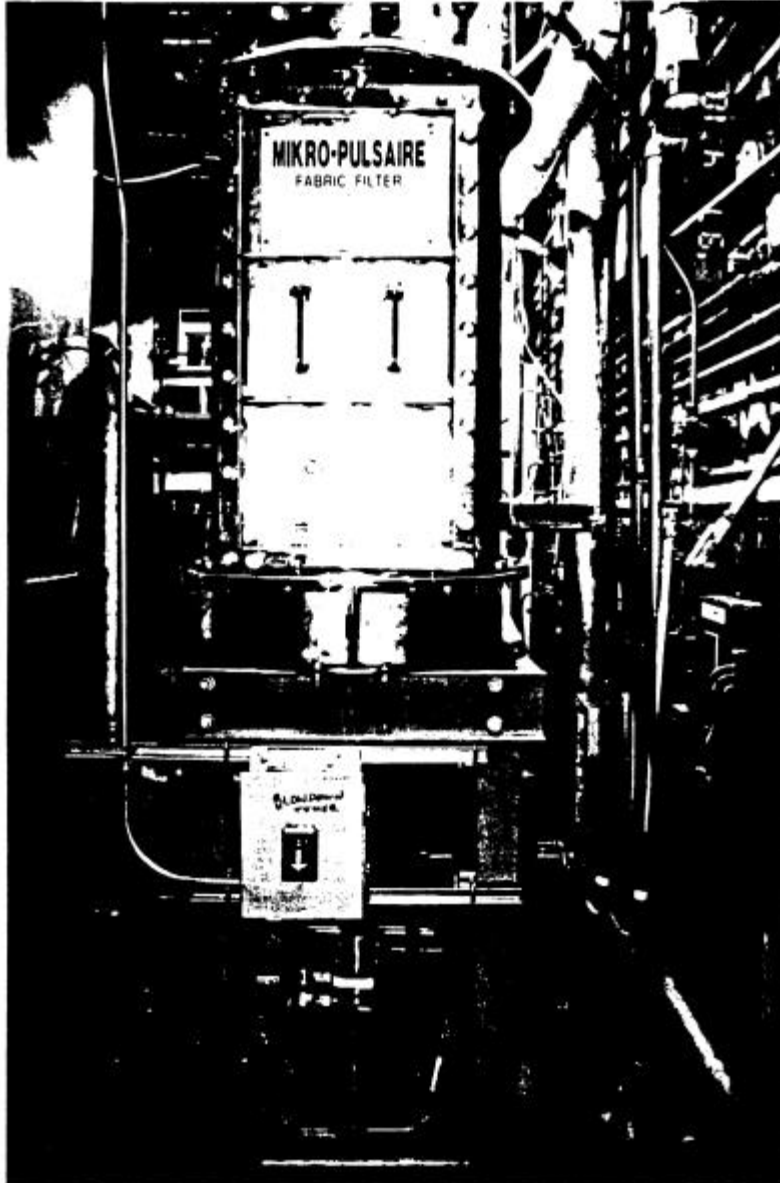


Figure 3.11. Baghouse and Dust Collection System

3.4.4 High Efficiency Mist Eliminator (HEME)

A HEME is located immediately down line from the EVS. The HEME removes water aerosols from the off-gas as well as micron and sub-micron particulate matter. The HEME utilizes a glass fiber element to remove mist and 99% of particulate below 3 microns in diameter. Collected water droplets flow by gravity down the fibers of the element and are drained to a sump at the bottom of the housing and then discharged. Figure 3.13 shows a schematic of the HEME.

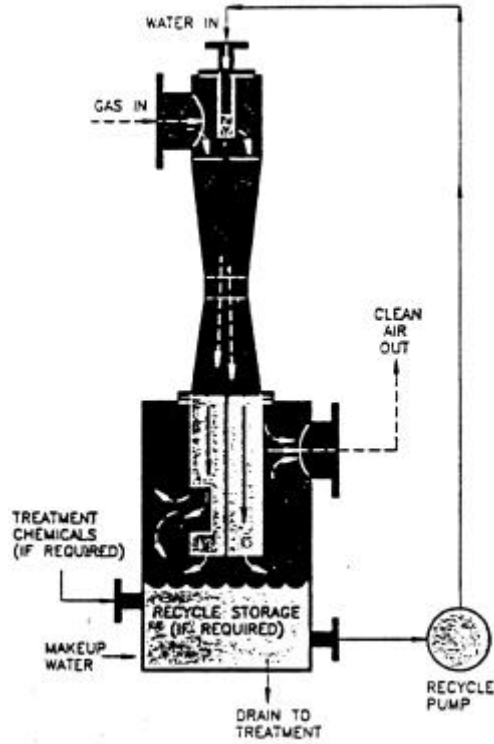


Figure 3.12. Ejector Venturi Scrubber (EVS)

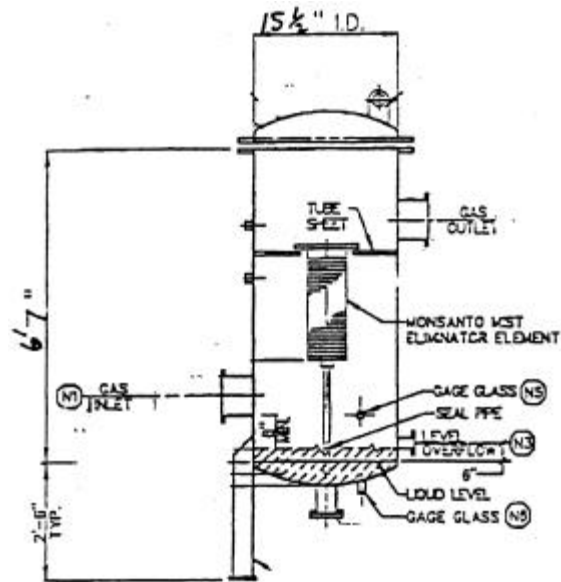


Figure 3.13. High Efficiency Mist Eliminator (HEME)

3.4.5 High Efficiency Particulate Air (HEPA) Filter

After leaving the HEME, the off-gas passes through a heater, followed by a HEPA filter designed to remove 99.9% of “hard to capture” particles (mean diameters of 0.3 μm -0.5 μm). The HEPA filter is nuclear grade, rated for 100 SCFM with filter pack dimensions of 12 in. x 12 in. x 5 7/8 in. The maximum allowable pressure drop through the HEPA is 50 “wc. The electric preheater provides up to 6.5 kW to the gas entering the HEPA in order to maintain the temperature of that gas near 100°C. These temperatures ensure that water will not condense in the HEPA filter.

3.5 Furnace Restart Equipment

If the furnace is allowed to cool without entirely removing the glass/slag, the frozen glass forms an electrically insulating layer between the negative stinger electrode and the positive hearth. To restart a filled or partially-filled furnace it is necessary to use a temporary electrical by-pass wired in parallel with the graphite hearth (anode). The by-pass circuit acts as the hearth inside the furnace until enough heat is generated to melt the glass layer, at which point the power can be switched from the by-pass circuit to the normal hearth anode.

The electrical by-pass consists of two braided steel cables with metal weights hung through a penetration in the top of the furnace down onto the solid glass surface. Nails are added to the surface of the glass to provide multiple contact points between the cable and the arc electrode. Figure 3.14 shows a schematic of the restart wiring configuration.

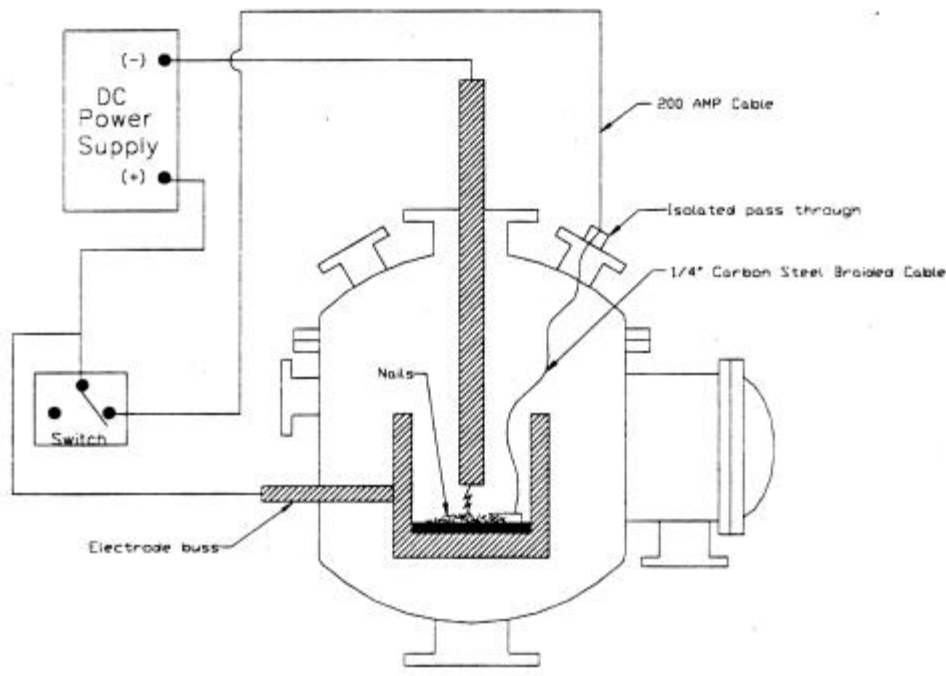


Figure 3.14. Furnace Restart Equipment

3.6 Data Acquisition and Control System

The control system for the engineering-scale furnace uses a Supervisory Control and Data Acquisition (SCADA) system working in conjunction with a Programmable Logic Controller (PLC). The SCADA software is FIXDMACS, version 5.0, manufactured by Intellution. This software runs on a Pentium 120 MHz computer and interfaces the PLC via an RS-422 connection. The PLC is a Square-D Class 8030. Each sensor input comes into the PLC input/output cards. The manufacturer's reported accuracy on those cards are within 0.1% of the total range for analog current and voltage signals and 0.25% of the total range for thermocouple signals. The system provides data logging, control, and alarming of critical data points. The total listing of input data points is in Appendix A.

3.7 Off-Gas Particulate Sampler

Off-gas particulate samples were collected using a Model 2010 A Nutech Isokinetic Stack Sampler manufactured by Graseby Anderson. The sampler is designed to meet all Environmental Protection Agency (EPA) standards for isokinetic source sampling equipment as outlined in the Office of Air Programs Publication No. APTD-0576.

The sampler consists of a control console, a sample case containing a heated filter, impinger glassware, an umbilical cord, heated sample probe and pitot tube. The isokinetic sampler is illustrated in Figure 3.15.

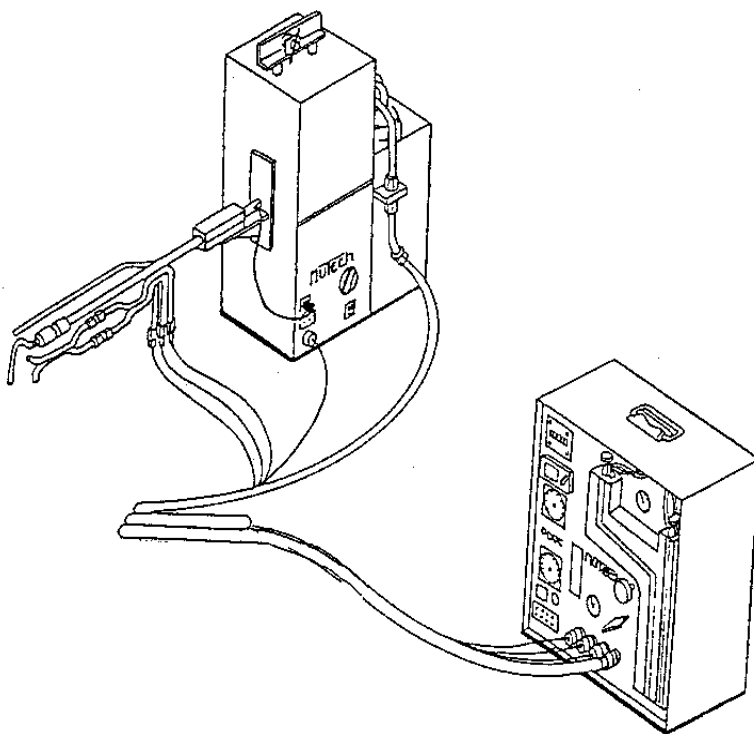


Figure 3.15. Isokinetic Sampler

The following is a brief description of operation of the sample equipment (see Figure 3.16):

1. Stack gases enter the probe nozzle at or near isokinetic conditions. The gases flow through the heated sample probe to the filter housing.
2. The pressure differential produced by a pitot tube near the sample probe is used to determine the off-gas velocity in the line. Using this ΔP , the operator calculates the desired sample nozzle velocity and flow rate, which is controlled by maintaining a differential pressure across a calibrated flow orifice.
3. The stack gases are drawn through a heated glass fiber filter that retains nearly all the entrained particulate. After the filter, the off-gas flows through a series of impingers contained in an ice bath to both cool the gases and remove condensables in the sample gas stream. The final impinger contains silica gel to remove water vapor from the gas.
4. The cooled gases enter the umbilical cord and are carried to the control unit. The control unit uses a fiber vane vacuum pump to draw the stack gases through the sampling train. A dry gas meter records the volume of gas sampled. Sampling rates are measured using a fluid manometer to measure the pressure drop across a calibrated flow orifice. Fine and coarse valves may be used to adjust the flow rate.

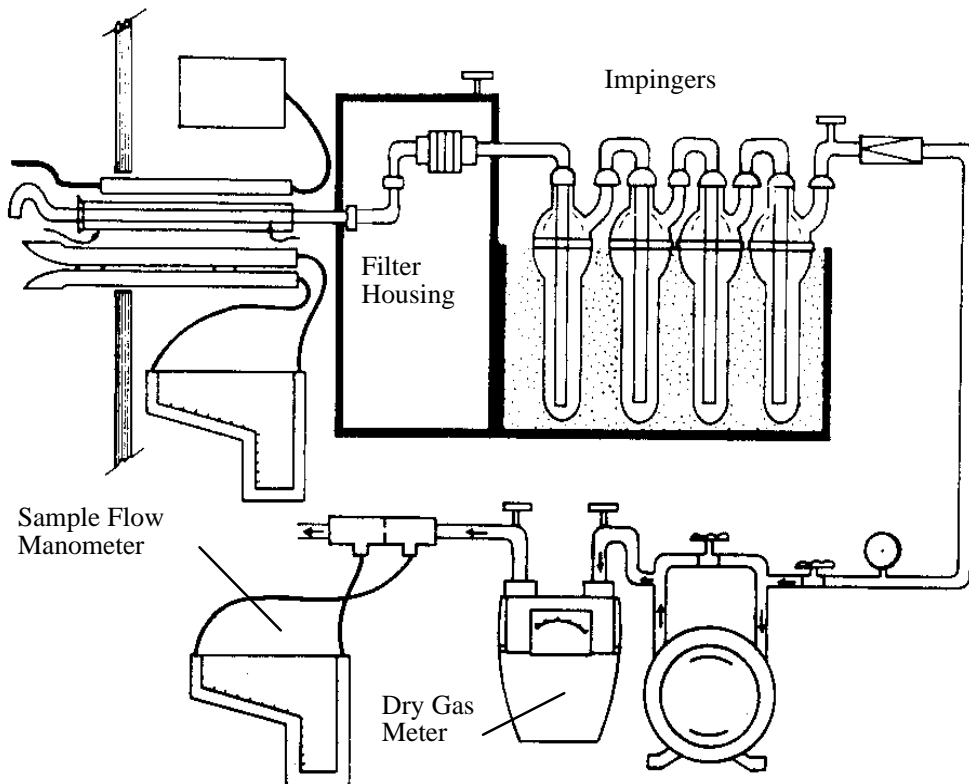


Figure 3.16. Typical Off-Gas Particulate Sampling System

4.0 Testing Campaign #1: Melter Performance Using Idaho National Engineering and Environmental Laboratory (INEEL) Soil

4.1 Objectives

The primary focus of the FY 1997 testing program at PNNL was to determine the fate of transuranic elements in high-temperature vitrification systems while demonstrating and evaluating the performance of the DC arc furnace. The engineering-scale test campaign described in this report was the first run of extended duration in the engineering-scale furnace; therefore, the primary focus of this testing was the operability of the system. Sampling and analysis were performed to both characterize the system operations and to verify the adequacy of the sampling and analytical procedures for subsequent testing.

The same feed material was run throughout the first test campaign; however, the campaign was divided into several segments in which certain key operating conditions were varied. The impact of the following test conditions on system operations was investigated:

- *Submerged/Exposed Arc* - The furnace was run with the electrode above the melt surface (exposed arc) or with the electrode submerged in the glass (submerged arc).
- *Cold-Cap Coverage* - Test segments with the electrode above the melt or submerged in the melt were run with either low or high amounts of feed covering the glass surface (cold-cap coverage) to obtain process data for both conditions.
- *Container vs. Bulk Feeding* - The feed material was fed to the furnace in closed containers or as a bulk material (screw feeder).

Data collected during test segments carried out at the above described conditions was used to meet test objectives which had been previously detailed in the FY 1997 test plan. The specific test objectives for the first engineering-scale test campaign were as follows:

1. System Operating Performance

- Evaluate the general operability of the DC arc furnace system and the effects of the various test conditions on the system performance.
- Measure operational performance data (processing rates, electrode consumption, specific melting energy, etc.).

- Evaluate the performance of prototypic product removal systems (overflow and bottom drains).
- Demonstrate the ability to restart the DC arc furnace after shut-down without draining the contents of the melt cavity.

2. Energy Balances

- Determine the overall energy balance for the engineering-scale system during the first test campaign.

3. Mass Balances

- Determine the overall mass balance for the duration of the entire test.
- Evaluate the impact of test conditions on the partitioning of metals to the off-gas and slag phases, specifically focusing on the hazardous metals and radionuclide surrogates.

4. Off-Gas

- Compare data obtained from sampling of the off-gas stream to that obtained from analysis of the collected baghouse solids.
- Evaluate the performance of the furnace off-gas system.

5. Product Characterization

- Characterize the durability of the slag product and determine the impacts (if any) of the test conditions on the product performance.
- Determine the TCLP leachate concentrations of heavy metals from the slag product.

4.2 Test Approach

The waste surrogate used for the first test campaign was actual INEEL soil spiked with various hazardous metals. Table 4.1 shows the normalized composition from the analysis of several soil samples.

Each of the metal elements in the table is assumed to be oxide in form. The primary constituents within the soil are silica, alumina, and calcia. The composition of the soil is such that the melting temperature is too high to be pourable from the engineering-scale furnace through the vacuum-assisted overflow section; therefore, lime was added to the soil to lower the viscosity into the desired range (about 100 poise at 1350°C to 1450°C). A similar lime addition scheme was used for INEEL Subsurface Disposal Area waste surrogates to assure they could be poured from test vitrification systems.

Table 4.1. Analyzed INEEL Soil Composition

Constituent	Amount (wt%)
Al	5.6
Ca	5.0
Fe	2.9
K	2.1
Mg	1.3
Na	0.9
Si	28.0
Ti	0.4
Other	0.2
O	42.1
Loss on Firing	11.5
Total	100

Table 4.2 gives the composition of the feed blend used for the first campaign of the engineering-scale furnace. Hazardous metals were spiked into the feed material at 1000 ppm (on a metal basis) in each form shown. Additionally, Zr, Nd, and Y were spiked at 2500 ppm (on a metal basis) into the feed blend. These three elements were added in three widely varying particle sizes in order to assess the impact of particle size on carryover to the off-gas during furnace operation. Off-gas partitioning of fine particulates is of key interest since debris wastes at the SRS contain finely ground ²³⁸Pu oxide, which may be much more dispersible than the rest of the waste material. Zr, Nd, and Y were added to the feed since they, like ²³⁸Pu, form very stable oxides with low vapor pressures at the target furnace operating temperatures. These elements were also chosen since they were not present in significant quantities in the INEEL soil or lime; the only source of these elements in the product streams was from the additive with the particle size of interest.

The effect of several variations in test conditions on the partitioning of metals to the off-gas phase and system operation was to be investigated in this test campaign. These tests will serve to identify the operating conditions to be used for subsequent testing. Following is a brief description of the conditions investigated:

- *Submerged/Exposed Arc* - Previous testing has shown that once a molten pool is established, the furnace may be run with the electrode submerged in the melt as opposed to arcing to the surface of the melt. The position of the electrode may affect a number of operating parameters including the thermal efficiency, volatile losses, melt redox, and processing rate.
- *Cold-Cap Coverage* - Previous testing has shown that a relatively cool feed pile can build up and cover the surface. Such an accumulation of a cold-cap can substantially reduce volatile and heat losses from the melt.

Table 4.2. Campaign #1 Feed Composition

Material	Amount
Base Materials:	
INEEL Soil	80 wt%
Lime	20 wt%
Hazardous Metals:	
AgNO ₃	1000 ppm (metal basis)
Ba(OH) ₂ •8H ₂ O	1000 ppm (metal basis)
CdO	1000 ppm (metal basis)
Cr(OH) ₃	1000 ppm (metal basis)
Pb(NO ₃) ₂	1000 ppm (metal basis)
Ni(OH) ₂	1000 ppm (metal basis)
Small Particulate:	
ZrSiO ₄ (<1 μm)	2500 ppm (metal basis)
Nd ₂ O ₃ (<44 μm)	2500 ppm (metal basis)
Y(OH) ₃ (<4760 μm)	2500 ppm (metal basis)

- *Container vs. Bulk Feeding* - Containerized feeding of the engineering-scale furnace lends considerable flexibility for radioactive operations. Additionally, this type of feeding may give some representative indications of drum feeding behavior in a full-scale system. On the other hand, bulk feeding (via an auger) may be more convenient for contaminated soils, glass forming additives, or homogenized wastes. The method of feeding may impact furnace processing rates, bulk carryover, and metals partitioning.

Five different test segments were planned in which operating conditions of the furnace were varied while using this soil/lime feed. These test segments included the following:

- Submerged arc/low cold-cap coverage
- Submerged arc/high cold-cap coverage
- Exposed arc/low cold-cap coverage
- Exposed arc/high cold-cap coverage
- Container feeding

Since problems were encountered with the ram in the container feeder, a segment with submerged arc and cold-cap coverage intermediate to the other two segments was substituted for the container feeding segment. The evaluation of container feeding operations was postponed until FY 1998 testing.

The strategy used in these tests was to run the system at one of the test conditions until it appeared that the operation of the furnace was fairly stable. A test segment would then be run for a duration of two to three hours, after which the test conditions would be changed to that of the next segment. When operation of the furnace again appeared stable, the next segment would be started. It was thought that since the same feed was used throughout the test, it was not necessary to “turn over,” or flush out the glass from the previous test segment. While this was true for the major, non-volatile elements, it became apparent during the analysis of the data from the tests that longer times between test segments or test segments of longer duration may have improved the mass balance data for some volatile metals such as cadmium.

4.3 Experimental

4.3.1 Feed Preparation and Furnace Operation

Feed was prepared for the test campaign in 100-pound batches. INEEL soil, lime, and hazardous metal and plutonium surrogate spike materials were individually weighed and added to a small cement mixer. Samples of all feed materials were analyzed for elemental content, as described in Section 6.4 of this report. The materials were mixed together for 30 minutes, after which the batch was removed to fill two 5-gallon pails. Additional batches were prepared to fill the needs of the test. Although all materials were dry, there was sufficient moisture in the soil to hydrate a portion of the added lime, which increased the temperature of the feed material to approximately 100°C to 150°C. This temperature is not high enough to result in the loss of any feed components, and the primary concern was the integrity of the plastic buckets.

A general overview of the method of operation (not including furnace start-up) is given here. The 5-gallon pails of feed were added to the bulk material feeder hopper as needed to maintain the mass of material in the feeder between 50 and 150 lb. The rate of feed was locally controlled at the bulk material feeder, and the position of the electrode was adjusted through the computer control interface to maintain the appropriate test conditions as described in Section 4.0 of this report. Glass was poured at the start and end of each test segment to ensure that there was no net accumulation of glass in the furnace during the test segment, and periodically poured as required to maintain the appropriate level in the furnace. The baghouse was also blown-back at the start and end of each test segment to allow collection of all baghouse solids generated during the segment. Sampling of the streams is described in Section 4.3.3 of this report.

4.3.2 Data Collection

Most of the data from the furnace was collected and logged by the data acquisition and control system that has been previously described. A list of all logged data points was provided in Appendix A. The historical data files were downloaded from the control computer at the completion of the test and converted to Microsoft Excel format, which allows easy analysis and graphing of the data. In addition, a number of data points were logged manually. These included instruments that did not have electronic output (flowmeters, pressure gauges, liquid levels, electrode positions, etc.), as well as logged data points

that were important for the operators to regularly monitor. This information was recorded hourly on data sheets. Data sheets were also used to record pertinent data from feed additions to the bulk material feeder and from every glass pour.

4.3.3 Sample Collection

Glass samples were taken by inserting a graphite boat (a block with a hollowed out depression) into the glass pour stream until filled. This sampler is identical to those that have been used extensively on other vitrification systems at PNNL. Samples were taken at the start, middle, and end of each test segment. The sampled glass was allowed to cool before being removed from the system and placed in a sample bottle.

Off-gas solids were collected by blowing back the baghouse, which knocked the accumulated solids off of the bags and down into the collection can. The baghouse was blown back at the start and end of each test segment; the solids collected at the end of each segment were retained as the sample for that segment.

Off-gas grab samples for gas analysis were periodically taken by pumping a slip-stream of the off-gas into gas sampling bags. Particulate sampling of the off-gas stream was performed using the equipment described in Section 3.7, using an approach similar to EPA Method 29 sampling (CFR 40 Part 60, Appendix A, Method 29—Determination of Metals from Stationary Sources). The off-gas line from which the samples were obtained was 4-in schedule 40 pipe. Because of the small line size, the type S Pitot tube and the sample nozzle were not co-located. Because of the configuration of the system, the pitot tube was placed over eight pipe diameters upstream of the sample point. The amount of material deposited on the pitot tube during operations was minimal, and thus, pitot tube performance was not affected. The probe was sealed to the line using a close-fitting plug, and the system was operated with only about 0.04 in. Hg vacuum at the sample point to minimize inleakage to the off-gas line at the sample point. Rather than attempt a traverse within such a small line, the sample probe was positioned at the approximate center of the line. The sample nozzle sizes used were 0.313 and 0.375 in. in diameter.

Only particulate data was obtained during sampling. The impingers were filled with water and were not analyzed at the conclusion of the test. After the first sampling, a nozzle and probe rinse was visually determined to have negligible solids. A small amount of solids was noted in the bend preceding the filter housing for some samples. This material fell onto the filter during disassembly of the filter housing and was included in the filter sample. Glass fiber filter papers, 110 mm in diameter, were used to collect the samples. The glass filter housing resulted in formation of deposits in an area approximately 100 mm in diameter. However, some leakage to the edge of the filter paper was noted in the deposition pattern of most filters. The filters were weighed before and after sample collection to determine the aerosol mass collected.

4.3.4 Analytical

Elemental analyses were performed by inductively-coupled plasma atomic emission spectroscopy (ICP/AES). Samples analyzed by ICP/AES must first be dissolved completely into solution. Acid

soluble compounds (some of the feed chemicals) were dissolved in concentrated nitric acid (heated if necessary) and diluted into 2% nitric acid to concentrations suitable for analysis. Most other materials were dissolved according to ASTM Procedure C1317-95, "Dissolution of Silicate or Acid-Resistant Matrix Samples." The sample of material was ground until it passed through a 200-mesh (74 μm) sieve. A portion of the ground sample was then fused using either potassium hydroxide in a nickel crucible, or sodium peroxide in a zirconium crucible. Both fusions were performed for all samples to allow determination of all four of these elements and to provide replicate analysis of all other elements. The fused samples were dissolved in HCl and diluted in 2% nitric acid prior to analysis.

The TCLP was slightly modified from the standard Method 1311. The major difference in the procedure used in these tests was a reduced sample size (5 g versus 100 g) in order to minimize waste generation. Additionally, experience has shown that the preliminary evaluation for any reasonably durable glass will show that the TCLP extraction fluid #1 (pH 4.93) should be used; therefore, the preliminary evaluation to determine the appropriate extraction fluid is usually omitted for glass samples.

4.4 Operating Performance

4.4.1 Furnace Restart

Prior to startup, the DC arc restart equipment was readied as described in Section 5. Approximately 8 kg of carbon steel nails were added on top of the residual frozen glass in the furnace. Next, the weights, on the ends of the 1/4 in. cables, were lowered so they were in contact with the nails. The DC power supply was started and continuity was checked before and after switching in the restart circuit. At this time it was discovered that enough continuity existed through the graphite hearth such that the restart circuit was not required. Therefore, the furnace was started without having to use the special set up. However, subsequent tests with deeper frozen glass levels are expected to require the restart circuit until continuity to the hearth is achieved. Consequently steel rods were inserted into the molten glass shortly after the furnace was shutdown to provide a conductive bridge to the hearth for the next furnace restart.

4.4.2 Operational Overview

The furnace startup and operation for the first test campaign in the engineering-scale furnace was completed during the week of April 6 and lasted approximately 6 days—144 hours of continuous operation. Figure 4.1 shows an event summary for the entire campaign.

The furnace preparations for start up were followed from the Safe Operating Procedure. As part of the preparations for start up, air and water cooling flows were started to the system. The nitrogen purge to the back side of the furnace's graphite hearth was also started. Next, the overflow section resistance heaters were used to ramp up the temperature in that section of the furnace at approximately 100°C per hour. By 0300 on 4/7/97 the temperature in the overflow section had reached over 500°C. At this time nitrogen flow was added to the plenum, via the electrode positioner enclosure, at 17 SCFM and the

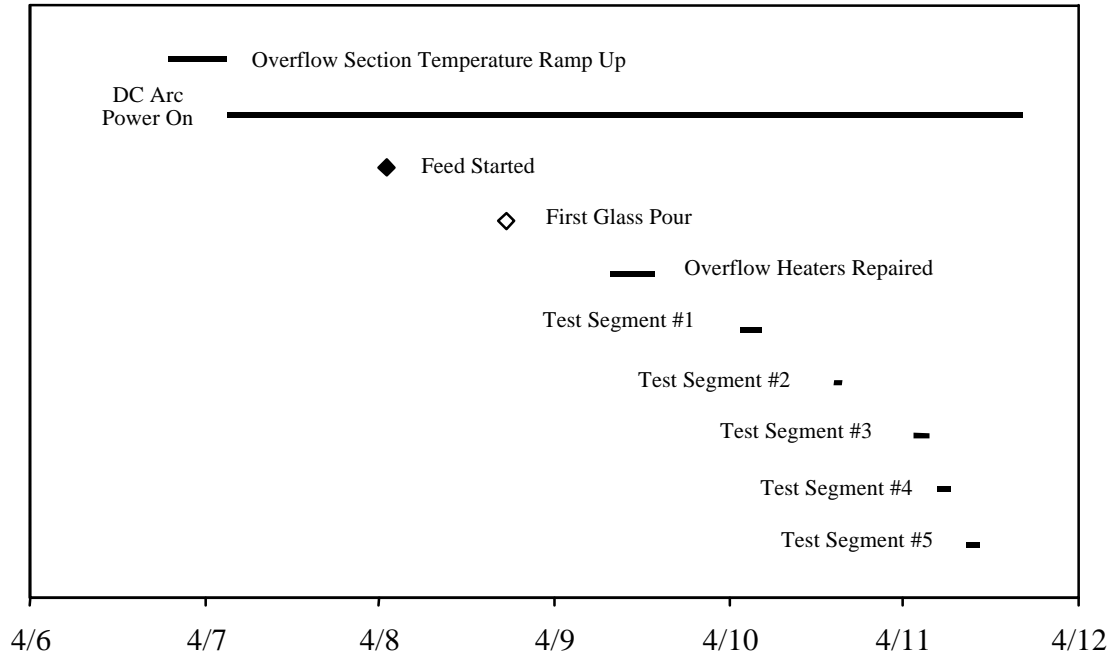


Figure 4.1. Campaign #1 Event Summary

off-gas blower started. Also at this time DC arcing was also initiated. Enough continuity existed from the electrode, through the residual slag, to the hearth that the restart circuit was not required.

A plot of the furnace DC power over the course of the run is shown in Figure 4.2. As seen in this plot, the first 7 hours of arc operation experienced erratic DC voltage behavior. The plenum vacuum was increased to -0.5 "wc to better force the nitrogen flow down the shaft of the electrode. Once this adjustment was made, the arcing potential and current stabilized to approximately 40 volts and 150 amps. The DC arc power was gradually increased over the next few hours. The plenum temperature also increased correspondingly with furnace power. Figure 4.2 also shows plenum temperature, as well as cumulative feed rate, over the course of the test.

The EVS was started at 2235 on 4/7/97 when the off-gas temperatures at the EVS had increased to over 100°C. A plot of the temperatures before (Post Film Cooler) and after the EVS are shown in Figure 4.3. Also shown in this figure is a plot of the post-HEPA temperature, which was elevated to approximately 80°C using the off-gas heater. By the time the EVS was started, the pressure drop across the bag house had increased from around 1 "wc to 4.4 "wc because of the buildup of a gray-colored dust. This was assumed to be from the residual material in the furnace from FY 1996 testing. A bag house blow down sequence was run and the pressure drop across the unit decreased back down to 1 "wc. This sequence was repeated throughout the test whenever the pressure drop across the bag house reached 4 "wc. The frequency of these blow downs was approximately once every 2 to 3 hours.

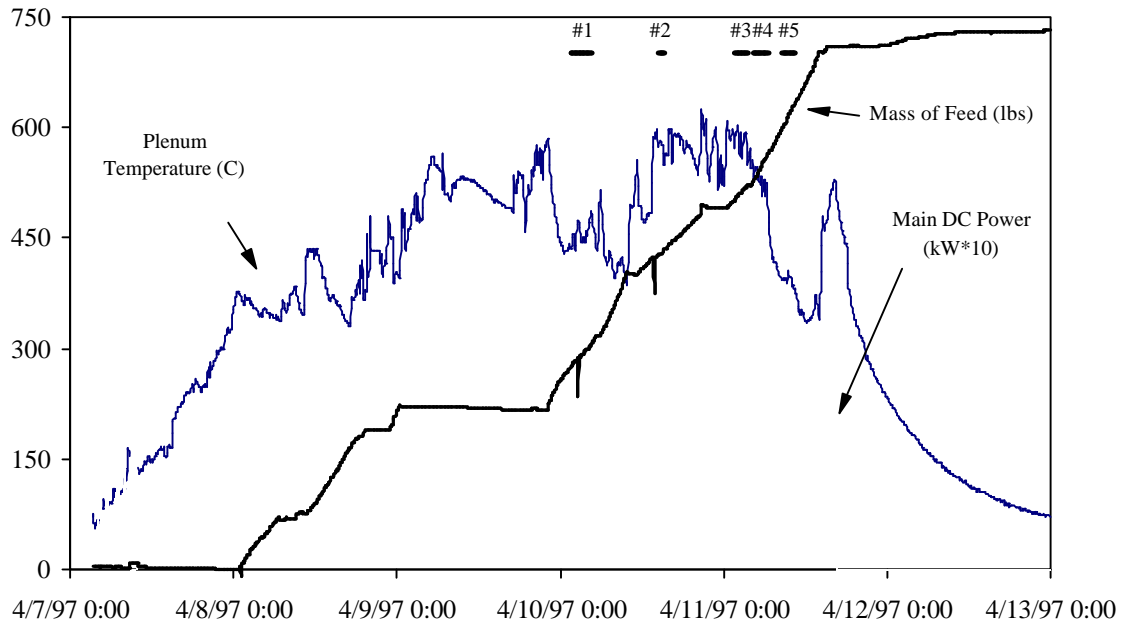


Figure 4.2. Main Furnace Plenum Temperature and DC Arc Power Data

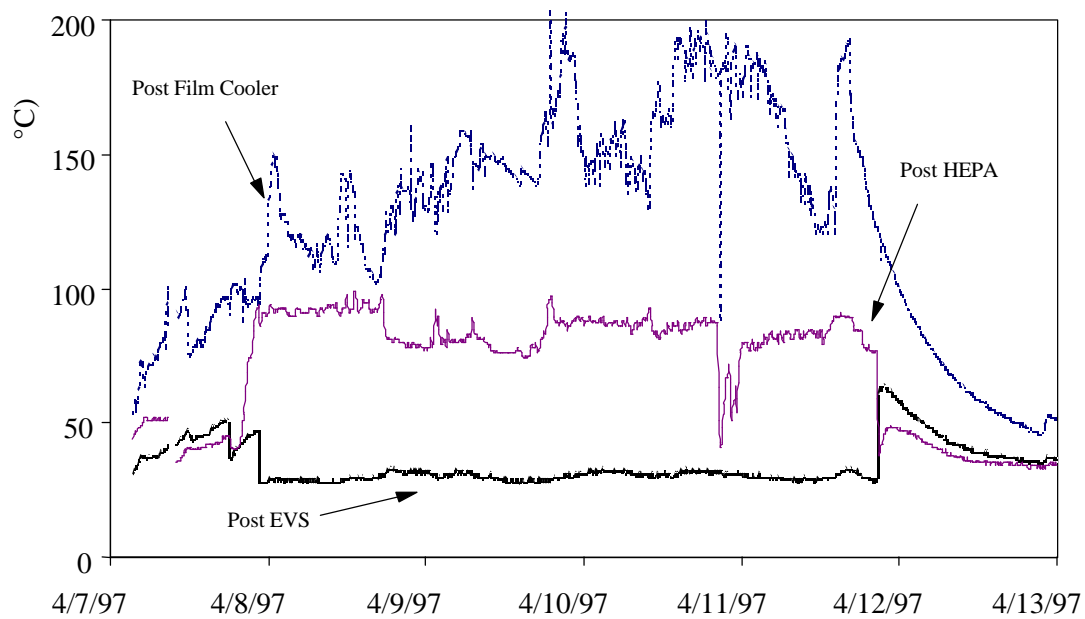


Figure 4.3. Measured Off-Gas Temperatures During Campaign #1

By approximately 0000 on 4/8/97 the DC arc power was operating steadily at 15 kW and the corresponding plenum temperature was at approximately 350°C. A substantial pool of molten material was visible in the furnace via the remote camera. This material was assumed to be glass/slag from the FY 1996 testing with the heavier metal, added prior to the test, having sunk underneath. This assumption

was substantiated by the fact that the graphite electrode was submerged within this molten material, yet the DC potential was still greater than 50 volts. If the molten pool had been primarily metallic the DC potential could not have been this high without arcing above the surface. Based on the conditions of the furnace at this time the solids auger was loaded and feeding to the furnace begun. Later in the campaign the plenum temperature was used as an operating parameter for feed rate determinations. However, during the first part of the campaign the rate of feed addition was controlled primarily by the appearance of the furnace melt, as seen by the remote camera. The feed was added so that a portion of the melt was in view at all times. Too high a feed rate during this point of operation could have cooled the molten material underneath too quickly, disabling the power input. During this time the electrode was kept submerged in the glass with no visible arc above the surface. Less than an hour after feeding was begun, convection currents in the molten glass underneath were visible as well as some bubbling up to the glass surface.

By 1500 on 4/8/97, the overflow section temperature had been increased to 1400°C in anticipation of the first glass pour. Figure 4.4 shows a plot of the overflow section temperature over the course of the campaign, along with the total power input to the resistance heaters. Also, by 0500 on 4/8/97, the furnace was estimated to be full enough (over 150 lb of glass) that pouring was imminent. A vacuum of 2 "wc was kept on the overflow section to assist the pour. At 1715, a 1/8 in. to 1/4 in. diameter glass stream began pouring from the furnace. This pour lasted for approximately 10 minutes before the pour stream diameter decreased to allow the formation of glass "hair" (small diameter, rapidly cooled glass) in and above the glass receipt canister. Pouring was stopped by reducing the vacuum on the overflow section and this "hair" was knocked into the overflow can by the glass sampler.

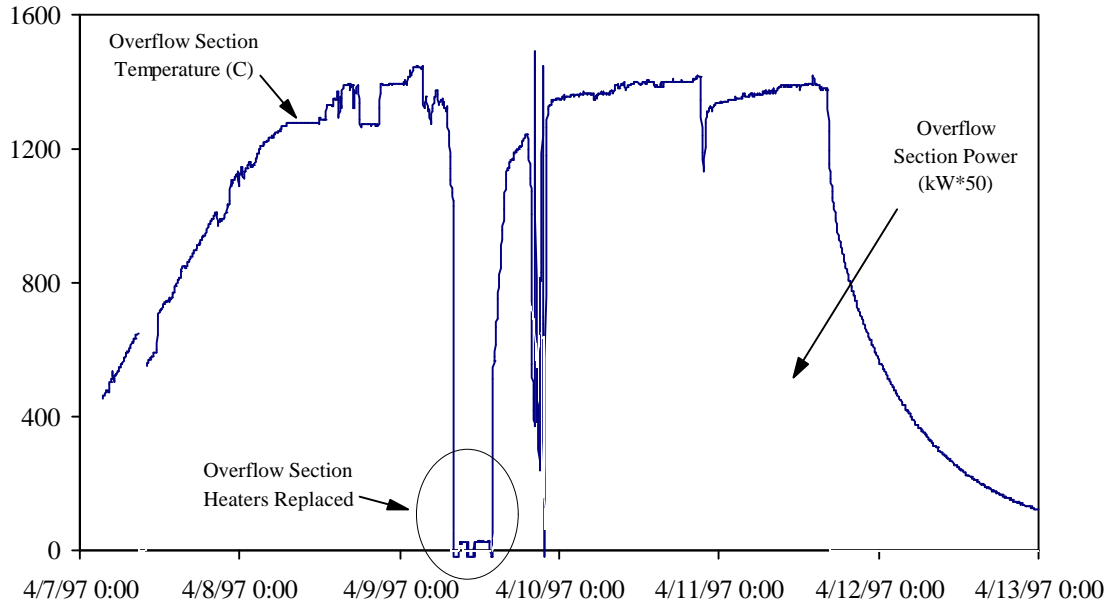


Figure 4.4. Overflow Section Temperature and Power Data

Shortly after the first glass pour, a metal stream spontaneously poured from the furnace bottom drain, even though no induction heating was being applied to the drain. Once the metal had poured (23 lb in a matter of seconds), glass entered the upper hole and rapidly solidified to form a plug. The bottom drain hole was sized (1/2 in. in diameter) to have this very effect. The initial pour of metal was assumed to be a result of an empty bottom drain hole. Since glass now plugs the hole, no future pouring through the bottom drain is likely without inductively heating the drain assembly.

For three hours following the first glass and metal pours, a noticeable change in the furnace operating current and potential occurred. The current decreased from nearly 300 amps to 100 amps and the potential increased from 80 to 110 volts, with no changes on the power supply settings. Furthermore, when the power supply settings were changed to increase output, there was no substantial effect on the current or potential. This behavior suggested a change in the load resistance. A previous test with the same feed material in the bench-scale DC arc furnace had shown a similar phenomenon; however, when a second test was performed with the same feed but with carbon steel shot added to the hearth at the beginning of the test, no unusual behavior was observed. Based on that experience, it was reasoned that, since glass does not wet graphite, molten metal is needed to provide a good conductive path between the molten glass and the melter's hearth. Therefore, approximately 4 lb of carbon-steel shot were fed into the furnace. Indeed, within minutes of adding the metal to the furnace the current increased to nearly 250 amps and the potential lowered to just under 100 volts. Due to oxidation and subsequent losses into the glass phase, periodic metal additions (around 2 lb each) were required throughout the test campaign when the current dropped substantially. In total, approximately 20 lb of carbon-steel shot were added to the furnace. Figure 4.5 shows the DC arc potential and currents plotted over the course of the campaign with each of the metal addition occurrences identified. Note that each addition of metal followed a drastic drop in current, which was remedied shortly after the addition.

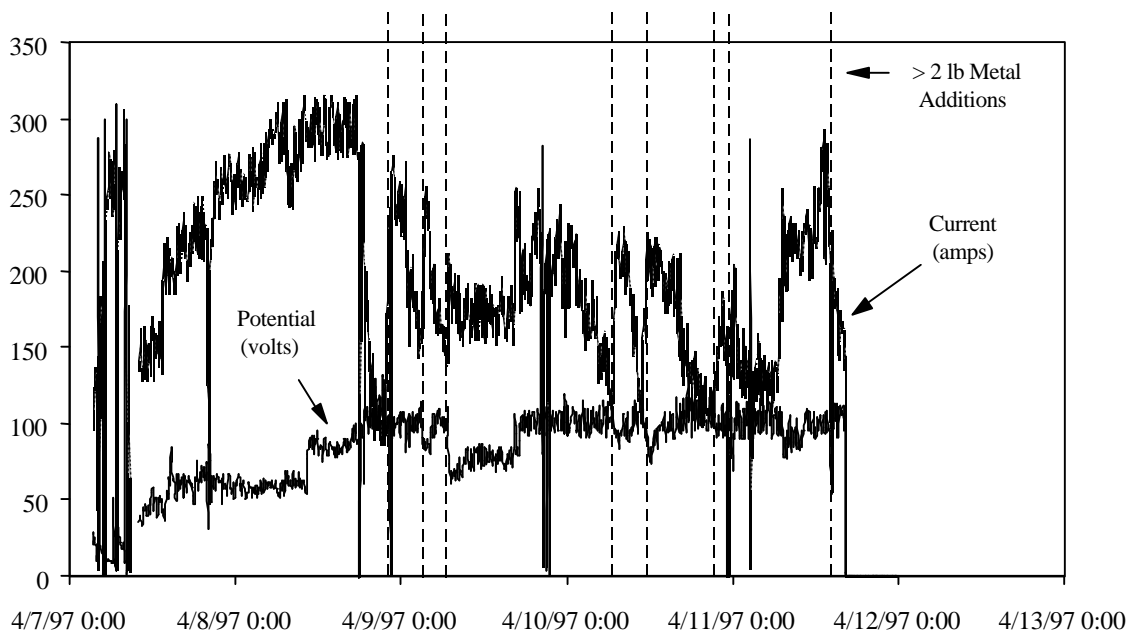


Figure 4.5. DC Arc Potential and Current Data with Metal Addition

Feeding and glass pouring continued for 8 hours following the first glass pour. During this time, problems began appearing with the overflow section heaters. An intermittent, short across the silicon-carbide heaters would periodically trip the power supply, resulting in difficulty maintaining the target temperature. Therefore, the power to the heaters was turned off and they were replaced. This replacement period is identified in Figure 4.4. Upon removal, an arc score, which may have been due to a manufacturing defect, was visible on one of the heaters. Once the heaters were replaced and the overflow section reheated to 1400°C (taking a total of 12 hours, between 0600 and 1800 on 4/9/97) feeding and glass pouring were resumed. Figure 4.6 shows a plot of the feed rate over the entire test campaign. Note that the steady feeding segments in this figure show average rates ranging from 4 to 10 kg/hr.

A photograph of the overflow section view port during a glass pour is shown in Figure 4.7. This pour shows a stream of approximately 1/8 in. - 1/4 in. in diameter. This size of pour stream only occurred during the first part of each semi-batch pour. Toward the end of the pour the stream diameter would decrease, forming rapidly-cooled glass “hair” in the overflow section. A larger system, with higher feed rates and glass pour rates, would not be as prone to this problem. If a continuously poured glass stream corresponds to a high enough mass flow, the stream diameter will stay large and won’t freeze as it pours. However, for systems the size of the engineering-scale furnace, glass must be poured in a semi-batch mode, using the vacuum-assisted gravity overflow, in order to maintain a sufficient pour stream flow to ensure the glass stream remains molten in the overflow section’s spellway. The reason for some glass hair buildup in the first test campaign was that the vacuum supply to the overflow section was not great enough. This resulted in more frequent, shorter-duration, glass pours with, correspondingly, more small streams at the end of each pour. The vacuum source to the overflow was increased at the end of the first test campaign to remedy this problem in the next tests.

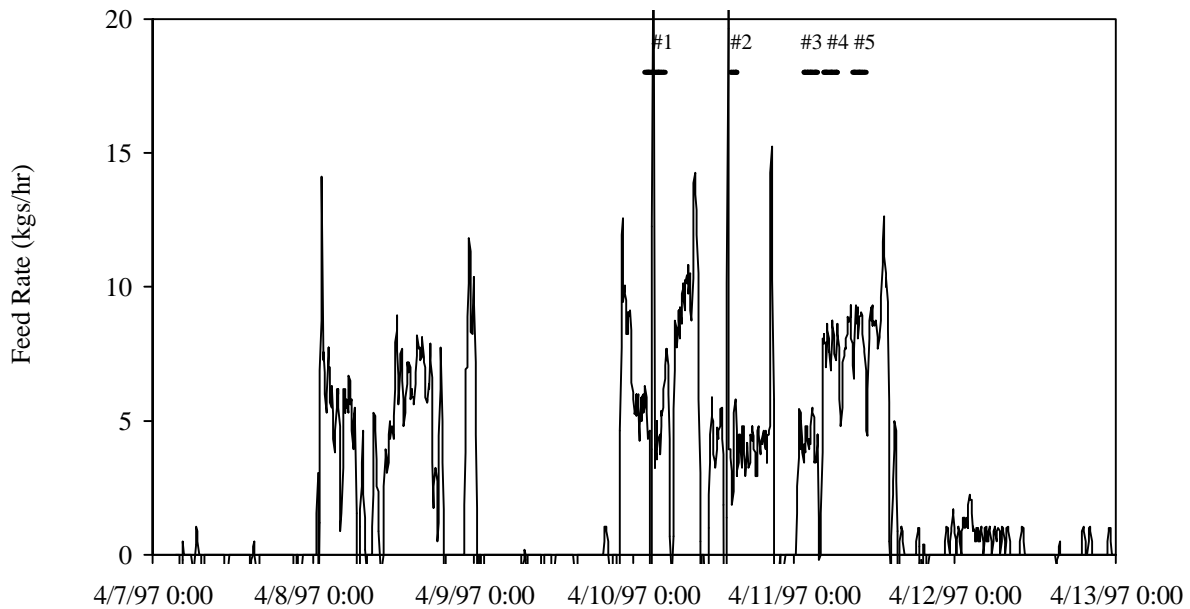


Figure 4.6. Measured Feed Rates During Campaign #1

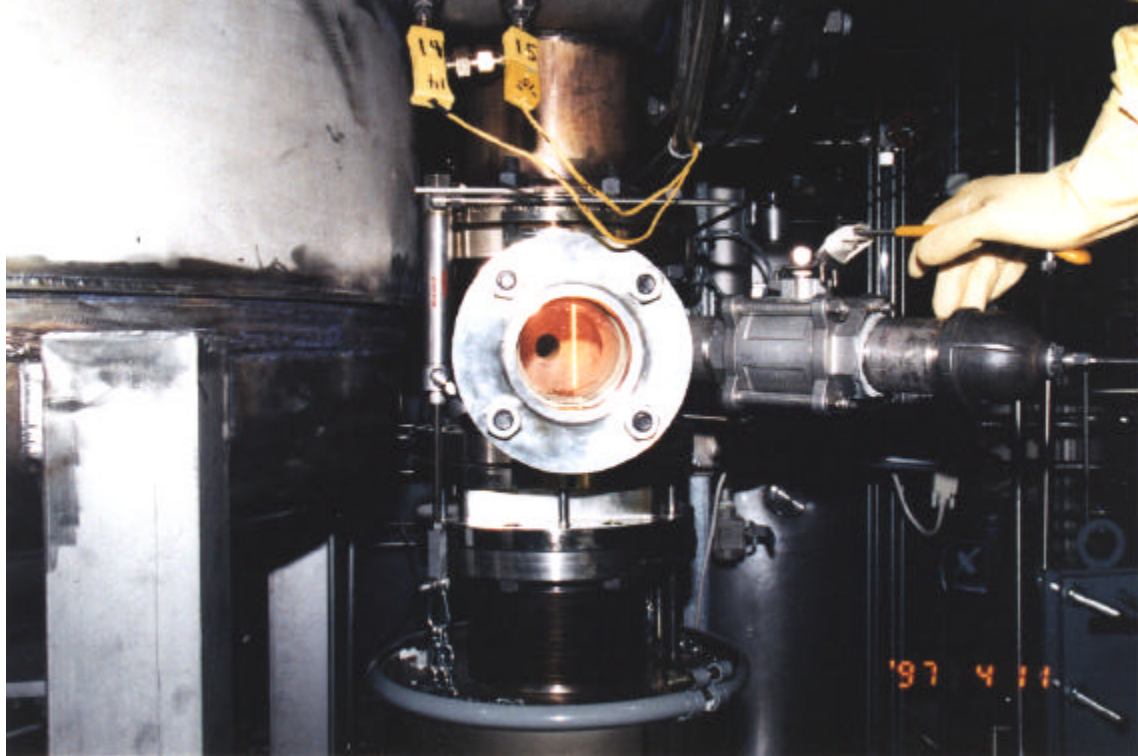


Figure 4.7. Glass Pour from Furnace Overflow During Campaign #1

4.4.3 Test Segment Descriptions

Prior to each test segment, glass was transferred from the furnace to reduce the melter's glass inventory to a minimal level, and the feed auger hopper and overflow canister weights were logged. Also, the bag house filter was blown down and all of the solids removed from the receipt drum. Prior to completing each segment, glass was poured from the furnace, post feed hopper and glass canister weights were logged, and the bag house was blown down and the collected solids removed and stored. Glass samples were taken before and after each test segment, as well as during each segment, depending upon its duration. Gas aerosols were measured for each test segment using a modified Method-29 procedure and hardware. These measurements lasted about 1 hour.

The conditions for the first segments were a submerged electrode (in the glass) and varying coverages of feed over the glass surface. This coverage is critical since it can affect the amount of volatilization of constituents to the off-gas. However, assessing the amount of glass surface coverage with feed can be difficult since the view port into the furnace has a limited field of view. Therefore, the plenum temperature was used to give a relative indication of the extent of coverage. The first test segment operated with a plenum temperature of approximately 455°C. This plenum temperature corresponded to a glass coverage of greater than 50%. The second test segment operated with a plenum temperature increased to approximately 570°C and a correspondingly lower glass coverage. The third and fourth test segments operated at plenum temperatures of 582°C and 526°C, respectively, but with the electrode

pulled up out of the glass to give an exposed arc. The final test consisted of resubmerging the electrode into the glass and operating at a maximum glass coverage. The plenum temperature during that segment averaged less than 400°C.

Figure 4.8 shows four still-shot photographs taken from recorded video during four of the test segments. This video was taken using a CCD camera mounted above the furnace lid view port. A gas welding optical filter was placed between the camera and the view port glass to reduce the glare of the arc. The top two photographs in Figure 4.8 show glass surface conditions when the electrode was submerged in the glass with high (left) and low (right) feed coverages of the glass. The two bottom photographs in Figure 4.8 show the glass surface conditions, again for high (left) and low (right) feed coverages of the glass, when the electrode and arc were exposed to the furnace plenum. As indicated by these photographs the exposed-arc segments, would be expected to produce substantially more activity in the furnace plenum than the submerged-arc segments. During these segments operators noted glass droplets flung from the arc zone and hitting the surrounding side walls of the furnace plenum.

Table 4.3 shows a compilation of the operating performance data from each test segment. The time and durations of each test segment, as well as the total masses of feed fed, glass poured, and solids collected in the off-gas are shown in this table. Additionally, averages of power, plenum temperature, feeding and glass pouring rates are shown.

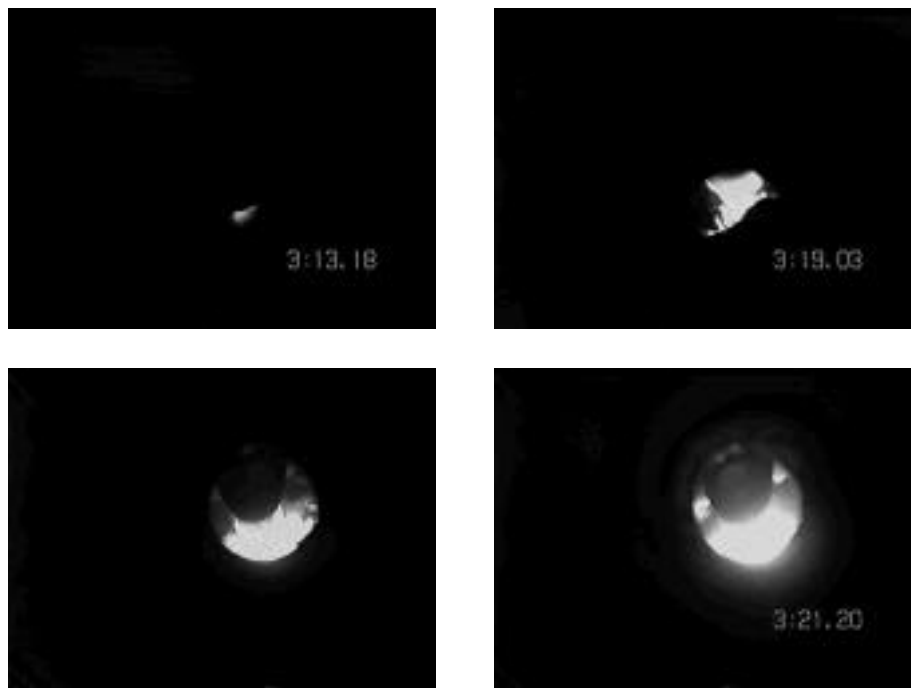


Figure 4.8. Photographs of Glass Surface Conditions During Testing (top left: submerged arc and high coverage of glass with feed, top right: submerged arc and low glass coverage, bottom left: exposed arc and high glass coverage, bottom right: exposed arc with low glass coverage)

Table 4.3. Processing Information for Each Test Segment

Test Segment Number	0	1	2	3	4	5
	Idle	Submerged Arc, Medium Glass Coverage	Submerged Arc, Low Glass Coverage	Exposed Arc, Low Glass Coverage	Exposed Arc, High Glass Coverage	Submerged Arc, High Glass Coverage
Test Segment Values:						
Date	4/9/97	4/10/97	4/10/97	4/11/97	4/11/97	4/11/97
Start Time	0100	0130	1428	0130	0430	0835
End Time	2200	0430	1528	0330	0630	1035
Duration (hours)	21.0	3.0	1.0	2.0	2.0	2.0
Feed Fed to Furnace (kg)	0.0	13.8	3.7	8.8	15.8	16.5
Glass Poured from Furnace (kg)	0.0	9.9	1.4	6.5	11.6	7.6
Solids Collected in Baghouse (g)	Not Measured	198	73	201	366	173
Gross Carryover to Off-gas (wt%)	Not Measured	1.4%	2.0%	2.3%	2.3%	1.0%
Average Test Segment Values:						
Power Consumption (kW)	16.2	17.3	18.6	13.5	13.5	20.2
Feed Rate (kg/hr)	0.0	4.6	3.7	4.4	7.9	8.3
Plenum Temperature (°C)	516	455	570	582	526	391
Glass Pour Rate (kg/hr)	0.0	3.3	1.4	3.2	5.8	3.8
Energy Input (kW-h/kg glass)	Infinite	4.2	5.6	3.5	1.9	2.7
Film Cooler Injection Flow (SCFM)		59	61	61	61	61
Post Film Cooler Flowrate (SCFM)		93	96	100	99	102
Gas Flow Out of Plenum (SCFM)		35	36	39	37	41
N ₂ Flowrate into Plenum (SCFM)		17	19	19	19	19

Typically, each test was designed to, at a minimum, feed an amount of material equivalent to four glass inventories. The individual test durations for the present effort were approximately one quarter of this. Primarily the shorter test durations impact the ability to generate steady-state glass compositions.

The data in Table 4.3 show that the test segments with the highest solids carryovers (shown as the percentage of baghouse solids from the given feed mass) were the exposed-arc segments. Indeed, those segments exhibited greater activity in the furnace plenum compared to the submerged-arc segments. Similarly, the gross carryover values appear to increase with the less coverage of glass with feed in the submerged-arc segments. A corresponding trend of higher plenum temperatures and activity was also observed for the low glass coverages in those segments.

The power consumption values in Table 4.3 are distinctly different between the submerged and exposed-arc segments. The exposed-arc segments show power consumption values of 13.5 kW, compared to over 17 kW for the submerged-arc segments. Despite this difference in power, consumption the exposed-arc segments processed feed at or above the rates in the submerged-arc segments. Although

this trend seems counter intuitive at first, it is assumed that the exposed-arc segments concentrated the power more directly into the feed material on the top of the glass. Conversely, the submerged-arc segments relied on heat transfer through the glass into the feed material, thereby increasing the bulk glass temperatures and heat losses to the surrounding refractory. Note that the suspected lower bulk glass temperatures in the exposed-arc segments were not low enough to affect glass pouring or total melt electrical resistance.

The power consumption per unit glass mass values in Table 4.3 were calculated based on the measured feed rates and loss on firing value (10.9%). These values ranged from 3 to 6 kWh/ kg of glass. The highest measured power consumptions were from the submerged arc segments. The lowest consumptions were from the exposed arc segments. This data substantiates that more heat losses were realized during the submerged-arc tests.

A comparison of the feed masses fed with the glass produced from each test segment was next made using the data in Table 4.3. This comparison is shown in Figure 4.9.

Figure 4.9 shows that all but two of the test segment data points fall on a straight line with a slope of 0.73. This slope is significant as it depicts the mass fraction of glass from a given mass of feed. Recall that laboratory assessments showed this ratio to be 0.89. Consequently, at least 16% of the feed mass is unaccounted for in Figure 4.9. Since Table 4.3 showed gross solids carryovers to the off gas of less than 3%, error in the feed or glass measurements are expected. Since many of the test segments were short in duration (less than 2 hours) the glass masses are assumed to be more suspect than the feed masses. Small accumulation factors within the furnace would account for the suspected error in the measured glass rate values. Additionally, problems encountered when measuring the poured glass mass after each test may also have affected the accuracy of those values.

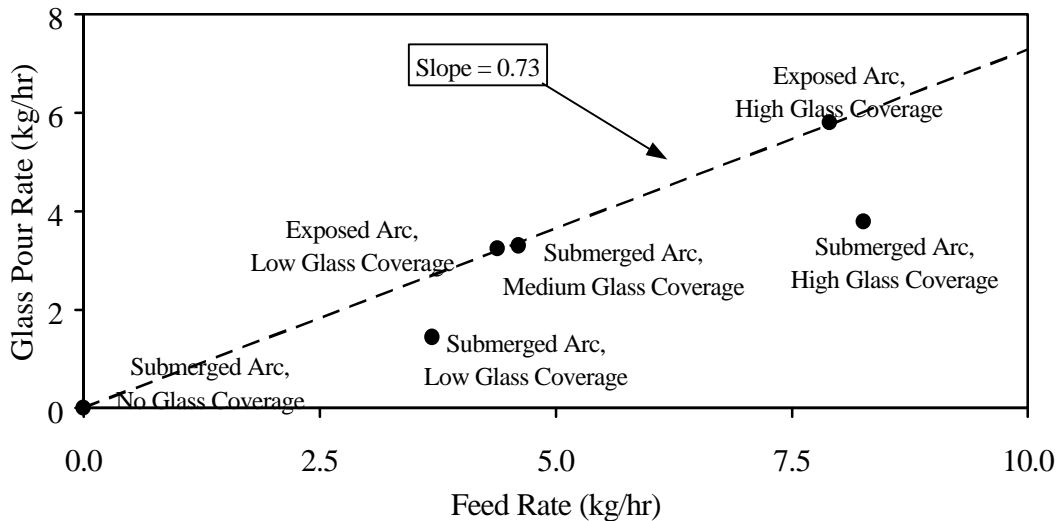


Figure 4.9. Glass Versus Feed Production for Each Test Segment

The flow rates given in Table 4.3 show the post film cooler flows, the point of aerosol sampling, to be around 100 SCFM. Approximately 60% of this flow was from the film cooler injection air. Correspondingly, 40% (or around 40 SCFM) of the flow came from the furnace plenum area. Table 4.3 shows that about one half of this flow was nitrogen introduced into the furnace plenum. As a result, the gases generated from the feed, along with inleakage, only constituted approximately 20 SCFM of the total flow into the off-gas system.

4.4.4 Post-Test Furnace Inspection

Inspections of the furnace and ancillary equipment were made once the test campaign was completed and the furnace had cooled. The primary areas of interest were the interior of the furnace, electrode positioner, hearth side busses, bottom drain, overflow section, internals of the baghouse, and the HEPA filter. The observations of each of these areas are discussed in the following section.

An access plug was removed on the top of the furnace to reveal the furnace plenum area. The surrounding side walls of the plenum had a 1 in. thick accumulation of spattered glass. The majority of this accumulation is suspected to have occurred during the exposed-arc test segments. Additionally, a dusting of unmelted feed material was observed on the surface of the cooled glass. This material is suspected to have fallen from the auger hopper after the furnace had been shut down. No refractory cracking or degradation was observed.

The electrode feeder/positioner was inspected for any obvious electrical arc scores or discoloring on the contact brushes or rollers. No problems were observed. Additionally, each of the four side graphite busses, which contact the graphite hearth, was inspected. Here, substantial oxidation of portions of each buss was observed. This bus exhibiting the worst oxidation is depicted in Figure 4.10.

As depicted in Figure 4.10, the graphite oxidation was severe enough that three of the four busses no longer contacted the graphite hearth. The reason for the oxidation was determined to be inadequate bake-out of the castable refractories inside the furnace. The predominant portion of the furnace refractory was cast into the furnace in a slurry form, much like concrete. The bound water in these refractories typically requires a substantial “bake-out” scheme to be released. Such a scheme was performed on the furnace; however, some residual water was still present in the refractories. During the test campaign small amounts of water were found to be accumulated in the side bus access ports. This water only began accumulating after molten-glass temperatures inside the furnace had been reached. The open penetrations through the castable refractory to the hearth provided a void where the water vapor accumulated. This water vapor then oxidized the graphite busses.

To properly dry melter refractories, the temperature of the entire melter needs to be raised to the bake-out value. Accomplishing this would require the melter with appropriately designed weep holes to be totally immersed in a large bake-out oven. Since this was not possible for a melter already situated in a radiologically controlled area, design features were employed to mitigate the recognized problems

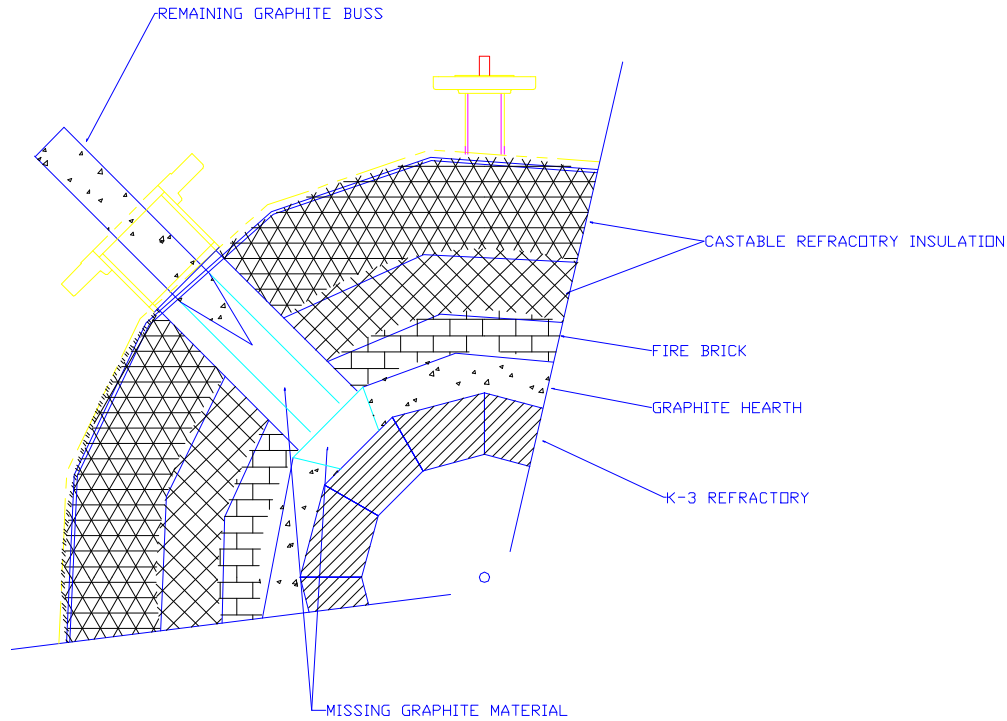


Figure 4.10. Observed Side Bus Oxidation

resulting from uncured refractories as were discussed in Section 3.11. Fortunately, the oxidation of the side busses were easily repaired after the April 1997 test using a moldable graphite clay and new graphite busses.

Both the bottom drain and glass overflow section of the melter appeared as they did when constructed. The filter bags in the baghouse were also undamaged. The HEPA filter was slightly darkened upon observation but had no other signs for needing replacement.

4.5 Energy Balance

Figure 4.11 summarizes an energy balance performed on the engineering-scale arc furnace during the first test campaign. The values used to perform this balance were averaged over the 30-hour testing period following 0500 on 4/10/97.

The average total power input from the DC arc and overflow section was 28.5 kW. A total of 9.1 kW were determined to be removed via the various cooling water and air streams. Additionally, an average of 6.3 kW were removed via the furnace off gas. The power transferred to the poured glass was approximately 3.3 kW. This value was estimated by using an assumed enthalpy change of 2.7 K joules per gram of feed and is based on a temperature increase of 1375°C. Note that a relatively small amount of the input power, less than 12%, was retained in the poured glass. A larger furnace with a, correspondingly, larger glass cavity is expected to have a higher percentage of the input power in the poured glass.

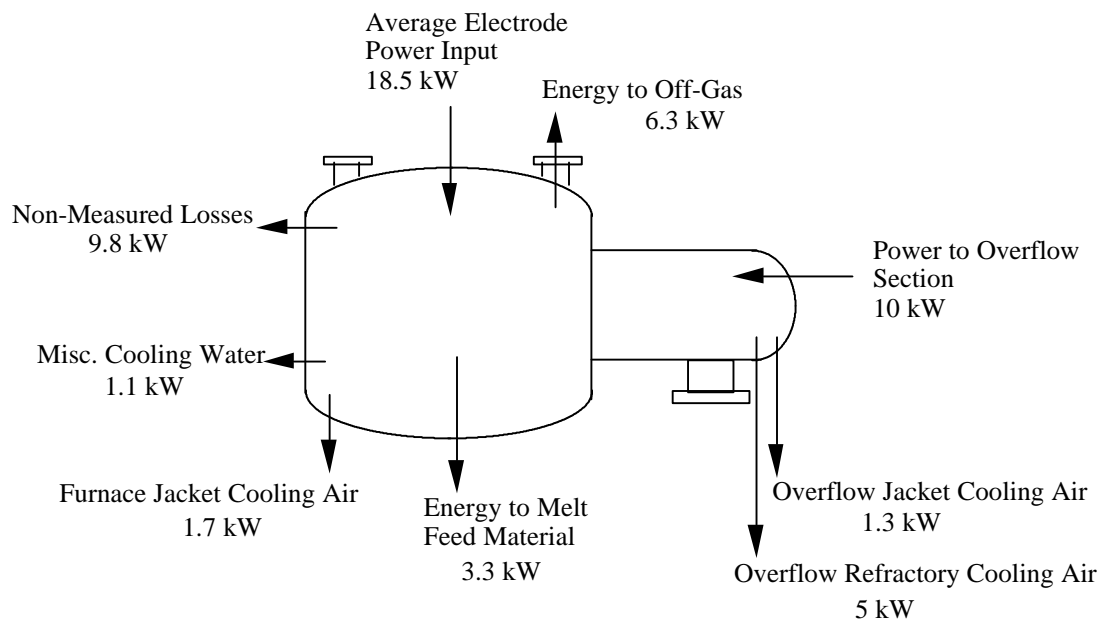


Figure 4.11. Energy Balance Summary

The “non-measured losses” in Figure 4.11 were determined by subtracting all of the other output power values from the sum of the input power values. The result of this calculation was 9.8 kW. The primary path for these losses was from the un-jacketed portions of the furnace (lid, bottom, penetration flanges, etc.). Figure 4.11 shows that the overflow section refractory cooling circuits pulled a total of 5 kW from those locations. This value was nearly 50% of the total power added to the overflow section. Since no unwanted glass migration was observed in the overflow section refractories, and glass was still poured from that section, its design criteria of those coils appears to have been achieved.

4.6 Off-Gas Analyses

Samples of the baghouse solids collected during each of the test segments were analyzed for total metals as described in Section 4.3.4 of this report. Table 4.4 presents the results of these analyses on an elemental basis. A comparison to the elemental composition of the feed shows that the off-gas solids are enriched in the volatile components, most notably silver, cadmium, and lead. Further analysis of the partitioning of the metals to the off-gas is provided in Section 4.8 of this report.

On-line monitoring equipment was not used for non-condensable gas analysis. However, several off-gas grab samples were obtained and analyzed using a Finnigan MAT-271 quantitative mass spectrometer. Analyses of these samples are summarized in Table 4.5. In all runs, the gas analysis failed to detect NO_x at a detection limit of 50 ppm or CO at a detection limit of 100 ppm.

Table 4.4. Elemental Composition of Collected Baghouse Solids (wt% Element)

Element	Test Segment					Batched
	1	2	3	4	5	Feed
Ag	0.56	0.51	0.45	0.34	0.50	0.10
Al	2.66	2.32	2.10	1.98	2.34	4.53
Ba	0.09	0.07	0.07	0.06	0.07	0.17
Ca	22.32	19.51	18.01	18.00	22.53	16.66
Cd	2.11	3.80	2.83	2.96	3.19	0.10
Cr	0.30	0.27	0.27	0.28	0.26	0.10
Fe	1.43	1.46	1.72	1.64	1.39	2.27
K	2.11	3.15	5.41	5.50	2.55	1.63
Mg	0.79	0.72	0.66	0.66	0.71	1.11
Mn	0.03	0.03	0.04	0.04	0.03	0.05
Na	0.71	1.49	2.60	2.28	0.98	0.67
Nd	0.66	0.59	0.52	0.54	0.67	0.35
Ni	0.28	0.27	0.26	0.27	0.25	0.10
Pb	1.87	3.30	2.46	2.65	1.83	0.10
Si	13.68	12.56	14.04	14.32	13.50	21.90
Sr	0.03	0.03	0.03	0.03	0.03	0.04
Ti	0.17	0.15	0.13	0.13	0.15	0.28
Y	0.29	0.28	0.27	0.27	0.30	0.24
Zr	0.34	0.33	0.34	0.31	0.30	0.23

Table 4.5. Mass Spectrometer Analysis of Off-Gas Grab Samples

Test Segment	N ₂ Mole%	O ₂ Mole%	Ar Mole%	CO ₂ ppm	H ₂ ppm
1	82.2	16.8	0.75	1930	110
2	82	17.1	0.76	1850	6
3	81.3	17.8	0.79	1390	<5
4	80.9	18.1	0.8	1920	7
5	77.9	21.1	0.94	390	<5

4.7 Slag Analyses

Thirteen samples taken from the slag pour stream at intervals throughout the test were analyzed for total metals as described in Section 4.3.4 of this report. Table 4.6 reports the results of these analyses normalized to 100 wt% oxide. It can be seen from this table that the composition of the glass was nearly constant throughout the test, which is as expected since the same feed material was used for the entire test. The standard deviations are less than $\pm 5\%$ for most of the elements. The largest variations are seen

Table 4.6. Normalized Composition of Slag Samples from the Engineering-Scale Furnace Test Campaign #1 (wt% oxide)

Oxide	4/10/97 0125	4/10/97 0250	4/10/97 0425	4/10/97 1405	4/11/97 0130	4/11/97 0230	4/11/97 0330	4/11/97 0430	4/11/97 0540	4/11/97 0630	4/11/97 0855	4/11/97 0946	4/11/97 1035	Average (±s)		±%s
SiO ₂	49.4	49.7	49.9	50.3	50.3	49.9	50.4	50.3	50.3	50.3	50.0	50.5	51.0	50.17	±0.4	0.8
CaO	24.1	24.3	24.3	25.1	25.0	25.2	25.0	24.7	24.7	24.7	24.9	24.8	25.2	24.76	±0.4	1.5
Al ₂ O ₃	10.8	10.8	10.8	10.5	10.4	10.5	10.6	10.4	10.3	10.3	10.2	10.2	10.3	10.48	±0.2	2.2
Fe ₂ O ₃	5.72	5.42	5.06	4.54	4.70	4.75	4.74	4.78	4.96	4.89	4.88	5.03	5.05	4.96	±0.31	6.4
K ₂ O	3.29	3.17	3.23	3.22	3.29	3.39	2.94	3.65	3.59	3.66	3.86	3.49	2.35	3.32	±0.38	11.5
MgO	2.19	2.20	2.23	2.17	2.16	2.16	2.18	2.14	2.13	2.13	2.13	2.09	2.10	2.15	±0.04	1.8
Na ₂ O	1.75	1.70	1.69	1.44	1.34	1.40	1.43	1.34	1.30	1.33	1.29	1.22	1.24	1.42	±0.18	12.5
Cr ₂ O ₃	0.696	0.683	0.658	0.607	0.648	0.653	0.640	0.629	0.618	0.612	0.556	0.576	0.588	0.63	±0.041	6.5
TiO ₂	0.511	0.514	0.508	0.521	0.512	0.518	0.515	0.513	0.514	0.512	0.515	0.515	0.522	0.51	±0.004	0.7
ZrO ₂	0.329	0.330	0.337	0.338	0.339	0.341	0.330	0.339	0.342	0.348	0.331	0.347	0.352	0.34	±0.007	2.2
Nd ₂ O ₃	0.412	0.419	0.448	0.443	0.443	0.449	0.468	0.444	0.444	0.447	0.457	0.447	0.441	0.44	±0.014	3.2
Y ₂ O ₃	0.300	0.305	0.305	0.332	0.326	0.329	0.327	0.327	0.328	0.328	0.332	0.333	0.341	0.32	±0.012	3.9
BaO	0.189	0.191	0.190	0.198	0.197	0.200	0.199	0.198	0.198	0.197	0.201	0.200	0.205	0.20	±0.005	2.3
Minor Components																
NiO	0.059	0.060	0.064	0.051	0.055	0.051	0.053	0.060	0.067	0.067	0.080	0.080	0.078	0.06	±0.011	16.7
CdO	0.015	0.017	0.026	0.008	0.021	0.012	0.011	0.013	0.015	0.022	0.019	0.017	0.018	0.02	±0.005	30.5
Ag ₂ O	0.050	0.055	0.059	0.040	0.045	0.030	0.028	0.030	0.031	0.037	0.046	0.044	0.046	0.04	±0.010	23.8
PbO	<0.08	<0.08	<0.08	<0.08	<0.08	<0.08	<0.08	<0.08	<0.08	<0.08	<0.08	<0.08	<0.08			
MnO	0.158	0.156	0.146	0.128	0.119	0.123	0.117	0.116	0.115	0.115	0.108	0.108	0.108	0.12	±0.018	14.2
SrO	0.041	0.042	0.046	0.042	0.042	0.044	0.046	0.042	0.042	0.043	0.043	0.043	0.044	0.04	±0.002	3.8

in the hazardous metal spikes. These metals are present near their detection limits and are expected to have greater error in the measurement. Additionally, the test operating conditions (cold cap coverage, exposed arc) are expected to impact the partitioning of these metals, and hence their concentration in the glass. Sodium, chromium, and magnesium show a downward trend in concentration throughout the test, which results in a slightly higher standard deviation. Potassium is present at near detection limit; hence the higher error in the measurement. The variability in iron is likely a result of oxidation/reduction reactions between the molten glass and molten metal phases.

The actual recovery in the analyses on an oxide basis was typically slightly less than 100 wt% for these samples. The recovered oxide ranged from 89.0% to 100.5% for the potassium fusions and from 97.4% to 99.8% for the sodium fusions. This range is typical for glass samples analyzed by this fusion method. A recovery of less than 100% oxide can result from volatile material in the sample (moisture, carbon, salts), failure to dissolve a particular component of the glass (bias of one or more elements), the presence of non-oxide constituents and/or the failure to dissolve a portion of the sample (uniform bias of all elements). Since these samples are from a slag processed at about 1500°C and the feed did not contain significant amounts of carbon, it was assumed that all volatile materials were lost from the melt and that the sample is 100 wt% oxide.

The low recovery observed in some of the potassium fusions relative to the sodium fusions typically results from the failure to dissolve the more refractory components of the sample. When this is the case, levels of most of the elements are comparable in both the potassium and sodium fusions of the sample, with one or two elements (typically silica) lower in the potassium fusion. In these instances, the sodium fusion is used with the values for sodium and zirconium taken from the potassium fusion. Sometimes, however, the levels of all the elements are proportionally lower in the potassium fusion, which indicates that the low recovery most likely results from failure to completely dissolve the sample (uniformly). In these instances, both fusions are used and the values are normalized to 100 wt% oxide.

The average recovery in all the samples was slightly less than 100%, being 96.4% and 98.2% for the potassium and sodium fusions respectively. As previously discussed, this deviation could be a result of failure to completely dissolve the sample. A comparison of the average glass composition to the batched composition in Table 4.7 shows good agreement in most cases between the average glass composition and the target batched composition.

The iron content in the slag product is significantly higher than the batched value. As previously discussed, a pool of molten metal was required to maintain control of power into the system, so steel shot was periodically added to the furnace. Throughout the test, the addition of more metal was required periodically, indicating that the pool of molten iron was being consumed by the slag melt. A comparison of the slag analyses to the batched composition confirms that the iron content of the slag was higher than expected. The measured difference represents about 3.5 kg of elemental iron dissolved into the slag. This is a significant fraction of the 10 kg of steel shot that were added during the run. The dissolution of metallic iron in the engineering-scale furnace contrasts with the behavior of iron in the bench-scale system. In the bench-scale tests, about 65% of the iron in soil/lime feed was reduced to metal, with a level in the glass of about 1.3 wt%. It appears that the conditions in the engineering-scale furnace are much less reducing than in the bench-scale system for the soil/lime feed used in these tests.

Table 4.7. Comparison of the Normalized Average Glass Composition to the Target Batch Composition

Oxide	Average Glass Composition	Target Batch Composition
SiO ₂	50.17	52.60
CaO	24.76	26.17
Al ₂ O ₃	10.48	9.61
Fe ₂ O ₃	4.96	3.64
K ₂ O	3.32	2.20
MgO	2.15	2.07
Na ₂ O	1.42	1.01
TiO ₂	0.51	0.52
Nd ₂ O ₃	0.44	0.45
ZrO ₂	0.34	0.35
Y ₂ O ₃	0.32	0.34
BaO	0.20	0.21
Cr ₂ O ₃	0.63	0.16
NiO	0.06	0.14
CdO	0.02	0.13
PbO	<0.08	0.12
Ag ₂ O	0.04	0.12
MnO	0.12	0.08
SrO	0.04	0.05

The data in Table 4.7 also show the chromium content of the glass to be several times higher than the batched value. The increase in chromium can be explained by corrosion of the high-chrome refractory brick that lines the interior of the furnace walls. Chrome contamination is highest when the bricks are first used, and should decrease in future testing as the bricks become seasoned. Assuming that all the excess chrome arises from the dissolution of the refractory, and that the dissolution of the refractory is uniform, then the concentration of other elements will also be somewhat affected, most notably aluminum and magnesium. Table 4.8 shows the estimated effects of contamination from refractory dissolution on the final glass composition. Significantly higher levels of aluminum, and possibly magnesium (in addition to chromium) are expected due to corrosion of the refractory. This issue will be considered further in the discussion of the mass balances.

Glass samples from the engineering-scale pour stream, as well as the baghouse solids, were subjected to the TCLP to characterize the product material as hazardous or non-hazardous. Results from these tests are reported in Tables 4.9 and 4.10. Leachate concentrations are well below regulatory limits for all glass samples, while the baghouse solids exceed the limits for lead in all samples and chromium in some samples. Cadmium, though present at significant levels in the baghouse solids, shows minimal leaching since the final pH of the TCLP leaching solution was about 12.5. This high pH results from the lime in the feed, which is carried over into the baghouse solids. Leaching of lead remains high, however, due to

Table 4.8. Mass in Feed Compared to Mass Dissolved from Refractory for Several Elements

Oxide	wt% in Refractory	Mass from Refractory (g)	Mass in Feed (g)	% Increase Over Feed
Cr ₂ O ₃	27.1	1,257	418	300.7
Al ₂ O ₃	58.6	2,718	25,117	10.8
Fe ₂ O ₃	6.1	283	9,514	3.0
MgO	6.1	283	5,410	5.2

Table 4.9. TCLP Leachate Concentrations from Glass Product (mg/L)

Element	TCLP Limit	ESF Sample Number					
		5	6	11	15	18	19
Ag	5	<0.03	<0.03	<0.03	<0.03	<0.03	<0.03
Ba	100	0.019	<.018	0.022	0.022	0.023	0.023
Cd	1	<0.036	<0.036	<0.036	0.435	<0.036	0.516
Cr	5	<0.12	<0.12	<0.12	<0.12	<0.12	<0.12
Ni	na	<0.12	<0.12	<0.12	<0.12	<0.12	<0.12
Pb	5	<0.24	<0.24	<0.24	<0.24	<0.24	<0.24
Element	TCLP Limit	ESF Sample Number					
		23	25	26	30	32	33
Ag	<0.03	<0.03	<0.03	<0.03	0.033	<0.03	0.033
Ba	0.024	0.023	0.03	0.032	0.035	0.027	0.051
Cd	0.062	<0.036	<0.036	<0.036	<0.036	<0.036	<0.036
Cr	<0.12	<0.12	<0.12	<0.12	<0.12	<0.12	<0.12
Ni	<0.12	<0.12	<0.12	<0.12	<0.12	<0.12	<0.12
Pb	<0.24	<0.24	<0.24	<0.24	<0.24	<0.24	<0.24

Table 4.10. TCLP Leachate Concentrations from Baghouse Solids (mg/L)

Element	TCLP Limit	ESF Sample Number				
		10	17	24	31	35
Ag	5	<0.03	0.121	0.152	0.3	0.355
Ba	100	8.82	4.08	1.09	1.28	8.05
Cd	1	0.098	0.152	0.167	0.112	0.097
Cr	5	1.16	1.37	10.19	5.02	0.88
Ni	na	<0.12	<0.12	<0.12	<0.12	<0.12
Pb	5	189.7	361.9	54.1	32.7	96.1

the formation of soluble complex ions. At a pH of 12.5, the solubility of lead is calculated to be about 130 mg/L. Recycling of the baghouse solids to the furnace may be considered as a means of minimizing the secondary waste stream, however, the buildup of volatile species within the recycle stream must be considered when evaluating such an option.

The low concentration of metals in the leachate from the glass samples does provide a regulatory measure of the durability of the glass product. However, the simple reporting of TCLP leachate concentrations does not take into account how much of these metals was actually present in the sample. A low leachate concentration of glass constituent may just mean that most of this substance was volatilized from the melt. However, the TCLP data can be used to calculate the fraction of the glass (or each element) that was leached from the sample. This is a standard means of representing leaching data to measure the durability of the sample. Comparing the fractional release for each element (mg element leached/g element in sample) to the overall fractional release for the sample (mg glass leached/g glass) can identify any preferential leaching, while the overall fraction release for a sample can be compared to that measured for other glasses to obtain a relative measure of the durability of the sample. Table 4.11 shows that the durability of the product from this test is comparable to that of natural basalt rock, a natural material of comparable composition. As a comparison, the overall leaching of the baghouse solids was about 50 mg/g. There does not appear to be any trend that would indicate that the test conditions (cold cap coverage, submerged arc) affected the durability of the product.

The INEEL soil bulk density was measured to be 1.23 g/mL, while post-test glass samples had an average measured density of 2.88 g/ml. Additionally, the laboratory measured mass loss of the feed, upon

Table 4.11. Overall Fractional Release of the ESF Glass Product (mg glass leached/g glass)

Sample	Overall Leaching (mg/g)
5	0.11
6	0.12
11	0.17
15	0.15
18	0.12
19	0.14
23	0.13
25	0.20
26	0.19
30	0.20
32	0.31
33	0.14
34	0.29
Natural Basalt	0.31

melting into a glass, was 10.9%. Each of these factors was used to calculate the volume reduction of original soil upon treating in the DC arc furnace as follows:

$$\text{Volume Reduction} = 100 * \left[1 - \left(\frac{1.23 \text{ g}_{\text{soil}}}{\text{ml}_{\text{soil}}} \right) \left(\frac{1 \text{ g}_{\text{feed}}}{0.8 \text{ g}_{\text{soil}}} \right) \left(\frac{0.891 \text{ g}_{\text{glass}}}{1 \text{ g}_{\text{feed}}} \right) \left(\frac{1 \text{ ml}_{\text{glass}}}{2.88 \text{ g}_{\text{glass}}} \right) \right] = 52.4\%$$

The equation shows that the resulting volume reduction of a given amount of INEEL soil was 52.4% upon melting. Soil is expected to yield the least reduction in volume of most candidate waste types for the DC arc furnace. Exceptions are large metallic or stone monoliths, which would not reduce substantially in volume. Wastes with substantial organic fractions may be reduced in volume by as much as 90% upon treatment.

4.8 Mass Balances and Partitioning

Closure of mass balances is vital to ensure that valid conclusions are drawn from the test data. All material must be accounted for by analysis of every stream supporting or generated by the process. If the amount of a material in one of the streams is obtained by difference, and there is no physical measurement verifying the presence of this material, significant uncertainties are created in this type of analysis. Alternatively, if all streams are analyzed and a balance fails to close (either more or less material in the outlet streams than present in the input streams), then there is the possibility of contamination, accumulation in the system, or analytical error. Prior to analysis of the partitioning information, mass balances were prepared and deviations from closure explained to ensure the validity of the data.

4.8.1 Overall Mass Balance

The overall mass balance considers the total masses of the feed material and the product streams, without regard to individual elements. Measured quantities include the mass of feed added to the system, the mass of slag product drained from the furnace, and the mass of off-gas solids collected. The mass of accumulated material in the furnace is estimated from the known dimensions and an approximate melt pool depth. The mass of volatile species lost to the off-gas is based on the measured properties of the feed. Figure 4.12 presents the overall mass balance for the first test campaign in the engineering-scale furnace.

The mass of feed material processed during the test was obtained from the load cell measurements on the bulk solids feeder. Off-gas solids mass was measured directly from the material collected during the entire test. The mass of the gaseous emissions was calculated from the total mass of feed material using the experimentally determined loss-on-ignition value of 10.9% for the feed material. The mass of poured glass was directly measured at the completion of the test. Subtracting the inputs from the outputs gives a difference of 65 kg, which represents the accumulation in the system. The estimated mass of glass remaining in the furnace, based on the dimensions of the system and the estimated glass level, is about 75 kg. The difference is accounted for by the approximately 12 kg of soil that was in the furnace at

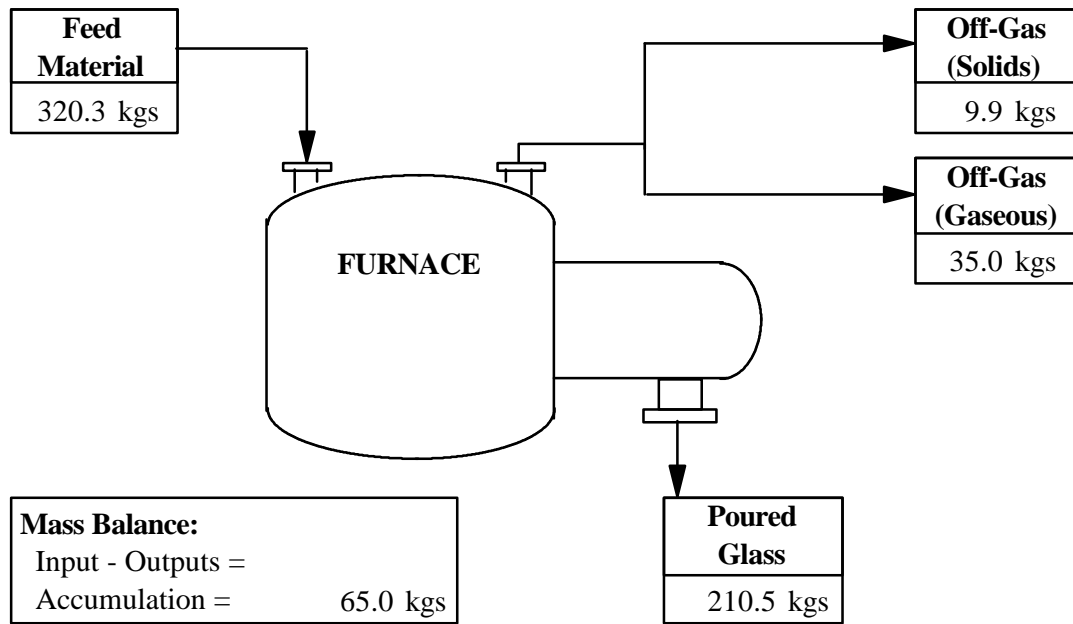


Figure 4.12. Overall Mass Balance for the Engineering-Scale Furnace Test Campaign #1

startup from past testing. The error in calculating the amount of glass remaining in the furnace is about ± 5 kg (1 in. of depth). The overall mass balance is found to account for all material fed to the system.

The partitioning of solids to the off-gas over the entire duration of the test is calculated from the above data to be 3.1%. This is significantly higher than the values measured during any of the individual test segments, due to higher off-gas loss rates occurring during nonsteady state operations (such as initial start-up, cold-cap burnoff after each test segment, idling between tests and during the repair of the overflow heaters.

4.8.2 Individual Test Segment Mass Balances

In order to ensure the validity of the data, all material must be accounted for in each of the streams. One cannot measure the lead content of the off-gas solids and assume that the remainder of the lead is in the glass. Each stream must be analyzed, and the amount of each element recovered in the product streams compared to that initially present in the feed material. To close the mass balance, the total amount of each element delivered by the feedstream should equal the cumulative quantity of this substance recovered from all product streams. Any significant deviations must be accounted for, or the data must be considered suspect. Once the balances are determined to close acceptably, then the data can be used to identify the partitioning behavior of the individual elements.

The composition of the feed material was determined by analyzing each of the components of the feed and calculating the batched feed composition based on the measured masses of each feed component. This method eliminates possible errors due to incomplete mixing and ensures the most accurate representation of the feed composition. The total mass of each of the product streams was measured

during each test segment, and samples of these streams were submitted for analysis (the total mass of the glass product was calculated from the mass of material fed during the test segment and the known oxide fraction of the feed. This was necessary because of the lack of accuracy in the measurement of the mass of slag product). From these analyses, the amount of each element in the product streams was determined. The amount of each element found in the glass and off-gas solids was expressed as a percentage of the amount of each element present in the material fed during that particular test segment. A value of 100% represents complete recovery.

Table 4.12 presents the mass balance data obtained for each of the five test segments. The analytical data supporting these values is included in Appendix B. The estimated error of each of the values reported in this table is $\pm 10\%$. Since the glass phase constituted the greater mass compared to the off-gas solids, the majority of the analytical error lies in the glass values.

The elements are grouped into three categories in Table 4.12. If the amount of an element measured in the product stream is equal to the amount fed (within the estimated $\pm 10\%$ error), then the recovery is deemed acceptable and the mass balance is assumed to close. If the amount measured is less than the amount fed, it is classified as low recovery. If the amount measured is higher than the amount fed, it is classified as high recovery. Deviations from acceptable recovery (failure to close the mass balance) are discussed below. Variations between test segments are discussed in subsequent sections dealing with partitioning.

All four elements with low recoveries (Ag, Cd, Ni, Pb) are readily reduced to their metallic form at high temperatures. The low recovery of silver and nickel is most likely explained by accumulation of a metal phase within the furnace since the feed in these tests did not include elemental metals, and iron actually had to be periodically added to the melter to maintain acceptable operating conditions, extraction and analysis of the melter's metal phase was not recovered for analysis. Previous testing in the bench-scale DC arc furnace demonstrated that nickel is fairly stable in the metal phase at the conditions in the furnace (Freeman and Seiler 1997). Both silver and nickel metals have relatively high boiling points, so significant volatile losses would not be expected. However, the low melting points of metallic cadmium and lead are expected to result in significant volatilization from the melt. The data in Table 4.12 show low volatile losses for silver and nickel, and high losses for cadmium and lead.

The low recovery of cadmium is likely a result of unsteady-state effects resulting from the short duration of the test segments. It is noted in the data of Table 4.12 that the recovery of cadmium approaches 100% for test segments 2 through 4, while only half of the cadmium is recovered in segments 1 and 5. This behavior may be explained by accumulation (refluxing) of the volatile elements in the cold cap, along with accumulation in the melt pool. Segments 2 through 4 were run with a high plenum temperature with either a low cold-cap coverage or an exposed arc. With the high plenum temperatures and limited cold cap coverage, most of the cadmium and lead which volatilize from the melt are carried directly into the off-gas. When a cold cap is present, however, the volatile metals are condensed by the cold cap. This increases the concentration of the volatile element at the surface of the melt, which will drive the concentration of the species higher in the molten pool. Since the test segments were relatively short, a steady state concentration in the glass pool would not be reached. An increase in concentration in

Table 4.12. Elemental Mass Balance for Test Segments 1 Through 5

Element	Test Segment 1			Test Segment 2			Test Segment 3			Test Segment 4			Test Segment 5		
	% in Glass	% in Off-Gas	% Total	% in Glass	% in Off-Gas	% Total	% in Glass	% in Off-Gas	% Total	% in Glass	% in Off-Gas	% Total	% in Glass	% in Off-Gas	% Total
Low Recovery															
Ag	45.51	7.78	53.29	33.32	11.88	45.20	28.56	10.37	38.93	27.37	8.04	35.41	37.32	5.06	42.38
Cd	14.98	29.65	44.63	6.10	88.09	94.19	11.56	66.06	77.62	13.06	70.45	83.52	14.34	32.09	46.43
Ni	43.28	4.03	47.31	36.02	6.30	42.32	37.36	6.10	43.46	45.59	6.49	52.08	56.25	2.57	58.83
Pb		26.25	26.25		76.35	76.35		57.29	57.29		62.96	62.96		18.42	18.42
Acceptable Recovery															
Ba	89.37	0.71	90.08	93.04	0.97	94.01	93.44	0.90	94.34	93.00	0.89	93.88	95.04	0.43	95.48
Ca	93.19	1.89	95.07	96.69	2.72	99.42	96.43	2.53	98.97	95.05	2.58	97.63	96.07	1.37	97.43
Mg	107.29	1.00	108.29	105.49	1.50	106.99	105.20	1.40	106.60	103.65	1.43	105.07	102.63	0.65	103.27
Nd	96.85	2.75	99.60	100.60	4.04	104.64	102.88	3.57	106.46	101.12	3.83	104.95	101.77	1.99	103.76
Si	93.69	0.87	94.56	94.85	1.31	96.16	94.73	1.48	96.21	94.93	1.54	96.47	95.29	0.61	95.91
Sr	90.82	1.37	92.19	89.51	1.97	91.48	93.39	1.86	95.25	89.19	1.83	91.02	91.16	0.96	92.12
Ti	96.96	0.83	97.79	98.77	1.22	99.99	97.70	1.10	98.80	97.29	1.08	98.38	98.12	0.54	98.66
Y	88.53	1.71	90.25	96.87	2.68	99.54	95.61	2.57	98.18	95.68	2.65	98.34	97.88	1.27	99.14
Zr	95.47	2.05	97.52	97.16	3.29	100.45	96.88	3.50	100.38	98.56	3.21	101.78	98.73	1.33	100.06
High Recovery															
Al	115.38	0.84	116.22	112.44	1.21	113.65	112.18	1.11	113.29	110.05	1.06	111.11	109.24	0.53	109.77
Cr	415.94	4.28	420.22	371.87	6.29	378.16	396.39	6.37	402.76	379.52	6.64	386.16	351.29	2.58	353.86
Fe	147.92	0.88	148.80	124.32	1.49	125.81	129.46	1.75	131.22	133.61	1.71	135.32	136.66	0.61	137.28
K	144.39	1.78	146.18	143.73	4.40	148.13	143.31	7.61	150.92	162.38	7.88	170.26	144.58	1.54	146.12
Mn	186.34	0.90	187.23	155.32	1.62	156.94	145.45	2.20	147.64	140.00	1.96	141.96	131.32	0.62	131.94
Na	166.44	1.46	167.90	140.42	5.08	145.49	134.88	8.89	143.77	128.58	7.95	136.53	121.86	1.45	123.31
Bulk Entrainment (%)															
		1.40			2.31			2.33			2.37			1.00	

the melt of only 0.01 wt% from the start to finish of the test segment would account for all of the missing cadmium in test segment 1. Such variation was observed in the glass composition, but sufficient analysis to determine the statistical significance of such variation has not yet been performed.

Lead was also shown to volatilize significantly from the melt (similar to cadmium); however, the detection limit by ICP analysis was not sufficiently low to measure the amount of lead remaining in the glass. The detection limit for lead represents a recovery of about 65% in the glass; therefore, there could be enough lead present in the glass to account for the remaining lead. Alternatively, some lead could be present in a metal phase that remained in the melter. Future analyses for lead in the glass should use alternative methods such as graphite furnace atomic absorption spectroscopy, which can detect much lower levels of lead in the sample.

A number of elements show high recoveries, which indicates a contamination source of this element in the test. Aluminum and chromium contamination results from leaching and corrosion of the high-chrome refractory (Monofrax K-3) lining the hearth. Assuming that all the excess chrome arose from refractory corrosion, and that corrosion of the refractory was uniform, the contamination by other elements present in the refractory may be estimated. These calculations estimate that the aluminum content of the glass would be increased by about 10%, while the magnesium content would increase by about 6.7% due to corrosion of the refractory. The data in Table 4.12 show the amount of aluminum recovered to be 9.8% to 16.2% over the input in the feed, while the amount of magnesium recovered was 3.3% to 8.3% over that input in the feed. Both of these differences are nearly completely accounted for by contamination from the corrosion of the refractory lining the hearth. Of note is the fact that the recovery for all three elements (Al, Cr, and Mg) trends down throughout the test, which would be expected as the corrosion of the refractory slows after the initial period of “rapid leaching.”

As previously discussed, the most likely source of the excess iron found in the product streams is the iron metal that was added to the system during processing. The excess iron in the glass product represents about 4 kg over the entire test. The 10 kg of iron metal added to the system provides an adequate source for contamination of this magnitude. The iron metal is also a likely source of manganese contamination. Along with the 10 kg of iron added during the test, about 8 kg of iron was added to the system during start-up. Carbon and other low alloy steels contain about 0.4 to 0.8 wt% manganese. Previous testing found manganese to primarily partition to the glass (Freeman and Seiler 1997); therefore, manganese in the added steel could end up in the glass. The manganese in the iron added to the system is sufficient to account for the extra manganese recovered in this test.

No source of contamination for the alkali metals (Na and K) could be identified. The potassium values in the glass are near the instrument detection limit; ICP-AES is a poor method for potassium analysis, and the values may be suspect. Sodium, on the other hand, has much lower detection limits and is typically reported with reasonable accuracy. There could have been an unknown source of contamination in the furnace or analyses.

4.8.3 Metals Partitioning

4.8.3.1 Bulk Material Partitioning

The bulk entrainment reported in Table 4.12 is the percent of the mass fed during the test segment, which was recovered in the baghouse solids. From this data, it appears that the degree of cold-cap coverage and the position of the electrode have a significant impact on the total solids carryover to the off-gas system. The bulk entrainment is plotted versus the measured plenum temperature in Figure 4.13. The plenum temperature is an indirect measure of the fraction of the surface covered with cold feed material in the submerged arc mode of operation, while in the exposed arc it is less relevant due to radiative heat transfer from the hot arc.

For the submerged arc operations, the plenum temperature and bulk entrainment both show an increasing trend with decreasing cold cap coverage. The exposed arc test segments showed high entrainment without a correlation to plenum temperature. Although certain elements are enriched in the off-gas solids (see in discussion in Section 4.8.3.3 on hazardous metal partitioning), most of the mass is still the bulk feed material, indicating that the physical characteristics of the system are affected by the different test conditions. At low cold-cap coverage, more of the melt surface is exposed, leading to more

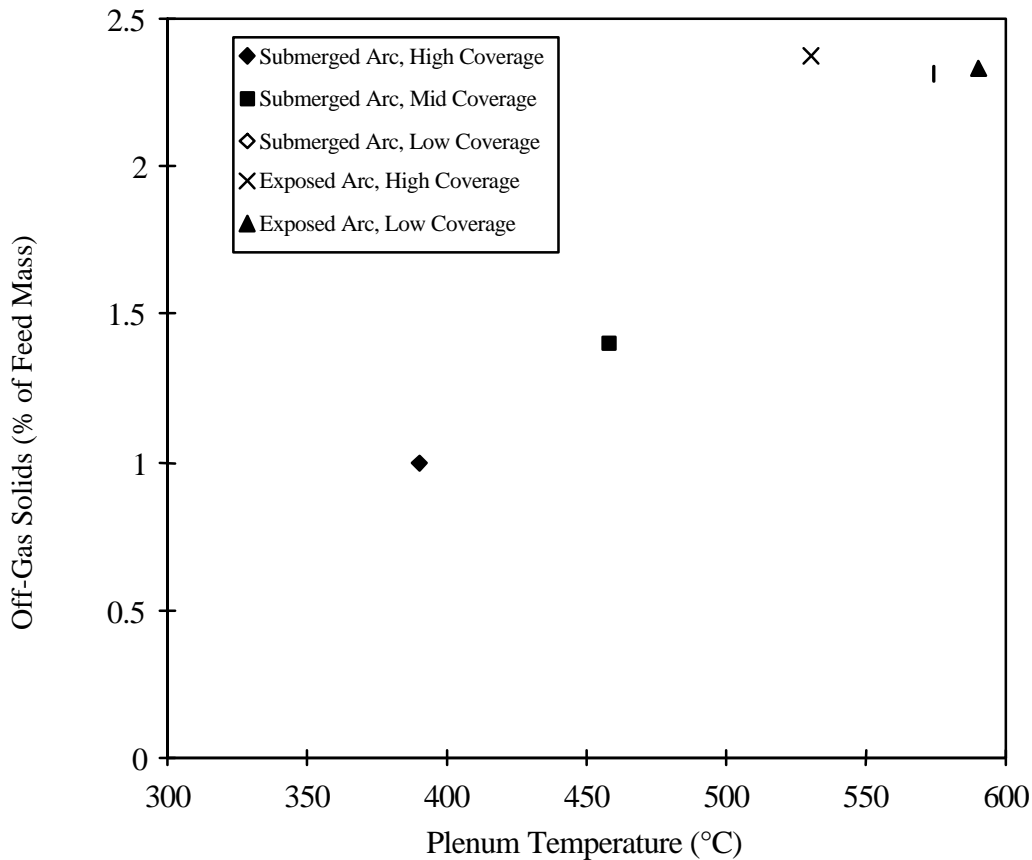


Figure 4.13. Total Off-Gas Solids Carryover Versus Plenum Temperature

bulk material being thrown up and entrained in the off-gas from the bubbling melt. With an exposed arc, the melt is violent in the vicinity of the arc regardless of cold cap coverage, which would explain the lack of effect of cold cap coverage with the exposed arc. To minimize bulk entrainment, it appears that the DC arc furnace should be run at a high cold cap coverage with the arc in the submerged arc mode.

4.8.3.2 Radionuclide Surrogate Partitioning

Previous testing in the bench-scale furnace with feeds spiked with plutonium found the partitioning of plutonium to the off-gas stream to be consistent with bulk entrainment of the feed as measured by the entrainment of stable, non-volatile oxides such as TiO_2 , CaO , and Al_2O_3 (Freeman and Seiler 1997). Since the first engineering-scale test did not include radioactive materials, the impact of the various test conditions on the partitioning of these and similar elements will be used to predict the impact on partitioning of plutonium. An additional concern with plutonium is the effect of particle size on the partitioning, since plutonium oxide is commonly present as a sub-micron particulate; therefore, several plutonium surrogates with a range of particle sizes were spiked into the feed. The surrogate materials used were $ZrSiO_4$, $<1\mu m$; Nd_2O_3 , $<44\mu m$; and $Y(OH)_3$, $<4mm$. The oxide form of all three surrogates is expected to represent plutonium oxide with respect to the physical entrainment mechanism. The melting point and free energy of formation of each surrogate oxide is comparable to that of plutonium oxide. Additionally, these three elements were not present in the bulk feed so that analytical error is minimized.

The off-gas partitioning values for the major non-volatile constituents are plotted in Figure 4.14. Note that these data appear to fall into two groupings. One group includes the soil components (Si, Al,

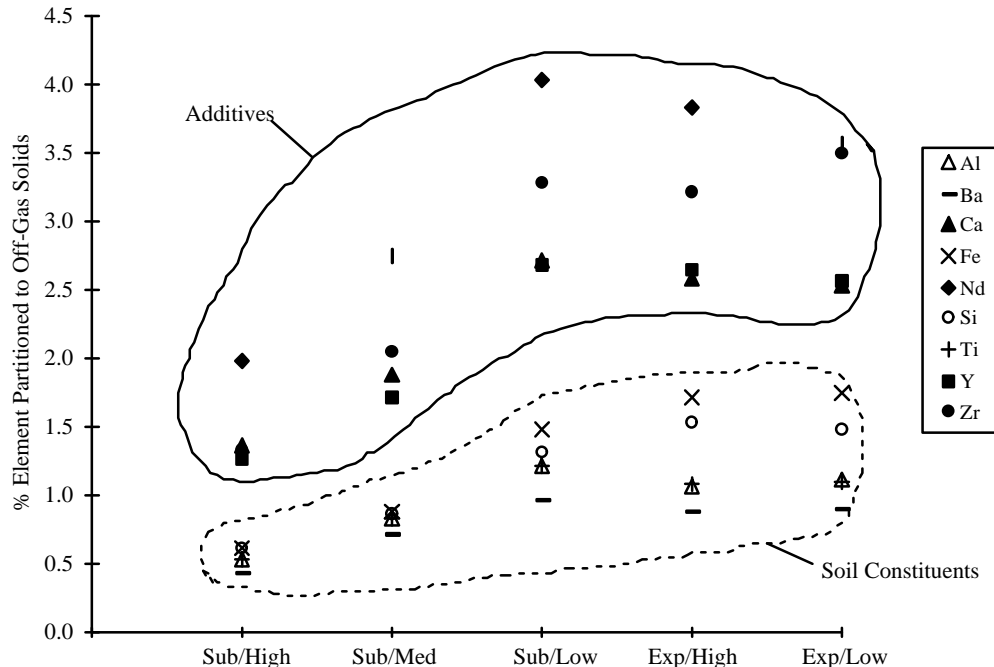


Figure 4.14. Partitioning of Primary Feed Constituents and Plutonium Surrogates at the Various Test Conditions

Fe, Ti) along with Ba, while the other group consists of additives to the soil (Ca, Nd, Y, Zr). The partitioning values of the soil components generally fall close together and are one-half to one-third the partitioning values of the additives. With the exception of Ba, this trend implies that the additives are entrained at a greater rate than the soil. The most likely reason for this behavior is differences in particle size. The soil is a coarse material with most of the mass found in larger particles, while most of the additives were much finer. Even the yttrium, which was of a nominally large particle size, was observed to contain substantial amounts of fine powder. The finer particles are more easily entrained, leading to higher partitioning values.

Figure 4.15 graphically depicts the higher rate of entrainment by plotting the percent of additive elements partitioned to the off-gas versus the percent of aluminum (soil component) partitioned to the off-gas. The slope of the line is about three times the one to one relationship which was observed for plutonium in the bench-scale testing, with the exception of barium, which partitioned nearly identically to the aluminum.

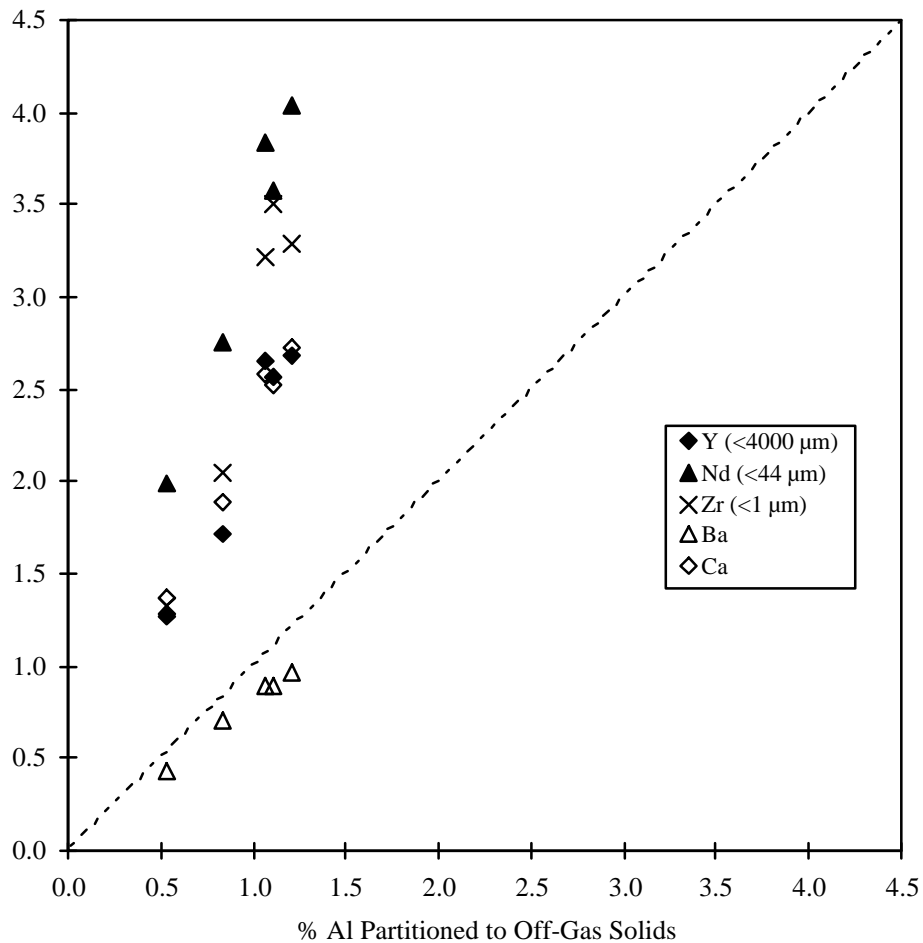


Figure 4.15. Partitioning of Plutonium Surrogates Compared to Aluminum

The exception of barium may be explained by the fact that the barium was added to the feed as $\text{Ba}(\text{OH})_2 \cdot 8\text{H}_2\text{O}$, which has a melting point of 78°C . During feed preparation, hydration of the lime with moisture from the soil raised the temperature of the feed to 100°C to 150°C . At these temperatures, the barium would melt and coat the soil particles, resulting in a physical attachment to the soil particles. This attachment would result in the partitioning of barium to follow closely that of the soil elements. Figure 4.15 shows that the barium partitioning did indeed closely track that of the soil components. Alternatively, the particle size of the barium crystals may have been similar to the particle size of the soil.

The behavior of barium may provide insight into why the plutonium partitioning in previous testing closely tracked the partitioning of the stable oxide components (mostly soil components). Plutonium was added to the feed as a nitrate solution, which would coat the feed particles and leave the plutonium physically attached to the feed particles when the solution dried, similar to the barium in these tests. It must also be considered that the smaller size of the bench-scale system may have resulted in smaller differences in the partitioning between the smaller and larger particles.

The difference in partitioning between the soil components and the additives suggests that particle size plays a role in the bulk entrainment of materials fed to the system. Particle size is of particular concern for waste streams contaminated with sub-micron plutonium oxide. The three plutonium surrogates in the engineering-scale tests ranged in size from <1 micron to about 4 mm to investigate any impacts of particle size on elemental partitioning. The data presented in Figure 4.15 appear to show that there is very little difference between the partitioning of these additives of widely differing particle sizes. This may be due to the agglomeration of small particles into larger particles. Additionally, small particles are easily attached to larger particles by electrostatic interactions. Another possible explanation for the similarity of partitioning over the range of particle sizes is that the different sizes of materials added were all “less than” fractions, rather than a definite size range. Therefore, even the additive with the largest particle size could contain a substantial mass of very fine particulate, which would bias the results. Future testing will use specific size fractions when investigating the effects of particle size.

The most important observation from the plutonium surrogate partitioning data is that the partitioning of all the non-volatile materials to the off-gas was low. Even extremely fine particles ($<1 \mu\text{m}$) only partitioned at less than two times the bulk entrainment rate, or a maximum of 4% in the engineering-scale system at these test conditions.

4.8.3.3 Hazardous Metals Partitioning

Partitioning of hazardous metals is of interest to identify the fate of these metals in the DC arc system. It is known that substantial loss of volatile metals is experienced during high temperature processing (Freeman et al. 1995). Of particular interest in these tests is determining conditions that will maximize the retention of the volatile elements in the glass phase. Experience with liquid-fed ceramic melters for waste processing, as well as cold-top melters in the glass industry, has demonstrated that maintaining a cover of cold feed material over the pool of molten glass will minimize volatility. Figure 4.16 shows the partitioning of the various hazardous metals for each of the test conditions.

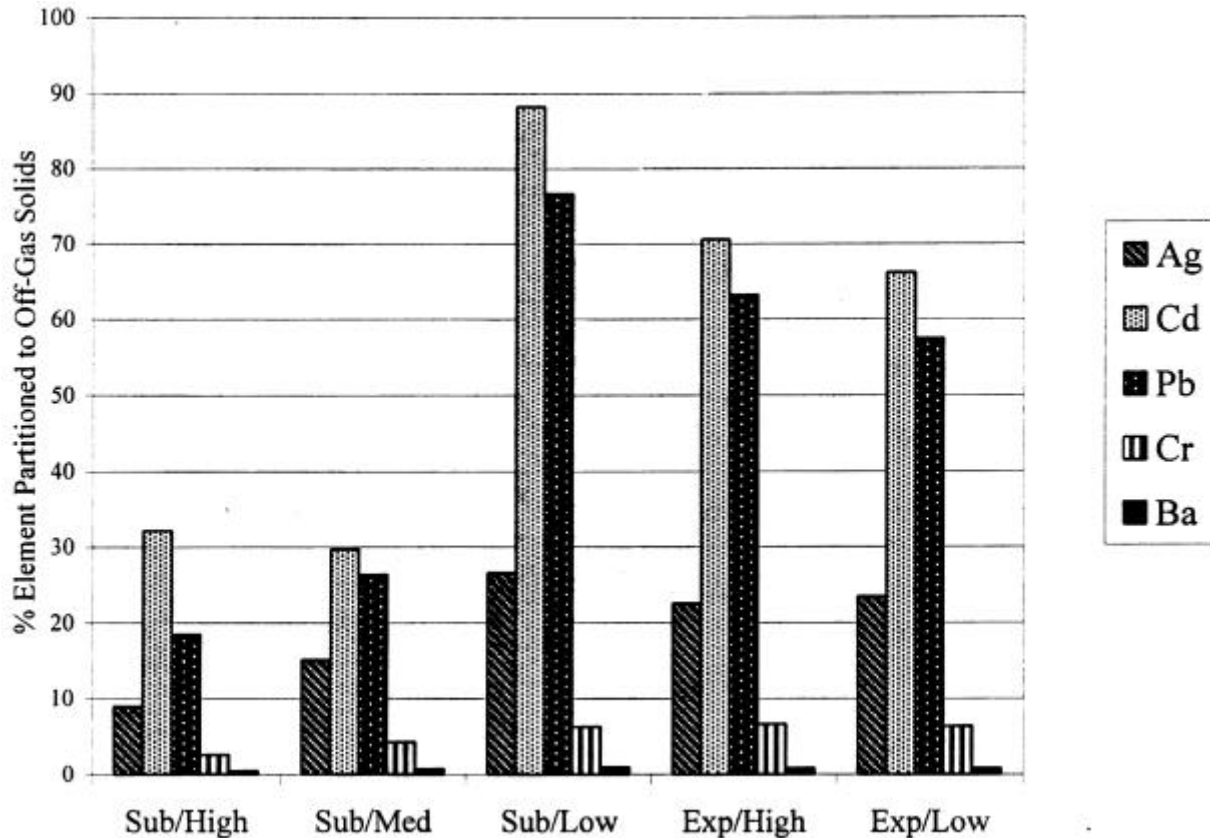


Figure 4.16. Partitioning of Hazardous Metals to the Off-Gas Solids at the Various Test Conditions

The trends parallel those previously discussed for the bulk partitioning and partitioning of the radionuclide surrogates. In the submerged arc operation, partitioning to the off-gas increases as the cold cap coverage decreases, while for exposed arc operation, partitioning is generally high regardless of the cold cap coverage.

Cadmium and lead are the most volatile elements at all test conditions, with about 50% to 90% of the element partitioning to the off-gas at low cold cap coverage or exposed arc conditions. These conditions are comparable to the operation of a plasma torch, which has been shown to have similar volatility for these metals (Freeman et al. 1995). The data appear to show, however, that partitioning of hazardous metals to the off-gas can be substantially reduced by running in the submerged arc mode with high cold cap coverage. This conclusion must be viewed as tentative given the fact that the mass balances at these conditions were not able to account for all the material, indicating that steady state conditions may not have been achieved. If volatile metals were refluxing in the cold cap, steady state partitioning to the off-gas or the glass could increase as the concentration built up in the cold cap. Future test segments will be of much longer duration to allow steady concentrations to be reached.

Chromium partitioning to the off-gas was much higher than expected given the low volatility and high stability of the oxide. As previously discussed, the chromium content of the glass was

approximately four times higher than the target value based on the feed. If entrainment from the glass is a significant source of off-gas solids, then the chromium content of the off-gas solids would be expected to increase by up to four times. If the partitioning value for chromium is divided by four, its value falls more closely in line with the non-volatile soil and additive components of the feed. This data suggests that substantial entrainment of material from the melt pool itself occurs, and not just from the unmelted feed.

Silver partitioning to the off-gas is relatively low, about 10% or less. Although silver is easily reduced to its metallic form, its melting and boiling points are much higher than cadmium or lead. Most of the unaccounted silver in the mass balance is expected to have accumulated in a metal phase within the furnace, although preliminary XRF analysis of the off-gas solids indicates that the ICP-AES results may be biased low. Barium partitioning to the off-gas was very low as would be expected based on the high stability and low volatility of the oxide.

5.0 FY 1997 Testing Campaign #2: SRS Debris Testing

After testing with soil-lime material, the engineering-scale furnace was placed in a cold standby mode for approximately 3 months before being restarted for the 2nd plasma arc test of FY 1997. The second test campaign was to investigate the effect of variation in feed composition and operating conditions on partitioning. Specifically a non-radioactive SRS debris surrogate was chosen as the baseline feed for this test.

5.1 Test Objectives

The objective of the second test campaign was to process a non-radioactive surrogate of SRS debris using the similar operating conditions utilized during the 1st engineering-scale test of FY 1997 (see Section 4). The primary focus of this test was to investigate the effect of feed composition, particle size, and melter operating conditions on the partitioning of hazardous metals and plutonium surrogates. The operating conditions to be varied in this testing campaign included: the degree of cold-cap coverage (unmelted, cool material floating on the surface of the melt) and the position of the electrode (submerged in the glass, or above the surface).

5.2 Flowsheet

The SRS waste debris surrogate was tested in the bench-scale DC arc furnace where glass forming additives and amounts were identified. The recipe for this surrogate is shown in Table 5.1.

Table 5.1. SRS Debris Waste Surrogate with Glass Forming Additives

Constituent	Amount	Constituent	Amount
Base Constituents:		Hazardous Metals:	
Ground Walnut Shells	5.3%	AgNO ₃	0.16%
Perlite (Harborlite)	5.3%	Ba(OH) ₂ •8H ₂ O	0.23%
PVC (Ground)	5.3%	CdO	0.12%
Soda/Lime Glass (Beads)	5.3%	CsNO ₃	0.14%
Steel BBs	5.3%	Pb(NO ₃) ₂	0.16%
Activated Carbon	2.4%	Ni(OH) ₂	0.16%
Portland Cement	2.1%		
Aluminum Tadpoles	0.77%	Varying Particle Sizes:	
Al(OH) ₃	7.4%	TiO ₂ (-400 mesh).	0.17%
CaO	16.2%	Ce(OH) ₄	0.37%
Fe ₂ O ₃	3.2%	ZrSiO ₄ , <1μm	0.51%
Dolomite Lime (CaMg(CO ₃) ₂)	7.4%		
Na ₂ CO ₃	0.58%		
SiO ₂	31.4%	Total	100%

Note that the SRS debris waste surrogate feed has 13% organic constituents by mass, comprising ground walnut shells, PVC, and activated carbon. Hazardous metals and non-volatile particulate of varying sizes were added to the surrogate to assess their carry over behavior.

5.3 Operations

The furnace was restarted using equipment described in Section 3.5. A deeper residual glass layer was in the furnace compared to that in the previous restart. This layer was approximately 12 to 14 in. thick. Approximately 10 lb of nails were added to the top of the glass to provide continuity. DC power was applied via the restart path for approximately 30 hours before current flow was achieved through the furnace hearth. At this time the furnace was probed to reveal a sticky glass layer on the bottom of the furnace that was assumed to be nonconductive. This suggested either a channel of molten glass to the bottom of the furnace or firing through a fissure or crack in the Monofrax K-3 sidewall to the graphite hearth behind was occurring. Nevertheless, the by-pass circuit was removed and the furnace heat up continued. Ten hours after current started passing to the hearth, soil-lime feed material was fed to the furnace. This material was used primarily to reestablish glass pouring from the furnace overflow. Approximately 110 lb of soil-lime feed were fed to the furnace over an 8-hour period during which time normal glass transfers occurred. Next, SRS debris surrogate feeding to the furnace was begun. Approximately 120 lb of debris was fed to the furnace over a 12-hour period. Glass pours were conducted approximately every 30 minutes. However, at the end of the 12-hour time period glass ceased pouring from the furnace. Attempts to resume pouring from the overflow were made. A higher vacuum was applied to the overflow section to try and force the glass out. Additionally, more feed was added to the furnace to give a larger hydrostatic head of glass inside of the furnace. Joule-heating down the overflow section throat was also attempted via a graphite rod inserted from the end of the overflow section. None of these attempts at restarting glass flow were successful.

An additional problem with the furnace was discovered during the period after glass had stopped pouring. Periodic probing of the furnace revealed that the glass level was dropping over time. Glass previously poured from the furnace was added to increase the level. Several additions of glass were made resulting in a cumulative glass addition of approximately 100 lb. The glass was believed to have leaked through an opening in the side of the graphite hearth, near one of the furnace's side buses. That opening would have enabled glass to fill one of the side-bus voids. Indeed, post inspection of the furnace found one of the furnace side bus voids full of glass.

Since attempts at restarting glass pouring from the furnace were unsuccessful, the furnace was shut down approximately 100 hours after pouring had ceased. Samples of the last glass poured from the furnace were used to estimate Monofrax K-3 corrosion during operation; the mechanism believed to have caused the glass to stop pouring. Concentrations of alumina were compared to those in the feed and the differences attributed to corrosion products from the Monofrax K-3. Chromia, another major constituent of Monofrax K-3, was not used as it had the potential of reducing to its metallic form and not exiting the furnace in the glass product. Not only were corrosion estimates made for the last SRS debris surrogate fed but for other periods of furnace operation as well. These results are summarized in Figure 5.1.

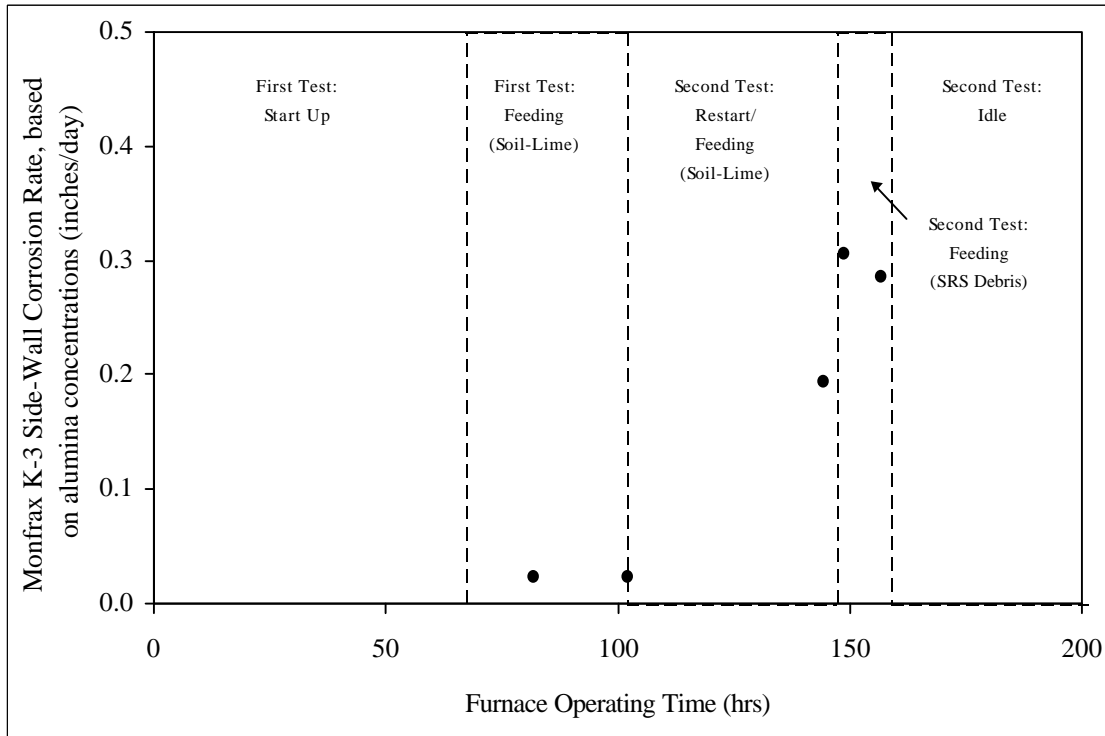


Figure 5.1. Monofrax K-3 Corrosion Rate Estimates for the Engineering-Scale Furnace

Figure 5.1 shows that little Monofrax K-3 corrosion occurred in the first test, with soil-lime feed, compared to the second test. Furthermore, the corrosion rate increase in the second test occurred before SRS debris was fed to the furnace. Subsequent feeding with SRS debris appears to have produced even more corrosion of the Monofrax K-3, however, not substantially more than during the furnace restart and feeding of soil-lime. These results help substantiate the theory that the arcing current shorted through the Monofrax K-3 side walls of the furnace during restart, producing enhanced corrosion of that material in those areas. The addition of reducing SRS surrogate debris further contributed to the overall corrosion of the Monofrax K-3. Laboratory corrosion tests, performed after the engineering-scale tests, showed similar Monofrax K-3 corrosion rates with SRS debris to those shown in Figure 5.1. Here, the organic content of the feed material was attributed to the corrosion, as chromia was believed to have reduced from the refractory leaving a weak alumina substrate.

5.4 Post-Test Furnace Inspection

A post inspection of the furnace revealed that an upper portion of the Monofrax K-3 side wall (approximately 3 in. by 4 in.) was entirely missing. The location of this missing Monofrax K-3 was near the side bus port that filled with glass. One possible cause for the glass pour stoppage is that a piece of the Monofrax K-3 side wall broke free and lodged itself in the throat of the discharge trough. An increase in glass viscosity from dissolution of Monofrax K-3 products into the glass bath is another possibility. The alumina concentrations in the last glasses poured from the furnace were 19% versus a target of 11%. It is

possible that the alumina content increased even more between the last pour and the following attempts to reestablish pouring, resulting in a glass with too high of a viscosity to pour from the furnace. The actual mechanism or mechanisms responsible for the pour stream stoppage, however, could not be conclusively established from the available analytical data.

6.0 FY 1998 Pantex Demonstration

Many of the DOE sites possess chemically toxic and radioactive materials that would be classified as “mixed waste” if the materials were not treated to destroy or somehow immobilize their hazardous constituents. Obsolete, classified, radionuclide-containing weapon components represent examples of DOE materials that may eventually have to be disposed of as mixed waste if left untreated. For classified materials, disposal costs can become quite excessive, as guarded, mixed-waste repositories would ordinarily have to be employed. Therefore a need exists (see Section 1.0) to develop a robust technology that can treat and demilitarize classified radionuclide-containing weapon components in order to minimize human exposures, environmental hazards, and life cycle management costs. Since the STCGs at the Pantex and SRS identified the plasma-fired, pyrometallurgical process (the DC arc technology) as a promising solution to this MWFA identified technology need, the focus of FY 1998 DC arc furnace activities was directed at demonstrating the demilitarization capability of this technology.

The obsolete weapon component chosen for this demilitarization demonstration was a ferroelectric neutron generator that exists in quantity at DOE’s Pantex Plant and contains both hazardous (Pb) and radioactive (^3H) constituents. Although the waste forms generated by the DC arc technology should have no appreciable capacity for tritium, and complete radionuclide release by the facility stack was a process expectation, the extent to which Pb could be immobilized in the vitreous waste product was of particular project interest. An unclassified photograph of the type of neutron generator tube processed during the Pantex Demonstration device is displayed in Figure 6.1.

The generator tube displayed is, in fact, a component of a larger neutron generator assembly that is visually classified. The triggers that contain energetics were separated from the tubes as part of the decommissioning/storage process at the Pantex Site. The tube component itself is designed, if appropriately triggered, to produce a neutron burst that enhances the fission yield of nuclear devices. However, being completely passive without their associated triggers, the hazards associated with processing these devices are limited to issues involving their chemical and radiological constituents. All discussions and calculations regarding tritium in this report are based on an unclassified bounding value for this isotope in the specific type of neutron generator that was processed during this demonstration.

6.1 Test Objectives

The primary focus of this testing program was to use the DC arc melter technology to treat and demilitarize weapon components (ferroelectric neutron generators) that containing hazardous and radioactive materials and to evaluate the ability of primary melter waste residuals to incorporate and immobilize hazardous feed stream constituents. This data will provide necessary information for assessing the ability of this technology to reduce the life cycle costs for managing obsolete, classified military hardware. Processing performance and the overall operability of the DC arc melter and its ancillary support systems were also of interest during the test. The efficacy of this high-temperature melter technology was also to be evaluated against the STCG-identified weapons materials processing needs.



Figure 6.1. Unclassified Photo of a Ferroelectric Neutron Generator Tube

The specific test objectives for the Pantex Demonstration as established in the FY 1998 Test Plan are summarized below.

- Develop flow sheet parameters for Pantex neutron generator feed stream.
- Demilitarize 200 ferroelectric neutron generators by converting all elemental constituents into glass and/or metal phases.
- Obtain partitioning and overall mass balance data for constituents in the feed stream.
- Determine the quality and durability of the slag waste product.
- Evaluate the operability of the furnace (electrode power stability, acceptable plenum vacuum fluctuations, electrode consumption, etc.).
- Evaluate performance of the induction heated-bottom and radiant-heated overflow drains for product removal.

- Obtain data to allow characterization of the performance of the furnace off-gas system.
- Determine TCLP leachate concentrations of specific regulated metals from the slag and metal product streams to support waste form classification.

6.2 Test Approach

The primary purpose of FY 1998 ESF testing was to demonstrate that the thermal DC arc process can be effectively used to sanitize classified, surplus neutron generators that contain both radioactive and chemically hazardous constituents. Specifically the ESF was used to melt the neutron generators and convert their base constituents into molten glass- and metal-phase waste streams. To accomplish this, each of the 200 neutron generators, individually packaged in cylindrical cardboard containers, was sequentially fed to the ESF using the melter's large object (can) feeder.

However, before the processing demonstration could begin, a process flowsheet had to be developed. Although the Pantex neutron generators could be melted and/or sintered alone, this material would not be readily removable from the furnace. Consequently strategies for dealing with the ceramic, refractory and mixed metallic neutron generator components had to be developed through crucible and bench-scale melter scoping tests using surrogate materials. These tests established the need for, and identity of, chemical additives necessary to produce well behaved waste streams and also served to identify refractory incompatibilities and operational vulnerabilities. In addition, the results identified the waste forms to be generated, allowed the melter to be prepared for these wastes, permitted a detailed processing plan to be formalized, and enabled a customized melter feed stream to be prepared.

Once a process flowsheet was developed and all melter repairs and preparatory work were complete, the processing campaign of the neutron generators commenced. Melter operations began with the processing of a preparatory feed that produced a molten bath designed to melt and/or dissolve the chemical components of the neutron generators when they were subsequently fed to the melter along with appropriate chemical additives. The melter's large object feeder was exclusively used to support all feed stream transfers. Once stable processing conditions had been achieved with the preparatory feed, processing of the canisterized neutron generators began.

The neutron generators were melted in a continuous processing campaign producing both metal and glass waste forms. Chemical additives were used to maintain the target glass composition while neutron generators were being processed. During this processing campaign, the molten metal and glass waste forms were to be periodically transferred to canisters using the melter's inductively heated bottom drain and resistively heated overflow section, respectively. However, an inadequate vacuum seal between melt and overflow sections of the melter precluded batch glass transfers; consequently, the process was operated in a continuous glass overflow mode. Although no need to tap the melter's metal phase presented itself during the demonstration, insufficient temperatures existing below the melter's hearth also prevented bottom draining the melter at the conclusion of the test. Despite these operational difficulties the Demonstration was successfully completed and the results obtained satisfied all major project goals.

6.3 Experimental

6.3.1 Flowsheet Development

The experimental design of the Pantex Demonstration test required use of both bench and engineering-scale DC arc melters. Initial bench-scale furnace scoping tests were required to develop a viable process flowsheet that would accommodate neutron generators. Although the Pantex neutron generators could be melted and/or sintered alone, this material would not be readily removable from the furnace—a requirement of a continuous or quasi-continuous process. In order to create a melt which can be easily transferred from the furnace, the waste must be blended with additives to reduce the viscosity of the melted material to a point that it can be removed at the operating temperature of the furnace. Based on past testing experience, additives may also be required to lower the organic content of the waste to provide stable furnace operations. The chemical and elemental constituents present in the neutron generators that needed to be accommodated by the process flowsheet are summarized in Table 6.1.

Because CaO-Al₂O₃-SiO₂ glasses have proven to be well behaved and readily pourable (Levin et al. 1964) (<100 poise) at ~1300°C, a glass based upon SiO₂ and CaO chemical additives in combination with Al₂O₃ present in neutron generators was chosen as the target vitreous waste product. However the presence of elemental aluminum in the flowsheet presented an operational problem for the DC arc melter. Because of its low density, elemental aluminum, if left unoxidized, could accumulate on top of the melter's molten glass pool as a separate phase, and ultimately produce melter arc electrical problems. Since such a phase could not be purged from the melter due to the melter's overflow design, Fe₂O₃ was added to the flowsheet design in order to promote oxidation of this elemental constituent (Gaskell 1990).

Prior to bench-scale flowsheet development testing, oven crucible melts were produced with glasses of varying Al₂O₃ content. The results obtained suggested the dissolution kinetics for granular alumina (present in neutron generators) in CaO-Al₂O₃-SiO₂ glasses are quite slow under the static soaking conditions used. Three tests using PNNL's Bench-Scale DC arc melter (Freeman and Seiler 1997) were

Table 6.1. Neutron Generator Composition (major constituents)

Chemical Composition		
Component	lb/unit	wt%
Al	0.044	5.7%
Al ₂ O ₃	0.365	46.6%
Steel(C)	0.068	8.7%
Pb(TiZr)O ₃	0.077	9.9%
Kovar	0.114	14.6%
Epoxy	0.114	14.6%
Total	0.784	100.0%

subsequently conducted to further examine the melting behavior of alumina refractory under more realistic, dynamic processing conditions. The feed used in all tests included appropriate proportions of all known neutron generator components in their proper physical and chemical states. Table 6.2 summarizes the composition of the feed streams tested.

All three formulations produced single-phase, high-quality glasses with little or no evidences for crystal growth. Moreover they exhibited low viscosity (<100 poise) characteristics at 1300°C and the ability to readily dissolve and incorporate high- density, monolithic alumina. Consequently these data served to establish the compositional basis for the reference target glass into which the neutron generators would be initially fed and dissolved. This reference glass also established the chemical composition of the glass former additives that were required to be processed with the neutron generators in order to maintain the target glass composition throughout the processing campaign. The compositional data regarding the target glass and glass former additives used during the Pantex demonstration test are also summarized in Table 6.2.

The waste loading adopted by this flowsheet development effort was limited to 20 wt% because of concerns about the dissolution kinetics of the high-density alumina feed stream constituents. Because of this, the adopted flowsheet could not be tailored to meet waste volume reduction objectives. However, all process operability constraints were satisfied by the resultant flowsheet design.

Table 6.2. Trial Pantex Flowsheet Compositions

Component	wt %				
	Feed #1	Feed #2	Feed #3	Target Glass	Glass Former
Al	1.1	1.3	1.2		
Al ₂ O ₃	9.2	10.6	10.3	13.2	
CaO	20.4	16.7	16.2	15.1	20.9
Co	0.5	0.6	0.5		
Fe	3.3	3.8	3.6		
Fe ₂ O ₃	9.9	11.5	11.1	16.3	14.2
Na ₂ O	3.4	3.0	6.3	6.1	3.7
Ni	0.8	1.0	0.9		
PbO	1.1	1.3	1.2		
SiO ₂	49.3	49.2	47.5	49.3	61.2
TiO ₂	0.4	0.5	0.4		
ZrO ₂	0.6	0.7	0.7		

6.1.2 Feed Preparation

Since the FY 1997 melter tests were not able to evaluate the ESF's large object feeder (can feeder) and neutron generators are discrete objects (2"OD x 4.5"L cylinders) requiring such a device, a decision was made to exclusively employ the can feeder system for all Pantex feed stream materials. A standard paper cylinder (3"OD x 5"L) was chosen to canisterize all materials to be fed to the melter. Metal canisters have been previously shown to create an unacceptable short circuiting problem when used with the ESF.

A small cement mixer was used to blend the target glass and glass former chemicals in the proportions indicated in Table 6.2. The homogenized mixtures were subsequently sampled and analyzed to demonstrate their conformity with the specified target values listed in Table 6.2. These chemical mixtures were also melted and fused to verify compliance with required viscosity and glass quality characteristics.

Once all quality assurance tests were complete, the chemical mixtures were canisterized. Since each paper cylinder could only accommodate ~600-grams of either chemical mix, 245 target feed and 422 glass former canisters were needed to accommodate the chemical blends. When the canisterization of the 200 neutron generators are included in the total, approximately 870 feed stream canisters had to be prepared in support the Pantex demonstration. Beyond the inconvenience of preparing such a large number of canisters, the use of paper canisters introduced over 50 lb of unnecessary cellulose reductant to the process flow sheet. The presence of this additional organic matter, moreover, has the potential to create off-gas processing difficulties in the engineering-scale system, which will be discussed in Section 6.5.1. In general, off-gas processing problems associated with feed stream organic matter can be easily handled by a secondary combustion chamber in the melter's off-gas system.

6.1.3 Furnace Operations

Table 6.3 presents an overview of the three operational segments making up the engineering-scale test campaign. The chemical compositions of all feed stream constituents are summarized in Table 6.2.

The first stage of the demonstration involved heating up the melter to operating temperatures. This involved ramping the temperature of the melter's overflow section using its resistive electrical heaters. Once the overflow temperature reached ~500°C, an arc was struck in the melt cavity between the central electrode and the hearth using iron nails as a conductive media. The heatup process continued until a 250°C plenum temperature was achieved, then melter feeding (Segment #2) was initiated.

Table 6.3. Pantex Demonstration Test Segments

Test Segment	Description	Feed Type	Feed Quantity (lb)
1	Warm Up	Nails/Graphite	10/0.5
2	Glass Production	Target Feed	300
3	Demonstration	Neutron Gen/Glass Frm	200/500

Target glass production involved feeding canisters of target feed to the melter using the large object feeder. A canister rack allows approximately 20 feed cans to be staged for sequential introduction into the melter. A SCADA System in conjunction with a PLC provides both logic and control of this automated feeding system. The feeding rate was locally controlled through the SCADA interface as was the electrode positioning and resultant processing power. Target feed was processed until glass pouring commenced and the equivalent of ~1-melt cavity turnover had been achieved, then the final test segment commenced.

The canisterized neutron generators were processed in a similar fashion as the target-glass feed material. However, for each neutron generator fed to the melter, two containers with glass forming chemical were sequentially fed to the melter in order to maintain the target glass composition in the melter. Thus three canisters (actually 3.1) had to be fed to the melter for each neutron generator processed. Although the automated can feeding system had to be ultimately abandoned during the final test segment due to mechanical difficulties, a functionally equivalent manual backup system (see Section 6.4.3) was successfully used to complete the test.

Although called for by the test plan procedure, the inability to establish a vacuum between the melter's process and overflow chambers precluded batch-pouring operations. The strategy of minimizing the use of water-bearing castable refractory in the repair of the melter may have contributed to the loss of vacuum isolation between these chambers. However, the tactic did prove successful in eliminating the operational threat of corrosive bus-bar failure that plagued both FY 1997 ESF tests (see Section 4.4.4).

Without the ability to establish a pressure drop between melt and overflow sections, the glass pool in the melt cavity could not be drawn down below its overflow point; consequently, melter operations during the Pantex Demonstration were conducted in a continuous overflow mode. This resulted in a continuous, low flow-rate glass stream discharge into the glass receipt canister. To minimize the potential of glass build-up in the overflow's spillway, due to glass-stream meandering, processing rates had to be maximized in order to maintain a reasonably hot pour stream. Consequently, operational plans to try to operate with a submerged center electrode were abandoned.

6.1.4 Data Collection

Most of the data from the furnace was collected and logged by the data acquisition and control system, which has been previously described. A list of all logged data points is provided in Appendix A. In addition, a number of test parameters were logged manually. These included instruments that did not have electronic output (flowmeters, pressure gauges, liquid levels, electrode positions, etc.), as well as logged data points, which were important for the operators to regularly monitor. This information was recorded hourly on data sheets. Data sheets were also used to record pertinent data regarding feed additions and sample collection.

6.1.5 Sample Collection

Sampling during the Pantex demonstration was complicated by the fact that radioactive materials were being processed. Since the glass produced during the test showed no evidence of smearable surface

contamination, sampling of this waste product was not restricted. However since hot batch pours could not be conducted due to vacuum isolation problems, glass sampling using a graphite boat was found to be unnecessary, as canisters could only hold ~30 lb of the loose-woven glass strands that collected in them. Consequently, samples were extracted from each full canister during change-out.

Off-gas system sampling was restricted to collection of EVS scrub liquor, baghouse solids, and non-condensable gases. However, since the baghouse filter assembly, due to its size, was located outside of the hood containment, no periodic samples of off-gas aerosol material could be collected during the test. An on-line gas chromatograph was used to obtain periodic analysis of the non-condensable melter exhaust gases. This gas data was primarily used to monitor oxygen levels in the melter, thereby allowing oxidative attack of the melter's graphite components to be controlled.

6.1.6 Analytical

Elemental analyses were performed by ICP/AES. Samples analyzed by ICP/AES must first be dissolved completely into solution. Acid soluble compounds (some of the feed chemicals) were dissolved in concentrated nitric acid or aqua regia (heated if necessary) and diluted to concentrations suitable for analysis. However most materials were dissolved according to ASTM Procedure C1317-95, "Dissolution of Silicate or Acid-Resistant Matrix Samples."

According to this procedure, the sample of material is ground until it passes through a 200-mesh (74- μm) sieve. A portion of the ground sample is then fused using either potassium hydroxide in a nickel crucible, or sodium peroxide in a zirconium crucible. Both fusions were performed for all samples to allow determination of all four of these elements and to provide replicate analysis of all other elements. The fused samples were dissolved in HCl and diluted in 2% nitric acid prior to analysis.

Because the dilutions required to reduce the concentrations of major constituents before using ICP/AES, the detection limits of minor constituents in the sample in many cases exceeded the trace concentrations in the sample. For this reason, glass samples were directly analyzed using x-ray fluorescence (XRF) spectrometry. This analytical technique was especially useful for determining the lead content of the melter's vitreous product.

Liquid scintillation counting techniques were employed in characterizing the tritium content of melter and off-gas system waste products. Because of the low penetrating nature of the tritium β , non-aqueous wastes were chemically dissolved before they could be counted. Because of the non-standard chemical nature of these solutions, internal calibration techniques were employed in characterizing the activity of these solutions.

The durability of the melter waste glass was also assessed using the TCLP. This procedure provides a standardized method for measuring the leach resistance of waste materials containing regulated hazardous materials. TCLP testing is necessary to demonstrate regulatory compliance when disposing of waste forms containing hazardous materials.

6.4 Operating Performance

A 4-day demonstration of the DC arc melter technology was conducted on April 13, 1998 through April 17, 1998, when 200 Pantex neutron generators were processed and successfully sanitized. The sanitization process involves feeding neutron generators along with appropriate glass-forming chemicals into a high temperature furnace that used a DC plasma discharge to melt and/or dissolve neutron generator constituents into molten glass and/or metal phases. The overall Pantex demonstration test can be broken down into three distinct segments, which were discussed in Section 6.3.3. An operational description of these test segments will now be discussed.

6.4.1 Test Segment 1

The first phase of the test, which commenced on April 13 at 0800 and concluded on April 14 at 0329, involved preparing the melter and off-gas system for operation and heating the melter to its operating temperature according to a previously established Safe Operating Procedure. During the day and part of swing shift on April 13, the resistive heaters were used to ramp-up the temperature of the melter's overflow section temperature to $\sim 500^{\circ}\text{C}$. When this had been achieved and all other melter support systems were operational (April 13 at 2045), the melter's arc was struck.

A plot of the furnace DC power over the course of the run is shown in Figure 6.2. As seen in this plot, the arcing power was increased over the first several hours to 20 kW as the voltage and current values stabilized at 80 volts and 250 amps, respectively. When the plenum temperature reached $\sim 250^{\circ}\text{C}$, feeding of the target glass chemicals commenced, which began the second phase of the melter demonstration.

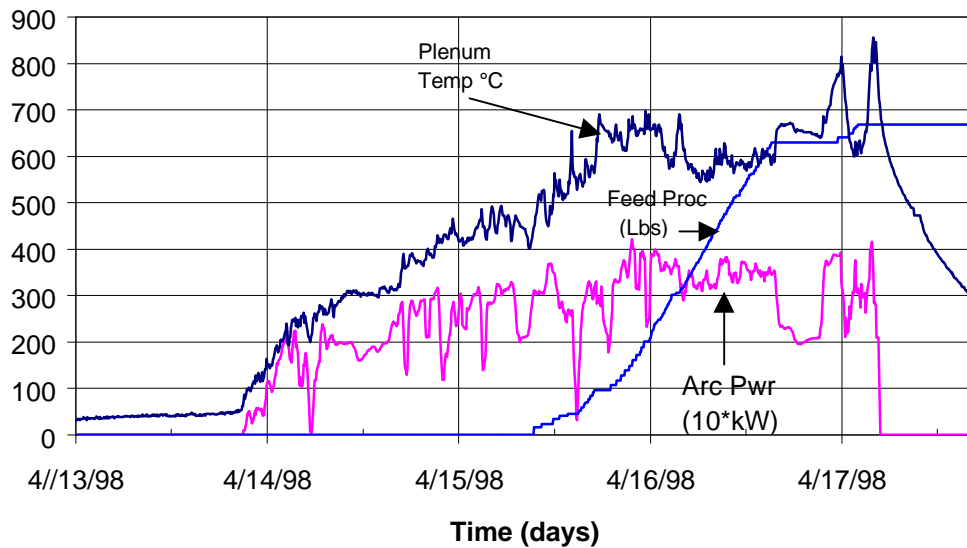


Figure 6.2. DC Arc Melter Operational and Processing Data

6.4.2 Test Segment 2

The second phase of the test was primarily concerned with preparing the molten bath into which the neutron generators would be incorporated. It also provided an opportunity to functionally test all necessary melter support functions before the commencement of phase 3, radioactive processing. The processing of the target glass chemicals did reveal significant functional deficiencies with the melter's large object feeder.

The problems encountered were both physical and electronic. The electronic difficulties involved the magnetic position sensors of the pneumatic ram that pushed the canisterized feed materials into the melter. For the most part, the electronic problem only created inconvenient delays, as the sequencing of the can feeder would only be interrupted by the fault. The physical problems, however, created significant canister jamming situations that could only be rectified by opening the system's protective airlock.

The source of the physical problems encountered was simply related to canister misalignment in the can feeder's air lock. The free-fall drop mechanism for introducing canisters into the airlock pipe (tee) resulted in canister alignment variations that would, under certain circumstances, jam the ram feeder during the delivery sequence. Various mechanisms were developed during the 2nd phase of testing to slow the canister's fall and to guide it into proper alignment. A decision was made to extend target glass feed processing in order to refine feeder design modification and to improve system reliability.

During this effort, the glass level in the melt chamber rose above the top of the overflow block and the first glass pour commenced. While trying to control this pour, it became apparent that a pressure differential could not be established between the melter's overflow section and its processing chamber (see Sect 6.3.3). This precluded the planned use of hot batch pours to transfer glass from the melter, which significantly complicated operations. In order to minimize the risk of developing a glass blockage in a continuous overflow mode, a priority had to be placed on maintaining high melter feeding rates. This placed additional importance on improving the reliability of the melter's can feeder. Refinements to the operation of the can feeder continued until all target glass feed canisters had been processed, whereupon the radioactive, 3rd and final phase of the test commenced.

6.4.3 Test Segment 3

On April 15 at 1025 the first neutron generator was fed to the melter. The processing of neutron generators continued in a more or less continuous manner until April 17 at 0245 when the 200th generator was fed to the furnace. However, the processing of neutron generators was slowed, during the initial 9 hrs of the radioactive portion of the test, by continued operational problems with the automatic feeding system. As a result of the time-consuming repairs and/or adjustments required to maintain the automatic feeding system, the average feeding rate over this period was less than 9 lb/hr. However, when the automatic system was replaced (April 15 at 1902) by a manual, gravity feed system, the processing rates increased significantly. During the ~21-hr period from April 15 at 1902 to April 16 at 1540, 75% of the neutron generators to be processed were continuously fed to the melter at a rate that maintained a ~90%

cold cap coverage of the melt pool (see Fig 4.8). Figure 6.3 graphically displays how uniformly consistent the processing rate was over this period where the average feeding rate achieved was 27 lb/hr. At the maximum processing rate achieved, a neutron generator was being processed every 6 minutes. This corresponds to a total (generator + glass-formers) hourly feed rate of 36 lb/hr. At an arc power of ~35 kW, this maximum processing rate could not be sustained, however, as excessive cold cap conditions were quickly produced. The project plan for the demonstration was based on a processing rate of 25 lb/hr or a neutron generator feeding period of 9-minutes.

With 25 neutron generators remaining, the processing campaign was suspended on April 16 at 1540 due to a blockage in the melter's overflow section. A slow change in waste glass viscosity apparently occurred during the processing of the 175 neutron generators, which caused ever increasing meandering of the continuously flowing glass stream as it dropped into the glass receipt canister (see Section 6.6). A buildup of glass below the overflow block finally choked off the transfer of melter glass. Attempts to clear the obstruction by increasing heater power to the overflow section failed and ultimately led to heater burnout when maximum power limits were used, as a last resort, to resolve the problem. Although the blockage could have been easily removed mechanically using an air-hammer and chisel, radiological safety concerns regarding the disruption of the airflow patterns in the process hood precluded the work from being performed.

While attempts to clear the overflow section progressed, efforts to initiate bottom draining of the melter were conducted. With 30 kW of power being supplied to the melter's freeze valve, metal draining could not be initiated. In order to increase temperatures in the proximity of the bottom drain, the melter's

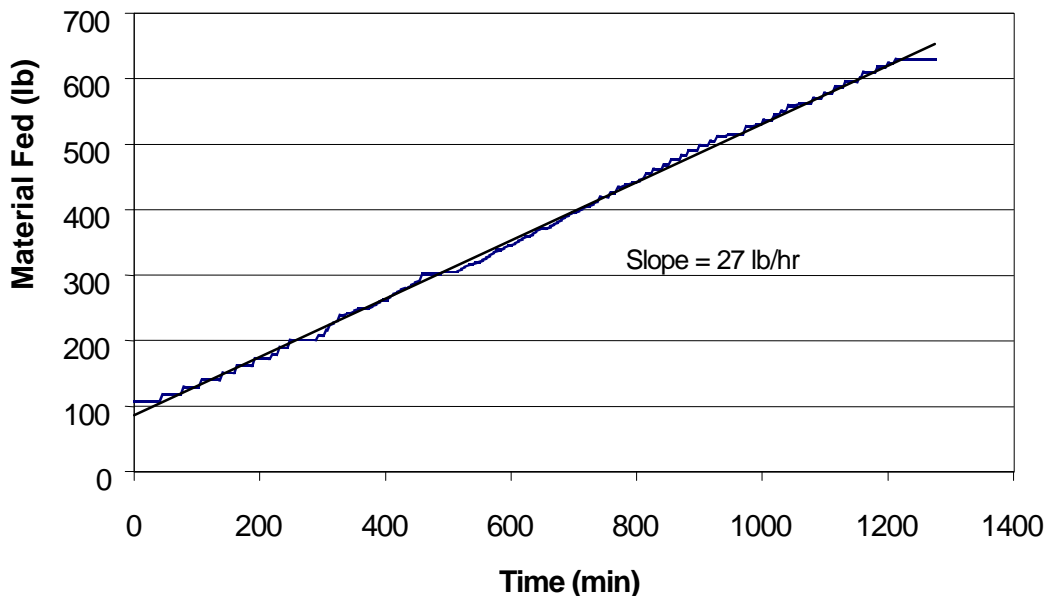


Figure 6.3. Steady-State Neutron Generator Processing Data

electrode was submerged and extended as far as possible into the melt cavity in an attempt to deliver more power to the bottom of the hearth and its drain port. Both internal and external heating of the melter's bottom drain area continued for several hours with no real success. Although very small drop-quantities of molten metal were observed to fall through the freeze valve during this heatup period, sustained flow from the melter could not be achieved.

With no available method to drain the melter, the remaining overflow heater was disabled and overflow cooling was increased to freeze the glass in the overflow transfer channel to preclude further glass transfers to the blocked overflow spillway. At 0115 on April 17, after the overflow temperature dropped below 1000°C, processing of the remaining 25 neutron generators resumed.

After all neutron generators had been fed to the melter, the furnace was operated at processing power levels (35 kW) for another 2 hours to ensure complete digestion of all feed materials. During this melter and glass pool heat up period, attempts to bottom drain the melt chamber continued, but without success. The melter's arc was finally extinguished at 0438 on April 17 after successfully processing and demilitarizing all 200 neutron generators, thereby satisfying all major project objectives and goals.

6.4.4 Post Test Melter Examination and Evaluation

The overflow section and bottom drain regions of the melter were examined after the melter had cooled down at the conclusion of the Pantex demonstration. As expected, the glass blockage occurred in the spillway below the overflow block. Meandering of the continuous-overflow molten-glass stream created the accumulation that finally blocked off the overflow section's spillway. No more than 6 inches of glass is believed to have accumulated in the 6 in.-diameter spillway.

Inadequate internal temperatures at or below the bottom of the melter's hearth were found to be responsible for the inability to bottom drain the melter's hearth. The obstruction (metal plug) in the graphite freeze valve was located midway through the 4 in. thick porous graphite slab that supports the melter's hearth. The construction details of this section of the melter are shown in Figure 3.4. Apparently the combined conductive heat transfers from the molten contents of the hearth and the heated portion of the freeze valve were insufficient to raise the temperature of the metal plug above its melting point. The unlined design of the melter's graphite hearth may have contributed to this cold bottom condition, as the arc's electrical current was not constrained to flow to the bottom of the hearth. No temperature information regarding this area of the furnace is available from testing data.

Two electrode segments were consumed throughout the 72-hour duration of melter operations. This consumption rate is consistent with previously reported, FY 1997 engineering-scale melter testing results.

6.5 Off-Gas Analyses

The chemical composition of neutron generators is fairly simple and is summarized in Table 6.1. The only chemically hazardous element present is lead, which, unfortunately, does possess semi-volatile characteristics. The first ESF test of FY 1997 clearly showed how important off-gas system losses for

lead can be. Consequently, the fate and behavior of this neutron generator component was of particular interest in the evaluation of the Pantex demonstration test.

The experimental results obtained demonstrated that feed component Pb partitions mainly to the off-gas system. Specifically 75% of the recovered Pb was found in the baghouse solids, and only 4% was incorporated in the melter's glass waste product. The remaining ~20% is believed to reside in the melter's unsampled metal phase.

Tritium represented the only radiological hazard associated with melter processing of neutron generators. Since melter waste products have very little capacity for this element or its oxide, complete release of this isotope to the melter's off-gas system was a project expectation. Moreover, since this isotope existed as a metal hydride in these neutron generator devices, it was further expected that the elemental chemical form would dominate the melter's tritium source term. Since the importance of tritium oxidation and exchange reactions during melter and off-gas system processing would be manifested by the tritium holdup in melter and off-gas system waste residuals, the specific activity of all collected waste streams were determined.

The radiological results obtained suggest that greater than a third of the tritium processed and released to the off-gas system was in the chemical oxide form. Moreover the aqueous EVS quench scrubber was, not unexpectedly, the major source of tritium accumulation. Specifically >15% of the total inventory of tritium released by the process was found to reside in the scrubber's aqueous media. Although a minor off-gas accumulation site, baghouse solids did exhibit the same specific activity as the EVS scrubbing liquor and, of course, the aqueous run-off of the HEME.

Off-gas system losses due to gross entrainment of feed was also investigated during the Pantex demonstration in order to compare containerized and bulk feeding techniques. All previous FY 1997 tests employed a bulk feeding method that continuously augered granular feed material into the furnace through the melter's lid. In the FY 1998 Pantex demonstration, granular feed materials were delivered to the melter in discrete canisterized packages.

Test results suggest that canister feeding may, indeed, reduce gross, off-gas system entrainment losses when compared to bulk melter feeding techniques. Total particulate off-gas partitioning measured during the target glass chemical feeding phase of the Pantex demonstration was determined to be 0.9%. Although attained under non-ideal processing conditions, this value is comparable to the best performance previously achieved when the melter was operated with a submerged arc and high cold-cap coverage during bulk feeding operations.

6.5.1 Baghouse Solids

The baghouse filter assembly described in Section 3.4.2 is the first off-gas device to treat the melter exhaust stream. This device is designed primarily to efficiently remove solid-state aerosols generated by the process. Having a 3 μ m pore size, the high temperature ceramic cloth filters quantitatively remove large diameter aerosols (i.e., entrained debris) but possess lower efficiencies for sub-micron fumes.

The processing of target glass feed during the 2nd segment of the Pantex demonstration provided an excellent opportunity to estimate feed entrainment losses associated with ESF containerized feeding operations. Neglecting the oxidizable, organic matter in the feed (canisters) and baghouse solids (pyrolyzed cellulose products), the aerosol mass partitioning to the off-gas system (baghouse filter assembly) was determined to be 0.9%. This value is comparable to a previous value obtained when the melter was operated with a submerged arc and high cold-cap coverage. All other previous ESF test segments produced significantly greater off-gas carry over values.

A comparison of baghouse solids and feed stream compositions in Table 6.4 shows a small degree of enrichment in elements that readily fume at melter operating temperatures. This suggests that both entrainment and boil-off mechanisms contributed to the observed off-gas system aerosol losses. This is quite reasonable since the processing of target glass feed in the current test was punctuated by nonsteady-state feeding conditions and low cold cap coverage. Furthermore since it has been previously demonstrated (see Section 4.1) that these process conditions act to increase off-gas partitioning, the low off-gas system losses sustained during this phase of processing suggests that the use of packaged or canisterized feed may significantly reduce gross melter off-gas losses relative to the bulk feeding alternative. However the feed packaging material (cellulose) introduces a considerable quantity of oxidizable material to the process flowsheet. Since the process was operated at low plenum oxygen levels (<1%), pyrolyzed organic material accounted for ~30 wt% of the baghouse solids collected during the nonradioactive processing phase of the Pantex demonstration. The addition of a secondary combustion chamber can, however, easily mitigate off-gas accumulations of pyrolyzed organic matter.

Despite the uniform feeding and high cold-cap coverage conditions that existed during most phases of neutron generator processing, significantly greater off-gas system losses of particulate matter occurred than was earlier experienced. This was primarily due to the impact of the semivolatiles: Pb and Zn. Although the presence of significant quantities of Pb in the process flow sheet were recognized, the magnitude of Zn in the neutron generators was totally unanticipated. Specifically these elements accounted for a major fraction of the inorganic material present in the baghouse solids that were collected at the conclusion of radioactive processing.

In addition to the these major semivolatile constituents, the presence of Ag and K in these off-gas solids suggest these unaccounted for semivolatiles must also be trace elemental constituents of neutron

Table 6.4. Baghouse Solids Composition (2nd segment)

Element	wt%	
	Baghouse	Flowsheet
Al	2.3	7.0
Ca	13.8	10.8
Fe	11.8	11.4
Na	7.4	4.5
Si	10.9	23.0

generators. The overall composition of the baghouse solids collected during neutron generator processing are compared with the feed stream flowsheet values in Table 6.5. This comparison clearly shows that fuming losses of semivolatile constituents totally dominate the overall melter effluent emission source term under the processing conditions (exposed arc/large cold-cap) used during this demonstration.

As mentioned earlier overall melter losses of particulate matter were significantly greater during neutron generator processing than during the non-radioactive operations (i.e., 2nd test segment). The difficulty in determining the overall particulate partitioning to the off-gas system during this test segment is accounting for the magnitude of pyrolyzed organic material that is present in these solids. Since the major cation constituents of these solids are probably not present as oxides, it is not necessarily justifiable to assume that the apparent sample weight losses during analytical fusion operations are associated with the organic fraction of the sample. However, lacking any better approach, this method has been used to estimate an overall off-gas aerosol partitioning value for inorganic feed stream components. Neglecting both the mass of cellulose packaging material and the organic neutron generator constituent, the off-gas particulate partitioning value estimated for the radioactive processing phase of the Pantex demonstration is 4%.

Although this estimated loss fraction is a factor of 4 greater than that observed during processing of target glass feed chemicals (2nd phase of testing), it is comparable to the overall losses sustained during the first ESF test in FY 1997, which used bulk feeding techniques (see Section 4.8.1). Since this FY 1997 test did not possess the high semivolatile feed stream loadings of the current test, the results of the 3rd segment of the Pantex demonstration also suggest that melter entrainment losses can be significantly reduced when feed stream materials are canisterized. However the magnitude and bulk of pyrolyzed organic material can create collection difficulties for the baghouse filter assembly if plenum or suitable

Table 6.5. Baghouse Solids Composition (3rd segment)

Element	wt%	
	Baghouse	Flowsheet
Ag	0.7	
Al	0.6	6.7
Ca	6.3	11.6
Co		0.5
Fe	2.6	11.4
K	2.8	
Na	2.2	4.7
Ni	0.1	0.9
Pb	24.7	1.1
Si	4.1	22.2
Ti	0.02	0.2
Zn	21.1	
Zr	0.1	0.5

afterburner oxidation is not used to reduce off-gas loadings of combustible effluents. During the processing of neutron generators, unoxidized organic matter produced a large volume of low-density material that influenced the composition and physical nature of the baghouse waste stream. Specifically, over 26 lb of baghouse solids, occupying a volume greater than 20 gallons, collected during the radioactive phase of melter processing.

To determine the tritium content of the baghouse solids, a known weight of collected material was dissolved in aqua regia, and diluted to a fixed volume. An aliquot of this solution was then mixed with a scintillator and counted using liquid scintillation techniques. The resultant tritium concentration data was then used to establish the specific activity of the baghouse solids. At $2\mu\text{Ci/g}$, the inventory of tritium contained in the baghouse solids collected during the processing of neutron generators was determined to be 23 mCi.

The chemical form or forms of tritium in the baghouse waste material has not been directly established. However the most likely candidates are tritiated water and labeled organic materials. Oxidation of thermally liberated tritium by glass oxides will readily form tritiated water, which certainly was a project expectation. Exchange reactions between organically bound hydrogen and tritium will also produce tritiated hydrocarbons (labeled organics) to a lesser extent. Either one or both sources are completely compatible with the measured specific activity of the material, as very small quantities of tritiated compounds are required to achieve the levels of activities observed.

In particular, only a nanogram (10^{-9} g) of HTO per gram of material would be required to create the observed specific activity of this particulate waste product. The fact that the temperature of the baghouse filter assembly was maintained at or above 250°C during radioactive processing is not a mitigating factor, as such exceeding small quantities of moisture are involved. Although tritiated water is the most likely source of activity in these baghouse solids, labeled organic matter may also be present, but in much smaller quantities. Tritium exchange reactions are expected to be significantly slower than the rate for direct oxidation.

6.5.2 Ejector Venturi Scrubber

The EVS is an aqueous contact scrubber in the melter's off-gas system that serves to quench the process off-gas stream, scrub-out condensable gases, and remove airborne particulate matter. The aqueous scrubbing media was maintained at or below 40°C throughout the duration of the Pantex demonstration and thus provided a very efficient exchange function for process-generated, tritiated water (vapor) emissions. Although an efficient HTO exchanger, the EVS did not provide high removal efficiencies for off-gas aerosols penetrating the upstream baghouse filter assembly due to their small aerodynamic size distribution. Consequently solids buildup in the EVS tank were not significant and, indeed, inconsequential when compared with the baghouse catch. Analyses of the EVS scrubbing liquor collected during the radioactive portion of the Pantex demonstration campaign are summarized in Table 6.6 along with compositional data on solids collected from the EVS tank after the test.

Only primary (wt% $> \sim 1\%$) elements are listed in this tabular compilation and these data are compared with the nominal composition of the process water used to charge the scrubber. Clearly the cations with

Table 6.6. EVS Effluent Compositional Data

Element	EVS Concentration (ppm)				Water Blank	EVS Solids Cation wt%
	4/16 0655	4/16 1300	4/17 0450	Average		
Ag						1.0
Al						6.1
Ca	290.4	265.7	316.6	290.9	20	47.6
Cd	0.3	0.4	0.8	0.5		6.4
Fe	0.1			0.1	0.04	14.6
K	18.6	14.6	17.6	17.0	1.4	2.9
Mg	30.9	29.5	37.5	32.6	4.7	1.9
Na	46.0	42.6	51.1	46.6	4.1	0.9
Nd	0.8	0.8	0.7	0.8		1.4
Pb					0.002	5.9
S	92.7	84.4	101	92.7		0.3
Si	17.0	16.9	21.7	18.6	5.9	5.3
Zn	1.0	0.9	1.4	1.11	0.06	1.4
HTO:μCi/cc	12.5	12.3	7.7	12.4	0	

major mass fractions in the EVS scrubbing liquor belong to natural constituents of the hard water used. Evaporative concentration of these elements during previous as well as current testing is most likely responsible for their mass buildup in the scrubber solution.

Similarly, the presence of volatile and semivolatile elements (e.g., Ag, Cd, Pb, S, and Zn) in soluble and insoluble EVS sampled matter can also be attributed to current as well as legacy waste residuals from previous ESF testing. Unfortunately, individual test contributions to the observed EVS data cannot be established because of insufficient historical analytical data. However, it can be easily shown that the cumulative masses of current flowsheet elements collected by the EVS are negligible in comparison to their presence in other process waste streams.

Unlike the other semi-volatile/volatile effluents listed in Table 6.6, the tritium constituent of the EVS scrubbing liquor is due exclusively to the Pantex demonstration. The two EVS sample solutions collected during the continuous processing period of the test (April 15 at 1902 to April 16 at 1540) suggest that at an average feeding rate of 27 lb/hr, an off-gas flow rate of 80 SCFM, and a scrubbing liquor temperature of 40°C, the tritium concentration of the EVS solution equilibrated at 12.4 μCi/cc. Evaporative losses and resultant dilution that occurred during the 8-hr process suspension period (April 16 at 1540 to April 17 at 0115), are responsible for the loss of tritium activity in the EVS sample collected at the conclusion of the test.

The equilibrated EVS tritium concentration can be used with processing rates, off-gas flow rates, scrubbing solution temperature, and the decay-corrected, bounding value for tritium in neutron generators

to estimate the minimum fraction of tritium converted to an oxide under the DC arc melter operating conditions. Assuming that 1) the evaporation process dominates EVS scrubbing liquor losses, 2) the off-gas exhausting the EVS is water-vapor saturated at 40°C, 3) the tritium vapor exchange in the EVS is quantitative, and 4) the decay corrected tritium content of the neutron generators processed are 40 mCi, the minimum fraction of tritium released by the process in the oxide form is estimated to be one third. Factors such as scrubbing liquor entrainment losses, non-quantitative exchange efficiency, baghouse tritiated water losses, and an actual neutron generator tritium content of <40mCi, will, if accounted for, act to increase the estimated fractional yield of process liberated tritiated water.

Because of the relatively large fraction of tritiated water released to the off-gas system by the DC arc process, a significant inventory of tritium will, in general, accumulate in any aqueous quench scrubber used to support the process. The actual inventory established under steady state conditions would, of course, be directly dependent on processing rate and off-gas processing conditions. For the Pantex demonstration, the equilibrated quantity of tritium that accumulated in the EVS during steady-state processing was 1.2 Ci. This inventory represents 15% of the total bounded value (8.1Ci) of tritium processed during the Pantex demonstration, and, therefore, represents a lower accumulation limit. However, no matter what the actual steady-state concentration becomes, the EVS will be a major off-gas system waste stream source for process tritium, as its cumulative inventory is 50 times that of the baghouse solids previously discussed.

6.5.3 HEME and HEPA Filter

No significant liquid waste stream volume was generated by the HEME during the Pantex demonstration. The water carry-over from the EVS was nominally counterbalance by off-gas evaporation. The HEME's seal pot fluid revealed only very low solids loadings when bottom drained from the vessel at the conclusion of the test. A sample of this fluid with suspended solids was analyzed and the results are summarized and compared to a similar suspension extracted from the EVS in Table 6.7.

The HEME slurry and the EVS suspension share common characteristic of being dominated by hard water constituents and semivolatile elements. Although the HEME seal pot slurry sample composition cannot be considered totally representative of the insoluble materials collected by the HEME filter element, these data do provide a semi-quantitative indication of the effluents being abated by this high efficiency filtration device, i.e., semi-volatiles.

Since the only source of water for the HEME's seal pot throughout the Pantex demonstration was EVS mist carry-over, one would expect similar tritium concentration in both off-gas system devices, and this is, indeed, what was found. The activity levels indicated in Table 6.7 are lower than concentrations previously described due to makeup water dilutions of the EVS scrubbing liquor during the 12-hr melter shut down period at the conclusion of the melter test. Because the HEME's seal-pot volume is small (0.2 gal) relative to the EVS tank reservoir (25 gal), the tritium holdup in this device is negligible in comparison to the EVS inventory.

Table 6.7. HEME/HEPA Effluent Compositional Data

Element	wt% of Major Detected Elements		
	HEME Slurry	EVS Slurry	Post HEME Pipe Deposits
Ag	0.2	0.8	1.5
Al	0.5	5.0	1.2
Ca	50.7	49.4	14.6
Cd	3.1	5.2	0.7
Cr	0.1	0.4	3.1
Fe	2.7	11.9	28.9
K	4.7	3.0	
Mg	5.5	2.7	0.5
Na	10.4	2.5	12.4
Nd	0.3	1.1	1.4
Pb	0.2	4.8	5.9
S	15.6	3.6	0.3
Si	3.6	5.0	5.3
Zn	0.7	1.2	1.4
HTO:μCi/cc	1.8	1.9	

Post-HEME pipe smear samples were also collected at the conclusion of the Pantex demonstration to obtain nominal compositional information regarding the condensed phase effluents penetrating the HEME and accumulating on the final off-gas HEPA filter. Beyond pipe corrosion products and hard water constituents, the residue samples were found to contain significant quantities of the flowsheet semivolatiles Ag, Pb, and Zn.

6.5.4 Melter Exhaust Gas Composition

Because of the vulnerability of exposed graphite components (crucible and overflow block) in the newly rebuilt ESF to oxidative attack, an on-line gas chromatograph was used throughout the Pantex demonstration to periodically monitor the composition of non-condensable gases present in the melter's plenum. Maintaining a plenum oxygen concentration below 3% was a necessary operation constraint to control corrosion rates of these critical melter components. The functional dependence of plenum oxygen concentration upon melter vacuum was measured at a fixed nitrogen injection rate of 30 SCFM prior to Pantex testing. The results obtained are summarized for various levels of vacuum, measured in inches of water column ("wc), in Table 6.8.

Based on this initial data and subsequent analyses conducted during the processing campaign, melter operations were conducted at a nominal 0.5"wc plenum vacuum.

Table 6.8. Plenum Oxygen Content (%) at Various Levels

Melter Vacuum	0.5"wc	1.0"wc	2.0"wc
% Oxygen	0.72	1.32	5.45

In addition to the oxygen concentration data, the gas chromatograph also provided non-condensable melter exhaust gas compositional data during all phases of testing. Table 6.9 summarizes the average data collected during the processing of target glass chemicals (Test Segment 2) and the neutron generator feed stream (Test Segment 3).

The compositional differences between the two processing phases are due primarily to feeding rate and organic loading parameters. No evidence for the presence of nitrogen oxides could be found in any of the chromatograms generated, although quantification of these effluents would have been difficult with the chromatographic columns employed.

Table 6.9. Average Melter Exhaust Composition of Process Generated Gases (mole %)

Process Segment	H ₂	O ₂	CO	CO ₂	CH ₄
Glass Chemicals	0.22	0.24	0.12	0.15	--
Neutron Generator	3.1	0.53	2.5	1.0	0.39

6.6 Slag Analysis

Having to operate the melter in a continuous overflow mode created cold pouring conditions that resulted in significant stringing or bird nesting conditions in the glass receipt canisters. Consequently, only about 30 lb of glass (12% of capacity) could be collected in each glass canister. In all, 18 glass canisters were produced during the Pantex demonstration, and glass samples were collected from each can.

The time dependent composition of the slag produced during the processing of the neutron generators is summarized and compared to flowsheet expectations in Table 6.10. The compositional variances of major glass forming oxides from their flowsheet values were not significant and were primarily caused by the unexpected loss of iron oxide from the glass. Ferric oxide, as previously discussed, was added to oxidize the elemental aluminum present in the neutron generator feed stream. The weight percentage of hematite used was based on a unity change (ferric to ferrous) in iron's oxidation state. It is clear that, unlike the bench-scale scoping tests, the iron oxide additive was being reduced to its elemental state under the operating conditions of the Pantex demonstration.

The degree to which iron oxide was being reduced to its elemental state, moreover, increased throughout the processing campaign as is graphically illustrated in Figure 6.4. The continual loss of iron

Table 6.10. Pantex Waste Glass Compositional Data

Oxide	wt%									
	Can #3	Can #4	Can #6	Can #8	Can #10	Can #12	Can #14	Can #16	Can #18	Flowsheet
SiO ₂	52.89	53.44	55.20	54.79	55.28	55.25	55.44	54.96	54.50	47.06
Fe ₂ O ₃	10.24	9.21	6.18	4.85	4.53	4.35	4.31	3.73	2.67	16.44
CaO	16.05	16.34	16.88	17.59	17.25	17.74	17.36	18.07	19.77	16.07
Al ₂ O ₃	14.90	15.15	15.88	16.54	17.43	17.08	16.85	17.83	18.33	13.34
Na ₂ O	5.29	4.72	4.10	3.96	3.54	3.41	3.31	3.33	3.60	2.80
PbO		0.08	0.06	0.10	0.04	0.05	0.03	0.03	0.02	1.30
NiO	0.04	0.03	0.06	1.44	0.04	0.03	0.03	0.03	0.03	1.25
Co ₂ O ₃			<1.4E-02		<8.5E-03	<1.2E-02	<8.0E-03	<9.2E-03	<9.0E-03	0.73
ZrO ₂	0.45	0.43	0.56	0.78	0.81	0.87	0.85	0.96	1.01	0.63
TiO ₂	0.05	0.06	0.07	0.08	0.08	0.08	0.09	0.09	0.09	0.37
	Undocumented Constituents									
Cr ₂ O ₃	0.072	0.078	0.094	0.104	0.194	0.277	0.278	0.327	0.338	
MgO	0.015	0.136	0.132	0.035	0.125	0.149	0.150	0.135	0.155	
MnO	0.069	0.061	0.068	0.060	0.061	0.066	0.067	0.070	0.069	
CuO	0.010	0.048	0.009	0.011	0.037	0.046	0.043	0.050	0.044	
SrO	0.023	0.024	0.030	0.025	0.026	0.027	0.027	0.027	0.028	
ZnO			0.017		0.022	0.033	0.014	0.012	0.014	
Ag ₂ O	0.008	0.004	0.009	0.010	0.010	0.011	0.010	0.008	0.008	
La ₂ O ₃	0.001	0.016	0.012	0.001	0.001	0.013	0.012	0.001	0.012	

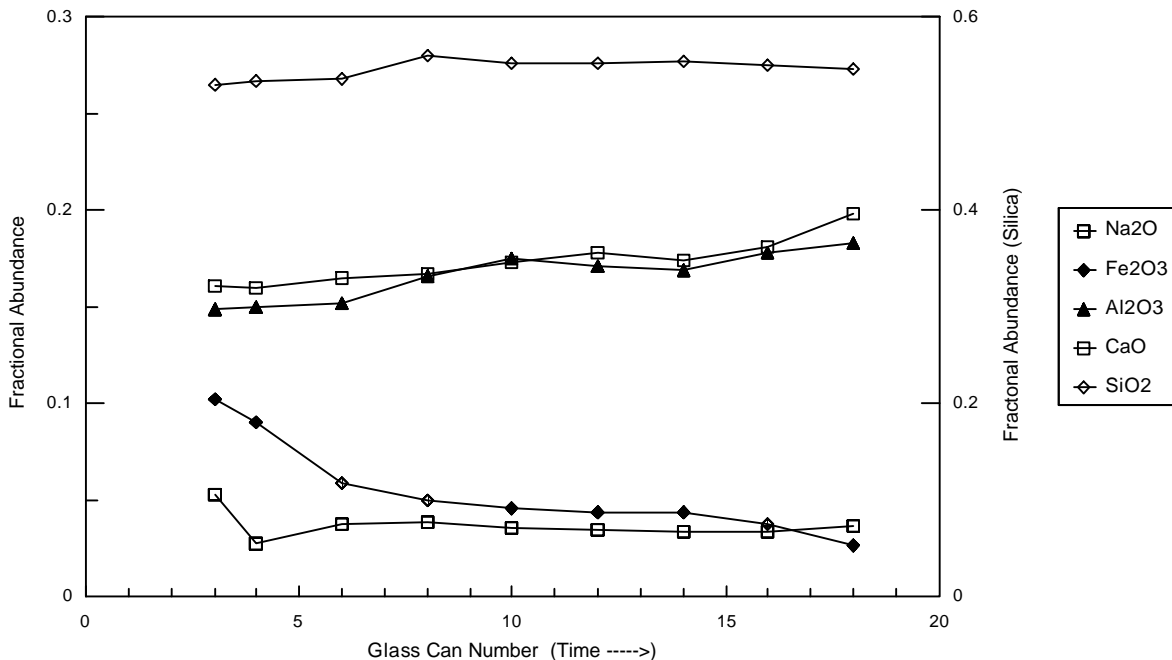


Figure 6.4. Temporal Compositional Changes in Pantex Slag

oxide from the process slag throughout the duration of the demonstration resulted in a corresponding compositional increase in all other glass forming oxides, as is shown in Figure 6.4.

Like Fe_2O_3 , the data in Table 6.10 also shows that the glass composition of PbO also decreased steadily throughout the Pantex test, presumably because of reduction. But unlike Fe, the loss of Pb was primarily to the off-gas system, although significant metal phase losses are also indicated (see Section 6.7.2). Partitioning to the glass could only account 4% of the Pb fed to the melter.

The processing behavior of the semi-volatile element Zn appears to be very similar to that of Pb. Although the Zn composition of neutron generators was undocumented, its impact, like Pb, upon the off-gas system was very significant. Over 20% of the 13 kg mass of particulate effluent collected by the off-gas system's baghouse filter was due to Zn. Without knowing the mass of Zn fed to the melter, the off-gas loss fraction of this element cannot be determined exactly. However based upon its previously determined plasma-arc processing behavior^(a) and the fact that glass accumulations account for only 2% of that found in baghouse solids, it is likely that off-gas system losses were essentially quantitative. Assuming this to be the case, a compositional estimate for Zn in neutron generators can be derived from the available off-gas and glass data. The resultant projected weight percent value for Zn in the neutron generator tubes processed is 3.2 %.

(a) March 1988 draft report, *Bench-Scale DC Arc Furnace Testing Using Simulated INEEL Sludge and SRS Debris Waste Feeds*, Pacific Northwest National Laboratory, Richland, Washington.

The slag compositional data for the non-volatile Ti and Zr feed constituents are also summarized in Table 6.10. Although these data don't compare very well with flowsheet expectations, there may be good reasons for the observed discrepancies. The presence of lead zirconium titanate material was the only documented source of Ti and Zr in neutron generators. Moreover the empirical formula used to provide this documentation implicitly indicated a 1:1 abundance ratio for these elements. However this may not reflect reality as this material, being a solid solution, has an infinite variability with regard to this abundance ratio (Hench and West 1990). To complicate matters further, the quantity of tritium getter material, Ti and/or Zr, assumed to be present in the neutron generators to be processed was never documented. Consequently the flowsheet values listed in Table 6.10 are only estimates based on the best available data provided to the project.

Beyond the actual weight percent values for Ti and Zr, the time dependent composition changes of these elements in the melter generated glass can provide interesting process insights. Since these elements were not present in the target glass produced to dissolve neutron generator components, the concentrations of these elements, if fully dissolved and incorporated in a uniformly mixed homogeneous glass, should rise exponentially [$C_{\infty} (1 - e^{-t})$] to a steady-state asymptote (C_{∞}). They do not as is clearly shown in Figure 6.5.

Since all past DC arc melter testing, bench- as well as engineering-scale, has shown quantitative partitioning of Ti and Zr to the glass,^(a) the temporal compositional changes shown in Figure 6.5 indicate a non-ideal stirred-tank condition and/or a glass assimilation problem for these feed constituents.

Although the glass compositional data for major constituents in Table 6.10 suggests uniform mixing in the melt cavity was occurring, the quality of the slag produced throughout the test was indicative of a significant processing problems. Specifically, phase separated slag was produced throughout the entire duration of the neutron generator processing campaign. However clear, single-phase glass was also contemporaneously produced with the phase-separated product.

Examination of the phase-separated slag showed it to be microscopically inhomogeneous. X-ray fluorescence analyses of the major constituents in ungranulated glass samples produced results that could easily vary by a factor of 2. However, whenever the macroscopic composition of clear glass was compared to that of contemporaneous phase separated slag, the results were found to be indistinguishable. Indeed, correlation coefficients of all comparisons made were well within ± 0.02 of unity. Consequently, it appears that a well-stirred tank of multi-phase slag was being produced throughout the entire duration of the neutron generator processing campaign.

Apart from the major undocumented Zn constituent in neutron generators, there were several other elements present in the waste glass that were undetected in the target glass blank. The more abundant of these constituents, Cr, exhibits the same general composition growth curve as Zr. The remaining elements exhibit a rather flat growth curve. The fact that these undocumented glass constituents are real and not analytical artifacts has been independently established by both ICP/AES and XRF analytical

(a) March 1998 draft report, *Bench-Scale DC Arc Furnace Testing Using Simulated INEEL Sludge and SRS Debris Waste Feeds*, Pacific Northwest National Laboratory, Richland, Washington.

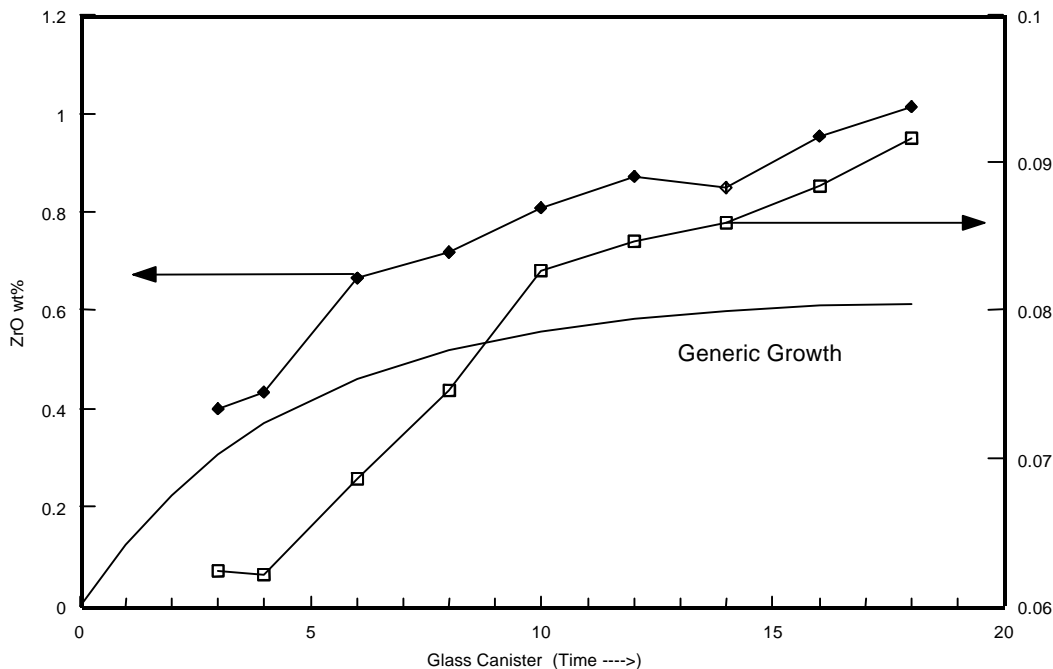


Figure 6.5. Temporal, Glass Compositional Changes of Ti and Zr

techniques. Co is the only known flowsheet constituent that could not be detected in the waste glass. Consequently, lower detection limits established by XRF analysis, have been assigned to this element in Table 6.10.

The specific activity of the melter's glass product was assessed by dissolving this glass and counting the resultant solution using liquid scintillation techniques. Indeed, the results indicated a residual low-level tritium content of $50\eta\text{Ci/g}$. Assuming the source of the activity is due to residual water in the glass matrix, the maximum quantity of tritiated water (HTO vs T_2O) that would have to be present to account for this activity is: 3.4×10^{-11} wt%. Since ppm quantities of water are common in melter glasses, this assumption is quite compatible with the observed specific activity value.

Glass samples collected at the mid point and end of the neutron generator processing campaign were also subjected to the standardized TCLP to determine if the waste glass would be classified as hazardous-mixed or simple low-level waste. The TCLP procedure is designed to establish the leachability of all EPA-declared (Environmental Protection Agency) hazardous elements that may be incorporated in waste materials to be disposed of. If test limits for one or more of these hazardous elements is exceeded, then the waste is declared hazardous and must be disposed of in specially designed and licensed repositories. The results obtained from TCLP testing of Pantex generated glasses are summarized in Table 6.11.

Because the levels of hazardous elements in the Pantex waste glass were quite low, leachate concentrations were found to be orders of magnitude below the regulatory limits. On the other hand, the level of Pb was so high (25 wt%) in the melter's baghouse solids, TCLP testing of this particulate matter was not attempted. Therefore, this off-gas system residual was disposed of as hazardous-mixed waste.

Table 6.11. TCLP Leachate Concentrations from Pantex Waste Glass

Element	Limit ($\mu\text{g/cc}$)	Concentration ($\mu\text{g/cc}$)	
		Mid Sample	End Sample
Ag	5	<0.008	<0.008
Cd	1	<0.011	<0.011
Cr	5	0.013	0.023
Pb	5	0.092	0.045

6.7 Mass Balance and Partitioning

Although the primary objective of the Pantex demonstration was to demilitarize neutron generators and to evaluate the ability of primary melter waste residuals to incorporate and immobilize hazardous feed stream constituent, characterizing the fate and behavior of all process components is necessary in evaluating operational realities and processing constraints. Toward this end mass balance calculations have been performed for the 3rd segment of this demonstration during which time the 200 neutron generators were processed. It must be noted that these calculations are limited by uncertainties in actual feed stream composition and radiation protection constraints imposed upon sampling and analyses activities during and after testing.

6.7.1 Overall Mass Balance

A gross or overall mass balance considers the total masses of the feed material, the waste products, and off-gas streams without regard to individual elements. Measured quantities include the mass of feed added to the system, the mass of slag product drained from the furnace, and the mass of off-gas solids collected. The mass of volatile species lost to the off-gas is based on the measured properties of the feed and off-gas system waste residuals. Figure 6.6 presents the overall mass balance for the 3rd phase of the Pantex demonstration during which time the 200 neutron generators were processed.

The measured difference between the derived melter input and output streams, 76 lb, can be ascribed to material accumulation in the melter's unmeasured molten metal phase. Indeed significant reductive losses of Fe from the slag phase did occur as reported earlier. As will be seen in the following section, the actual projected losses of slag phase Fe to the melter's molten metal phase represents a large fraction of the accumulation predicted by the simple mass balance calculation discussed above. On the basis of the average Fe content of the slag waste product, ~50 lb of Fe appear to have accumulated in the melter's metal phase over the duration of the Pantex demonstration.

To estimate solids partitioning to the off-gas system, as discussed previously, the masses of cellulose packaging material and the organic neutron generator constituent in the feed stream were neglected and the baghouse solids were corrected for the presence of organic and/or volatile constituents. The results obtained suggest a relatively large 4% loss of inorganic matter to the off-gas system. This is in stark contrast to the 0.9% loss fraction experienced during non-radioactive operations (i.e., 2nd test segment)

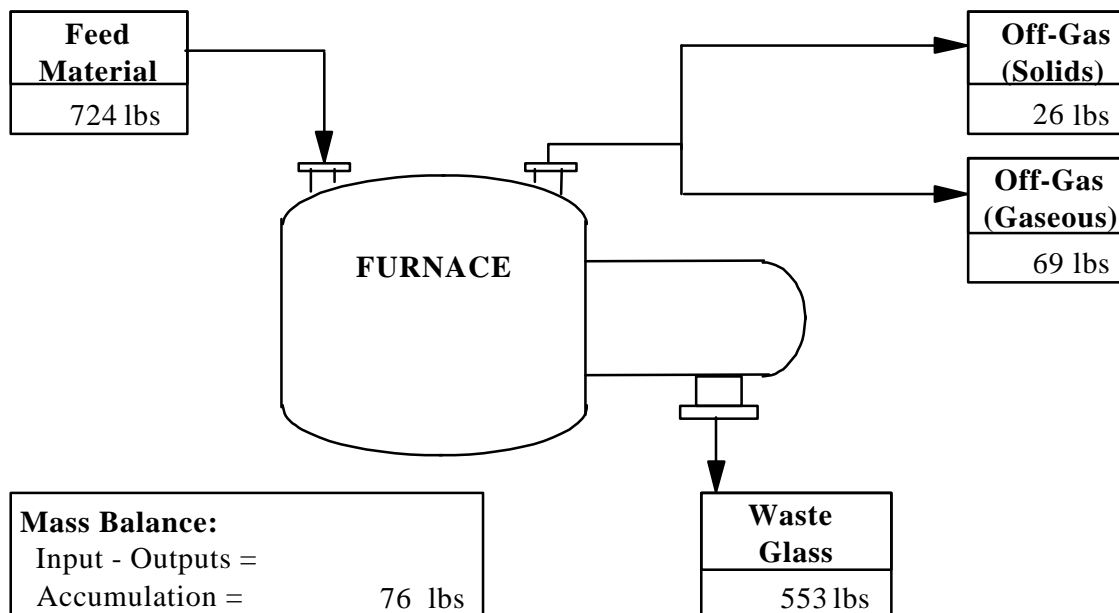


Figure 6.6. Pantex Demonstration Mass Balance Processing Data

when melter target glass was being produced. The relatively large loss of performance sustained during the 3rd test segment is totally attributable to the presence of feed stream semi-volatiles (i.e., Pb and Zn).

6.7.2 Partitioning of Flowsheet Constituents

The available (average) compositional information of the melter's feed stream, glass product, and off-gas wastes were combined with the overall masses of these constituents to estimate process partitioning of flowsheet constituents. Table 6.12 presents the mass balance data for the 3rd test segment during which time the 200 Pantex neutron generators were processed. The estimated error in reported values is nominally $\pm 10\%$ provided that corresponding compositional data is correct.

Table 6.12. Flowsheet Partitioning Data

Element	Total Mass (lb)			% Partitioned To		Total %
	Feed	Glass	Off-Gas	Glass	Off-Gas	
Al	47.5	48.8	0.10	102.8	0.2	103
Ca	74.2	69.0	1.27	93.0	1.7	95
Co	3.9	<0.06	0.00	<1.4	0.0	<2
Fe	75.2	21.5	0.62	28.6	0.8	29
Na	13.6	16.1	0.59	118.0	4.3	122
Ni	6.6	0.8	0.02	12.6	0.3	13
Pb	8.1	0.3	6.08	3.5	74.7	78
Si	142.2	141.4	0.97	99.4	0.7	100
Ti	1.9	0.3	0.00	13.6	0.2	14
Zr	3.6	3.1	0.02	85.4	0.4	86

The mass balance data for the major glass constituents except for Fe and possibly Na are all quite reasonable. The magnitude of the loss of Fe from the product glass during neutron generator testing, as discussed in the previous section, is clearly demonstrated in these data. Only 1/3 of the iron fed to the melter can be accounted for in these documented process streams. Moreover, these data as well as the information provided in the previous off-gas system discussion clearly indicate that reductive loss and subsequent accumulation in the melter's molten metal phase is responsible for the reported mass balance deficit of this feed stream constituent.

Similarly, the low recovery of Ni and Co is also most certainly caused by accumulation within the melter's undocumented molten metal phase. Previous bench^(a) as well as engineering-scale DC arc melter tests have shown Ni to partition almost exclusively to the metal phase. Similar behavior would also be expected from chemically similar Co.

Unlike the previous iron-alloying elements, the non volatile elements, Ti and Zr, have been shown by past DC arc testing data to strongly accumulate in the melter's slag phase. The current results for Zr are consistent with this expectation, but those for Ti are not. Since Ti is a non-volatile and it isn't reasonable, on the basis of past data, to assume any significant accumulation in the melter's metal phase, the low recovery of Ti can only be explained by either assuming that constituent assimilation problems were encountered during processing, or that constituent flowsheet information is incorrect. Since DC arc melter-processing problems involving Ti have never been previously reported, the apparent low recovery of this element is probably due to inaccurate compositional information.

The presence of lead zirconium titanate material was the only documented source of Ti and Zr in neutron generators. Moreover the empirical formula used to provide this documentation implicitly indicated a 1:1 abundance ratio for these elements. However this may not reflect reality as this material, being a solid solution, has an infinite variability with regard to this abundance ratio (Hench and West 1990). To complicate matters further, the quantity of tritium getter material. Ti and/or Zr, used in the neutron generators to be processed, was not documented. Consequently the flowsheet values listed in Table 6.10 are only estimates based on the best available data provided to the project.

From the above, it also follows that the good mass balance achieved for Zr may just be fortuitous. Indeed, the Zr glass composition changed throughout Pantex campaign, and its final recorded concentration was 60% greater than the flowsheet value. The averaging process can, at times, obscure reality, which may very well be the case in this particular situation.

The data involving Pb, although not tightly balanced as Zr, is probably more definitive than this non-volatile element. The fate and behavior of Pb has been very well characterized in previous bench- and engineering-scale DC arc melter tests.^(a) Specifically, high off-gas losses due to semi-volatile fuming would be ordinarily expected unless a high cold-cap coverage was maintained under submerged electrode processing conditions. Since submerged electrode operations were not used, in order to maximize

(a) March 1988 draft report, *Bench-Scale DC Arc Furnace Testing Using Simulated INEEL Sludge and SRS Debris Waste Feeds*, Pacific Northwest National Laboratory, Richland, Washington.

processing rates, low retention of lead (~200ppm) in the process glass resulted. Consequently, most of the Pb, (75% of the flowsheet value) was accounted for in the baghouse solids as is indicated Table 6.5.

Previous bench-scale testing^(a) has clearly shown that as much as 20% of the Pb fed to DC arc melter can accumulate in the melter's molten metal phase. This explanation if accepted and adopted could, therefore, easily close Pb's mass balance. However, because of the large volume of accumulated off-gas solids collected (~20 gal) and the resultant difficulty of representatively sampling such a large radioactive-waste stream, the unaccounted for Pb could also be present in these baghouse solids. Since it was not possible to sample the melter's metal phase or improve upon the radioactive-waste sampling techniques used for the baghouse solids, closure of Pb's mass balance could not be unequivocally resolved. What is certain, however, is that the vitreous product of the DC arc process could only accommodate (on the average) a maximum of 5% of the Pb fed to the melter under the processing condition used during the Pantex demonstration.

Tritium, unlike the other hazardous constituents of neutron generators, was not expected to be retained by process waste forms to any significant extent and its accumulations in off-gas waste streams, which would be determined by process dependent oxidation and exchange reaction rates, was also expected to be small. Table 6.6 confirms this expectation, although a greater oxidation rate created a larger than anticipated tritium holdup in the off-gas system's quench scrubber. Since the actual quantity of tritium in neutron generators is classified, minimum partitioning values, based upon the decay corrected bounding value of the tritium processed, had to be reported in the mass balance table. Based on these data less than 85% of the tritium process was directly released to the process stack.

(a) March 1988 draft report, *Bench-Scale DC Arc Furnace Testing Using Simulated INEEL Sludge and SRS Debris Waste Feeds*, Pacific Northwest National Laboratory, Richland, Washington.

7.0 Economic Analysis of the DC Plasma Arc Melter

The cost a graphite electrode DC arc furnace system capable of processing heterogeneous mixed waste is presented in this section. This cost estimate was prepared not only as an estimate for the cost of fielding this technology, but also as a basis for comparison with competing options for management of contact-handled mixed waste in the Department of Energy complex. The waste management options chosen for comparison are a standard plasma torch system such as the SAIC Plasma Hearth Process (PHP) and a no treatment option.

The basis of the graphite electrode DC arc cost estimate is a complete system capable of processing 10 tons/day. This system includes a furnace system, waste feed system, off-gas treatment system, secondary combustion chamber, power supplies (arc power, glass overflow heating power, and metals drain), instrumentation and control system, and product removal and handling system. To allow cost comparison with other waste management options, a value for the processing facility, site preparation, and permitting cost are included. The cost for the facility and permitting are rough-order of magnitude costs and are only present to allow reasonable comparison of the various option costs. Table 7.1 contains a summary of the graphite-electrode DC arc system cost estimate.

Costs to operate the DC arc system have also been estimated and presented in Table 7.2. These costs are presented on a cost per ton basis. The capital costs are applied to the treatment cost per ton on a straight-line depreciation rate over the estimated life of the system. The estimate assumes that the waste being treated has an activity level that allows for refurbishment of the furnace refractory without replacement of the furnace shell, thus extending the life of the furnace system. The system life is assumed to be 15 years. Cost parameters included in the operating costs include operating staff labor, electrical power, and consumable usage (e.g., inerting gas usage, arcing electrode consumption, etc.).

Table 7.1. Estimated Capital Cost for a Graphite Electrode DC Arc Furnace System

Component	Price
Furnace System	\$3,092,000
Off-Gas Treatment System	\$370,000
Secondary Combustion Chamber	\$605,000
System Design	\$687,000
Total System Cost	\$4,754,000
Facility/Site Prep. Costs	
Facility Cost	\$20,000,000
Site Preparation	\$2,000,000
Permitting Cost	\$5,000,000
Total Facility/Site/Permitting Cost	\$27,000,000
Total System Cost	\$31,754,000

Table 7.2. Graphite Electrode DC Arc System Operating Costs

Item	Per Ton
Capital Cost Contribution	\$734
Operating Power	\$99
Operating Labor	\$1,440
System Maintenance	\$11
DC Electrode Replacement	\$100
Overflow Heater Replacement	\$8
Nitrogen Use	\$11
Off-Gas Blowdown Disposal	\$6
Glass Formers Additives	\$14
Total Operating Costs	\$1,689
Final Product Disposal (per processed ton)	\$2,245
Total Costs to Install and Operate	\$4,668

A comparison of the life-cycle cost for the graphite electrode technology versus a plasma torch system, and a non-treatment scenario where the wastes are just repackaged and compacted prior to shipment and disposal is presented in Table 7.3. A capital cost estimate for a similar sized plasma torch treatment system was prepared to allow for comparison. The primary differences between the graphite electrode and torch plasma systems are as follows. It is estimated that the cost for the plasma torch furnace is about 40% higher due to a more complex furnace chamber as a result of tilt pouring of product. The off-gas system cost is estimated to be about 50% higher due to increased gas flow rate resulting from the torch gas, and the primary power supply cost is higher cost because of torch cooling water. The primary operating cost difference between the two thermal treatment technologies results from energy efficiency differences; the graphite electrode system is about twice as efficient. There are other minor differences such as higher nitrogen usage in the torch system (torch gas usage), lower costs for torch maintenance in comparison with graphite consumption, and no overflow heater replacement requirement for torch system. Operating labor as well as other cost factors is estimated to be equivalent for the two technologies.

Capital costs for the no-treatment option are assumed to be approximately the same as that required for the graphite electrode system. It assumed that a processing facility of the same size is required to house the sorting and compaction equipment. The operating labor requirement is estimated to be higher than the two thermal treatment options because of increased handling of the waste material. Though these parameters contribute to the waste management cost, the primary cost element of this option is the increased disposal cost resulting from disposal of a substantially higher volume of waste because of the small waste volume reduction. The disposal costs for all waste forms were assumed to be \$400 per ft³ for this analysis.

Table 7.3. Waste Management Option Cost Comparison

Item	Per Ton Cost		
	No Treatment	Plasma Torch	Graphite Electrode
Capital Cost Contribution	\$652	\$815	\$734
Operating Power	\$1	\$198	\$99
Operating Labor	\$1,920	\$1,920	\$1,440
System Maintenance	\$9	\$18	\$11
Consumable Usage	\$0	\$34	\$119
Off-Gas Blowdown Disposal	\$0	\$6	\$6
Glass Formers Additives	\$0	\$14	\$14
Total Operating Costs	\$1,930	\$2,190	\$1,689
Final Product Disposal (per processed ton)	\$4,596	\$2,245	\$2,245
Total Costs to Install and Operate	\$7,178	\$5,250	\$4,668

8.0 References

Freeman, C. J. and D. K. Seiler. 1997. *Treatment Studies of Plutonium-Bearing INEEL Waste Surrogates in a Bench-Scale Arc Furnace*, PNNL-11568, Pacific Northwest National Laboratory, Richland, Washington.

Freeman, C. J., G.P. Abrigo, P. J. Shafer, and R. A. Merrill. 1995. *Literature Review of Arc/Plasma, Combustion, and Joule-Heated Melter Vitrification Systems*, PNNL-10666, Pacific Northwest National Laboratory, Richland, Washington.

Gaskell, D. R. 1990. *Introduction to Metallurgical Thermodynamics*, 2nd Edition, McGraw-Hill Series in Materials Science Engineering, New York.

Hench, L. L. and J. K. West. 1990. *Principles of Electronic Ceramics*, John Wiley & Sons, New York.

Levin, E. M., C. R. Robbins, and H. F. McMurdie. 1964. *Phase Diagrams for Ceramists*, The American Ceramic Society, Columbus, Ohio.

Mixed Waste Focus Area Technology Development Requirements Document (TDRD). 1997a. *Radionuclide Partitioning*, INEL/EXT-97-00304.

Mixed Waste Focus Area Technology Development Requirements Document (TDRD). 1997b. *Plasma and Graphite DC Arc Electric Melters*, INEL/EXT-97-003-1.

MWFA: see Mixed Waste Focus Area.

Appendix A

Data Point Listing

Table A.1. Data Point Listing for the Engineering-Scale DC Arc Furnace

M&TE Label	Sensor I/O Category	Sensor I/O Type	Sensor Location and Description	Value Range	Accuracy (of full scale value)
<i>Electronically Logged Data:</i>					
TCS-01	Thermocouple	Type S	Plenum Temperature	-20 to 1760 C	0.50%
TCS-02	Thermocouple	Type S	Bottom Drain Temperature	-20 to 1760 C	0.50%
TCS-03	Thermocouple	Type S	Overflow Section Temperature #1	-20 to 1760 C	0.50%
TCS-04	Thermocouple	Type S	Overflow Section Temperature #2	-20 to 1760 C	0.50%
TCK-01	Thermocouple	Type K	North West Electrode Bus	-80 to 1240 C	0.30%
TCK-02	Thermocouple	Type K	South West Electrode Bus	-80 to 1240 C	0.30%
TCK-03	Thermocouple	Type K	North East Electrode Bus	-80 to 1240 C	0.30%
TCK-04	Thermocouple	Type K	South East Electrode Bus	-80 to 1240 C	0.30%
TCK-05	Thermocouple	Type K	Bottom Cooling Water Outlet	-80 to 1240 C	0.30%
TCK-06	Thermocouple	Type K	Overflow Jacket Cooling Air Outlet	-80 to 1240 C	0.30%
TCK-07	Thermocouple	Type K	Film Cooler Air Inlet Temperature	-80 to 1240 C	0.30%
TCK-08	Thermocouple	Type K	Off-Gas, Post Film Cooler	-80 to 1240 C	0.30%
TCK-09	Thermocouple	Type K	Off-Gas, Post Venturi Scrubber	-80 to 1240 C	0.30%
TCK-10	Thermocouple	Type K	Off-Gas Heater Temperature	-80 to 1240 C	0.30%
TCK-11	Thermocouple	Type K	Off-Gas, Post Blower (for SCFM calc.)	-80 to 1240 C	0.30%
TCK-12	Thermocouple	Type K	Off-Gas, Post HEPA	-80 to 1240 C	0.30%
TCK-13	Thermocouple	Type K	Venturi Scrub Water	-80 to 1240 C	0.30%
TCK-14	Thermocouple	Type K	Overflow Refractory Cooling (Circuit #1) Air Outlet	-80 to 1240 C	0.30%
TCK-15	Thermocouple	Type K	Overflow Refractory Cooling (Circuit #2) Air Outlet	-80 to 1240 C	0.30%
TCK-16	Thermocouple	Type K	Side Bus #2 Cooling Water Outlet	-80 to 1240 C	0.30%
TCK-17	Thermocouple	Type K	Venturi Heat Exchanger Cooling Water Outlet	-80 to 1240 C	0.30%
TCK-18	Thermocouple	Type K	Chiller Water Supply Temperature	-80 to 1240 C	0.30%
TCK-19	Thermocouple	Type K	Side Bus #1 Cooling Water Outlet	-80 to 1240 C	0.30%
TCK-20	Thermocouple	Type K	Side Bus #3 Cooling Water Outlet	-80 to 1240 C	0.30%
TCK-21	Thermocouple	Type K	Side Bus #4 Cooling Water Outlet	-80 to 1240 C	0.30%
TCK-22	Thermocouple	Type K	Overflow Refractory Cooling (Circuit #3) Air Outlet	-80 to 1240 C	0.30%
TCK-23	Thermocouple	Type K	Overflow Refractory Cooling (Circuit #4) Air Outlet	-80 to 1240 C	0.30%
TCK-24	Thermocouple	Type K	Chiller Water Header Temperature	-80 to 1240 C	0.30%
TCK-25	Thermocouple	Type K	Process Air Header Temperature	-80 to 1240 C	0.30%
TCK-26	Thermocouple	Type K	EVS Tank Temperature	-80 to 1240 C	0.30%
ET-01	Analog Input	4-20ma	DC Power Supply Voltage Sensor	0 to 400V	0.05%
CT-01	Analog Input	4-20ma	DC Power Supply Current Sensor	0 to 600A	0.05%
ET-03	Analog Input	0-5 Vdc	Overflow SCR #1 Voltage Sensor	0 to 240V	0.05%
CT-03	Analog Input	0-5 Vdc	Overflow SCR #1 Current Sensor	0 to 380A	0.05%
ET-04	Analog Input	0-5 Vdc	Overflow SCR #2 Voltage Sensor	0 to 240V	0.05%
CT-04	Analog Input	0-5 Vdc	Overflow SCR #2 Current Sensor	0 to 380A	0.05%
ET-05	Analog Input	0-5 Vdc	Off-Gas Heater SCR Voltage Sensor	0 to 240V	0.05%
CT-05	Analog Input	0-5 Vdc	Off-Gas Heater SCR Current Sensor	0 to 50A	0.05%
ET-06	Analog Input	0-5 Vdc	3-Phase Bottom Drain Heater SCR Voltage Sensor	0 to 208V	0.05%
CT-06	Analog Input	0-5 Vdc	3-Phase Bottom Drain Heater SCR Current Sensor	0 to 380A	0.05%
POS-01	Analog Input	0-5 Vdc	Stinger Positioner Motor Position (relative to initial '0')	-100 to 100cm	0.05%
TRQ-01	Analog Input	0-5 Vdc	Stinger Positioner Motor Torque	0 to 100%	0.05%
PT-01	Analog Input	4-20 ma	Plenum Vacuum	-30 to 30"WC	0.05%
PT-02	Analog Input	4-20 ma	Pressure Drop Across Film Cooler	-20 to 20"WC	0.05%
PT-03	Analog Input	4-20 ma	Pressure Drop Across EVS	-20 to 20"WC	0.05%
PT-04	Analog Input	4-20 ma	Pressure Drop Across HEME	-30 to 30"WC	0.05%
PT-05	Analog Input	4-20 ma	Pressure Drop Across HEPA	0-100"WC	0.05%
PT-06	Analog Input	4-20 ma	Post HEPA Vacuum	0-130"WC	0.05%
PT-07	Analog Input	4-20 ma	Melter Plenum to Overflow Pressure Differential	-20-20"WC	0.05%
PT-08	Analog Input	4-20 ma	EVS Nozzle Pressure	0-100psig	0.05%
PT-09	Analog Input	4-20 ma	Film Cooler Air Inlet Pressure	0-130"WC	0.05%
FT-01	Analog Input	4-20 ma	Blower Air Bleed Flow Rate	0-25"WC	0.05%
FT-02	Analog Input	4-20 ma	Off-Gas Air Flow Rate	0-25"WC	0.05%
PT-12	Analog Input	4-20 ma	N2 Pressure	0-100psig	0.05%
LC-01	Analog Input	4-20 ma	Auger Feeder Hopper Load Cell	0-500 lbs	0.05%
LC-02	Analog Input	4-20 ma	Overflow Glass Can Load Cell	0-500 lbs	0.05%

Table A.1. Data Point Listing for the Engineering-Scale DC Arc Furnace (continued)

M&TE Label	Sensor I/O Category	Sensor I/O Type	Sensor Location and Description	Value Range	Accuracy (of full scale value)
AO-01	Analog Output	4-20 ma	DC Power Supply Control Signal		0.05%
AO-02	Analog Output	4-20 ma	Auxilliary AC Power SCR Control Signal		0.05%
AO-03	Analog Output	4-20 ma	Overflow SCR #1 Control Signal		0.05%
AO-04	Analog Output	4-20 ma	Overflow SCR #2 Control Signal		0.05%
AO-05	Analog Output	4-20 ma	Off-Gas Heater SCR Control Signal		0.05%
AO-06	Analog Output	4-20 ma	Bottom Drain SCR Control Signal		0.05%
AO-07	Analog Output	4-20 ma	Solids Feed Control Signal		0.05%
AO-08	Analog Output	4-20 ma	Off-gas Air Control Valve Signal		0.05%
DI-01	Digital Input	120V	Chiller Water Header Flow Switch		
DI-02	Digital Input	120V	Auxilliary AC Power SCR Short/High Current Alarm		
DI-03	Digital Input	120V	Overflow SCR #1 Short/High Current Alarm		
DI-04	Digital Input	120V	Overflow SCR #2 Short/High Current Alarm		
DI-05	Digital Input	120V	Off-Gas Heater SCR Short/High Current Alarm		
DI-06	Digital Input	120V	Bottom Drain SCR Short/High Current Alarm		
DI-07	Digital Input	120V	Ram Gate Valve Position		
DI-08	Digital Input	120V	Bottom Drain Gate Valve Position		
DI-09	Digital Input	120V	Overflow Drain Gate Valve Position		
DI-10	Digital Input	120V	Top View Port Gate Valve Position		
DI-11	Digital Input	120V	Not Used (Was Overflow View Port Valve Position)		
DI-12	Digital Input	120V	Ram Pusher Fully Retracted Switch		
DI-13	Digital Input	120V	CAM Alarm		
DI-14	Digital Input	120V	Top Ram Can Gate Valve Position		
DI-15	Digital Input	120V	Stinger Positioner Motor Direction (forward or reverse)		
DO-01	Digital Output	Dry Contact	Stinger Positioner Motor Control (UP)		
DO-02	Digital Output	Dry Contact	Stinger Positioner Motor Control (DOWN)		
DO-03	Digital Output	Dry Contact	Not Used (Was Stinger Motor Control (STOP))		
DO-04	Digital Output	Dry Contact	Not Used (Was Stinger Motor Control (JOG))		
DO-05	Digital Output	Dry Contact	AutoDialer Output		
DO-06	Digital Output	120V	#1 Film Cooler Air Source Valve		
DO-07	Digital Output	120V	#2 Film Cooler Air Source Valve		
DO-08	Digital Output	120V	Overflow Vacuum Source Valve (OPEN)		
DO-09	Digital Output	120V	Ram Gate Valve Solenoid		
DO-10	Digital Output	120V	Bottom Drain Gate Valve Solenoid		
DO-11	Digital Output	120V	Overflow Drain Gate Valve Solenoid		
DO-12	Digital Output	120V	Top View Port Gate Valve Solenoid		
DO-13	Digital Output	120V	Not Used (Was Overflow View Port Valve Solenoid)		
DO-14	Digital Output	120V	Top Ram Can Gate Valve Solenoid		
DO-14	Digital Output	120V	Overflow Vacuum Source Valve (CLOSED)		
Manually-Logged Data:					
FI-01	Rotometer	N/A	Electrode Sheath Cooling Water	0-10gpm	1.00%
FI-02	Rotometer	N/A	Electrode Housing Nitrogen Purge	0-25scfm	1.00%
FI-03	Rotometer	N/A	Overflow Block Cooling Coil # 1	0-25scfm	1.00%
FI-04	Rotometer	N/A	Overflow Block Cooling Coil # 2	0-25scfm	1.00%
FI-05	Rotometer	N/A	Overflow Block Cooling Coil # 3	0-25scfm	1.00%
FI-06	Rotometer	N/A	Overflow Block Cooling Coil # 4	0-25scfm	1.00%
FI-07	Rotometer	N/A	Bottom Drain Cooling Water	0-10gpm	1.00%
FI-08	Rotometer	N/A	Bottom Drain Nirtrogen Purge	0-100scfm	1.00%
FI-09	Rotometer	N/A	Hearth Nitrogen Purge	0-100scfm	1.00%
FI-10	Rotometer	N/A	Main Shell Cooling Air	0-100scfm	1.00%
FI-11	Rotometer	N/A	North West Electrode Bus Cooling Water	0-1gpm	1.00%
FI-12	Rotometer	N/A	South West Electrode Bus Cooling Water	0-1gpm	1.00%
FI-13	Rotometer	N/A	North East Electrode Bus Cooling water	0-1gpm	1.00%
FI-14	Rotometer	N/A	South East Electrode Bus Cooling Water	0-1gpm	1.00%
FI-15	Rotometer	N/A	Overflow Shell Cooling	0-100scfm	1.00%
FI-16	Rotometer	N/A	Heat Exchanger Cooling Water	0-20gpm	1.00%

Appendix B

Analytical Data

Test Seg1

Test Segment 1						
Feed Mass (lb)	31.2					
Glass Product (lb)	27.8					
Baghouse Solids (g)	197.8					
Feed						
ESF-1 Feed Composition						
	Conversion	Actual	Normalized		Actual Wt%	Total g
	Factor	Feed Oxide	Feed Oxide		Feed Element	Element
Ag ₂ O	1.074	0.107	0.120	Ag	0.100	14.14
Al ₂ O ₃	1.890	8.350	9.373	Al	4.419	625.37
B ₂ O ₃	3.220			B		
BaO	1.116	0.189	0.213	Ba	0.170	24.00
BeO	2.775			Be		
Bi ₂ O ₃	1.115			Bi		
CaO	1.399	23.144	25.981	Ca	16.541	2340.89
CdO	1.142	0.114	0.128	Cd	0.100	14.10
CeO ₂	1.228			Ce		
Co ₂ O ₃	1.407			Co		
Cr ₂ O ₃	1.462	0.145	0.163	Cr	0.099	14.08
CuO	1.252			Cu		
Dy ₂ O ₃	1.148			Dy		
Eu ₂ O ₃	1.158			Eu		
Fe ₂ O ₃	1.430	3.253	3.652	Fe	2.275	322.01
K ₂ O	1.205	1.993	2.238	K	1.655	234.20
La ₂ O ₃	1.173	0.005	0.006	La	0.005	0.66
Li ₂ O	2.153			Li		
MgO	1.659	1.832	2.057	Mg	1.105	156.36
MnO	1.582	0.073	0.082	Mn	0.046	6.55
MoO ₃	1.500			Mo		
Na ₂ O	1.348	0.916	1.028	Na	0.680	96.19
Nd ₂ O ₃	1.166	0.392	0.440	Nd	0.336	47.60
NiO	1.273	0.126	0.141	Ni	0.099	13.99
P ₂ O ₅	2.291			P		
PbO	1.078	0.108	0.121	Pb	0.100	14.12
SO ₃	2.497			S		
SiO ₂	2.139	47.204	52.991	Si	22.067	3122.95
SnO ₂	1.270			Sn		
SrO	1.183	0.042	0.047	Sr	0.036	5.05
TeO ₂	1.251			Te		
TiO ₂	1.668	0.470	0.527	Ti	0.281	39.84
VO ₂	1.628			V		
Y ₂ O ₃	1.270	0.305	0.343	Y	0.240	34.01
ZnO	1.245			Zn		
ZrO ₂	1.351	0.310	0.348	Zr	0.229	32.45
LOI		10.921				
Total		100.000	100.000			

Test Seg1

Test Segment 1									
Glass Product									
	Conversion	Glass Product Wt % Oxide				Actual Wt%		Total g	
	Factor	ESF-1-05	ESF-1-06	ESF-1-11	Average	Glass Elemer	Element		
Ag2O	1.074	0.05	0.05	0.06	0.05	Ag	0.051	6.43	
Al2O3	1.890	10.83	10.81	10.81	10.82	Al	5.724	721.57	
B2O3	3.220					B			
BaO	1.116	0.19	0.19	0.19	0.19	Ba	0.170	21.45	
BeO	2.775					Be			
Bi2O3	1.115					Bi			
CaO	1.399	24.10	24.27	24.27	24.21	Ca	17.303	2181.39	
CdO	1.142	0.01	0.02	0.03	0.02	Cd	0.017	2.11	
CeO2	1.228					Ce			
Co2O3	1.407					Co			
Cr2O3	1.462	0.70	0.68	0.66	0.68	Cr	0.464	58.56	
CuO	1.252					Cu			
Dy2O3	1.148					Dy			
Eu2O3	1.158					Eu			
Fe2O3	1.430	5.72	5.42	5.06	5.40	Fe	3.778	476.32	
K2O	1.205	3.29	3.17	3.23	3.23	K	2.682	338.17	
La2O3	1.173					La			
Li2O	2.153					Li			
MgO	1.659	2.19	2.20	2.23	2.21	Mg	1.331	167.77	
MnO	1.582	0.16	0.16	0.15	0.15	Mn	0.097	12.20	
MoO3	1.500					Mo			
Na2O	1.348	1.75	1.70	1.69	1.71	Na	1.270	160.09	
Nd2O3	1.166	0.41	0.42	0.45	0.43	Nd	0.366	46.09	
NiO	1.273	0.06	0.06	0.06	0.06	Ni	0.048	6.06	
P2O5	2.291					P			
PbO	1.078					Pb			
SO3	2.497					S			
SiO2	2.139	49.37	49.65	49.93	49.65	Si	23.210	2926.04	
SnO2	1.270					Sn			
SrO	1.183	0.04	0.04	0.05	0.04	Sr	0.036	4.58	
TeO2	1.251					Te			
TiO2	1.668	0.51	0.51	0.51	0.51	Ti	0.306	38.63	
VO2	1.628					V			
Y2O3	1.270	0.30	0.30	0.31	0.30	Y	0.239	30.11	
ZnO	1.245					Zn			
ZrO2	1.351	0.33	0.33	0.34	0.33	Zr	0.246	30.98	
		100.00	100.00	100.00	100.00				

Test Seg2

Test Segment 2							
Feed Mass (lb)			7				
Glass Product (lb)			6.2				
Baghouse Solids (g)			73.3				
Feed							
ESF-1 Feed Composition							
	Conversion	Actual	Normalized		Actual Wt%	Total g	
	Factor	Feed Oxide	Feed Oxide		Feed Element	Element	
Ag ₂ O	1.074	0.107	0.120	Ag	0.100	3.17	
Al ₂ O ₃	1.890	8.350	9.373	Al	4.419	140.31	
B ₂ O ₃	3.220			B			
BaO	1.116	0.189	0.213	Ba	0.170	5.39	
BeO	2.775			Be			
Bi ₂ O ₃	1.115			Bi			
CaO	1.399	23.144	25.981	Ca	16.541	525.20	
CdO	1.142	0.114	0.128	Cd	0.100	3.16	
CeO ₂	1.228			Ce			
Co ₂ O ₃	1.407			Co			
Cr ₂ O ₃	1.462	0.145	0.163	Cr	0.099	3.16	
CuO	1.252			Cu			
Dy ₂ O ₃	1.148			Dy			
Eu ₂ O ₃	1.158			Eu			
Fe ₂ O ₃	1.430	3.253	3.652	Fe	2.275	72.25	
K ₂ O	1.205	1.993	2.238	K	1.655	52.54	
La ₂ O ₃	1.173	0.005	0.006	La	0.005	0.15	
Li ₂ O	2.153			Li			
MgO	1.659	1.832	2.057	Mg	1.105	35.08	
MnO	1.582	0.073	0.082	Mn	0.046	1.47	
MoO ₃	1.500			Mo			
Na ₂ O	1.348	0.916	1.028	Na	0.680	21.58	
Nd ₂ O ₃	1.166	0.392	0.440	Nd	0.336	10.68	
NiO	1.273	0.126	0.141	Ni	0.099	3.14	
P ₂ O ₅	2.291			P			
PbO	1.078	0.108	0.121	Pb	0.100	3.17	
SO ₃	2.497			S			
SiO ₂	2.139	47.204	52.991	Si	22.067	700.66	
SnO ₂	1.270			Sn			
SrO	1.183	0.042	0.047	Sr	0.036	1.13	
TeO ₂	1.251			Te			
TiO ₂	1.668	0.470	0.527	Ti	0.281	8.94	
VO ₂	1.628			V			
Y ₂ O ₃	1.270	0.305	0.343	Y	0.240	7.63	
ZnO	1.245			Zn			
ZrO ₂	1.351	0.310	0.348	Zr	0.229	7.28	
LOI		10.921					
Total		100.000	100.000				

Test Seg3

Test Segment 3						
Feed Mass (lb)	19					
Glass Product (lb)	16.9					
Baghouse Solids (g)	200.5					
Feed						
ESF-1 Feed Composition						
	Conversion	Actual	Normalized		Actual Wt%	Total g
	Factor	Feed Oxide	Feed Oxide		Feed Element	Element
Ag2O	1.074	0.107	0.120	Ag	0.100	8.61
Al2O3	1.890	8.350	9.373	Al	4.419	380.83
B2O3	3.220			B		
BaO	1.116	0.189	0.213	Ba	0.170	14.62
BeO	2.775			Be		
Bi2O3	1.115			Bi		
CaO	1.399	23.144	25.981	Ca	16.541	1425.54
CdO	1.142	0.114	0.128	Cd	0.100	8.58
CeO2	1.228			Ce		
Co2O3	1.407			Co		
Cr2O3	1.462	0.145	0.163	Cr	0.099	8.57
CuO	1.252			Cu		
Dy2O3	1.148			Dy		
Eu2O3	1.158			Eu		
Fe2O3	1.430	3.253	3.652	Fe	2.275	196.10
K2O	1.205	1.993	2.238	K	1.655	142.62
La2O3	1.173	0.005	0.006	La	0.005	0.40
Li2O	2.153			Li		
MgO	1.659	1.832	2.057	Mg	1.105	95.22
MnO	1.582	0.073	0.082	Mn	0.046	3.99
MoO3	1.500			Mo		
Na2O	1.348	0.916	1.028	Na	0.680	58.58
Nd2O3	1.166	0.392	0.440	Nd	0.336	28.98
NiO	1.273	0.126	0.141	Ni	0.099	8.52
P2O5	2.291			P		
PbO	1.078	0.108	0.121	Pb	0.100	8.60
SO3	2.497			S		
SiO2	2.139	47.204	52.991	Si	22.067	1901.80
SnO2	1.270			Sn		
SrO	1.183	0.042	0.047	Sr	0.036	3.07
TeO2	1.251			Te		
TiO2	1.668	0.470	0.527	Ti	0.281	24.26
VO2	1.628			V		
Y2O3	1.270	0.305	0.343	Y	0.240	20.71
ZnO	1.245			Zn		
ZrO2	1.351	0.310	0.348	Zr	0.229	19.76
LOI		10.921				
Total		100.000	100.000			

Test Seg3

Glass Product									
	Conversion	Glass Product Wt % Oxide				Actual Wt% Total g		Glass Elemer Element	
	Factor	ESF-1-18	ESF-1-19	ESF-1-23	Average				
Ag2O	1.074	0.04	0.03	0.03	0.03	Ag	0.032	2.46	
Al2O3	1.890	10.45	10.49	10.61	10.52	Al	5.565	427.22	
B2O3	3.220					B			
BaO	1.116	0.20	0.20	0.20	0.20	Ba	0.178	13.66	
BeO	2.775					Be			
Bi2O3	1.115					Bi			
CaO	1.399	25.03	25.15	24.99	25.05	Ca	17.906	1374.72	
CdO	1.142	0.02	0.01	0.01	0.01	Cd	0.013	0.99	
CeO2	1.228					Ce			
Co2O3	1.407					Co			
Cr2O3	1.462	0.65	0.65	0.64	0.65	Cr	0.443	33.98	
CuO	1.252					Cu			
Dy2O3	1.148					Dy			
Eu2O3	1.158					Eu			
Fe2O3	1.430	4.70	4.75	4.74	4.73	Fe	3.307	253.87	
K2O	1.205	3.29	3.39	2.94	3.21	K	2.662	204.39	
La2O3	1.173					La			
Li2O	2.153					Li			
MgO	1.659	2.16	2.16	2.18	2.16	Mg	1.305	100.17	
MnO	1.582	0.12	0.12	0.12	0.12	Mn	0.076	5.80	
MoO3	1.500					Mo			
Na2O	1.348	1.34	1.40	1.43	1.39	Na	1.029	79.01	
Nd2O3	1.166	0.44	0.45	0.47	0.45	Nd	0.388	29.82	
NiO	1.273	0.06	0.05	0.05	0.05	Ni	0.041	3.18	
P2O5	2.291					P			
PbO	1.078					Pb			
SO3	2.497					S			
SiO2	2.139	50.30	49.91	50.39	50.20	Si	23.467	1801.63	
SnO2	1.270					Sn			
SrO	1.183	0.04	0.04	0.05	0.04	Sr	0.037	2.87	
TeO2	1.251					Te			
TiO2	1.668	0.51	0.52	0.51	0.51	Ti	0.309	23.70	
VO2	1.628					V			
Y2O3	1.270	0.33	0.33	0.33	0.33	Y	0.258	19.80	
ZnO	1.245					Zn			
ZrO2	1.351	0.34	0.34	0.33	0.34	Zr	0.249	19.14	
		100.00	100.00	100.00	100.00				

Test Seg4

Test Segment 4						
Feed Mass (lb)	34					
Glass Product (lb)	30.3					
Baghouse Solids (g)	365.9					
Feed						
ESF-1 Feed Composition						
	Conversion	Actual	Normalized		Actual Wt%	Total g
	Factor	Feed Oxide	Feed Oxide		Feed Element	Element
Ag2O	1.074	0.107	0.120	Ag	0.100	15.41
Al2O3	1.890	8.350	9.373	Al	4.419	681.49
B2O3	3.220			B		
BaO	1.116	0.189	0.213	Ba	0.170	26.16
BeO	2.775			Be		
Bi2O3	1.115			Bi		
CaO	1.399	23.144	25.981	Ca	16.541	2550.97
CdO	1.142	0.114	0.128	Cd	0.100	15.36
CeO2	1.228			Ce		
Co2O3	1.407			Co		
Cr2O3	1.462	0.145	0.163	Cr	0.099	15.34
CuO	1.252			Cu		
Dy2O3	1.148			Dy		
Eu2O3	1.158			Eu		
Fe2O3	1.430	3.253	3.652	Fe	2.275	350.91
K2O	1.205	1.993	2.238	K	1.655	255.22
La2O3	1.173	0.005	0.006	La	0.005	0.72
Li2O	2.153			Li		
MgO	1.659	1.832	2.057	Mg	1.105	170.39
MnO	1.582	0.073	0.082	Mn	0.046	7.14
MoO3	1.500			Mo		
Na2O	1.348	0.916	1.028	Na	0.680	104.82
Nd2O3	1.166	0.392	0.440	Nd	0.336	51.87
NiO	1.273	0.126	0.141	Ni	0.099	15.25
P2O5	2.291			P		
PbO	1.078	0.108	0.121	Pb	0.100	15.39
SO3	2.497			S		
SiO2	2.139	47.204	52.991	Si	22.067	3403.22
SnO2	1.270			Sn		
SrO	1.183	0.042	0.047	Sr	0.036	5.50
TeO2	1.251			Te		
TiO2	1.668	0.470	0.527	Ti	0.281	43.41
VO2	1.628			V		
Y2O3	1.270	0.305	0.343	Y	0.240	37.06
ZnO	1.245			Zn		
ZrO2	1.351	0.310	0.348	Zr	0.229	35.36
LOI		10.921				
Total		100.000	100.000			

Test Seg4

Glass Product									
	Conversion	Glass Product Wt % Oxide				Actual Wt%	Total g		
	Factor	ESF-1-25	ESF-1-26	ESF-1-30	Average	Glass Elemer	Element		
Ag2O	1.074	0.03	0.03	0.04	0.03	Ag	0.031	4.22	
Al2O3	1.890	10.38	10.30	10.26	10.32	Al	5.459	749.98	
B2O3	3.220					B			
BaO	1.116	0.20	0.20	0.20	0.20	Ba	0.177	24.33	
BeO	2.775					Be			
Bi2O3	1.115					Bi			
CaO	1.399	24.68	24.72	24.69	24.70	Ca	17.650	2424.73	
CdO	1.142	0.01	0.02	0.02	0.02	Cd	0.015	2.01	
CeO2	1.228					Ce			
Co2O3	1.407					Co			
Cr2O3	1.462	0.63	0.62	0.61	0.62	Cr	0.424	58.22	
CuO	1.252					Cu			
Dy2O3	1.148					Dy			
Eu2O3	1.158					Eu			
Fe2O3	1.430	4.78	4.96	4.89	4.88	Fe	3.413	468.83	
K2O	1.205	3.65	3.59	3.66	3.63	K	3.017	414.43	
La2O3	1.173					La			
Li2O	2.153					Li			
MgO	1.659	2.14	2.13	2.13	2.13	Mg	1.286	176.60	
MnO	1.582	0.12	0.12	0.11	0.12	Mn	0.073	9.99	
MoO3	1.500					Mo			
Na2O	1.348	1.34	1.30	1.33	1.32	Na	0.981	134.78	
Nd2O3	1.166	0.44	0.44	0.45	0.45	Nd	0.382	52.45	
NiO	1.273	0.06	0.07	0.07	0.06	Ni	0.051	6.95	
P2O5	2.291					P			
PbO	1.078					Pb			
SO3	2.497					S			
SiO2	2.139	50.32	50.28	50.31	50.30	Si	23.516	3230.66	
SnO2	1.270					Sn			
SrO	1.183	0.04	0.04	0.04	0.04	Sr	0.036	4.91	
TeO2	1.251					Te			
TiO2	1.668	0.51	0.51	0.51	0.51	Ti	0.307	42.24	
VO2	1.628					V			
Y2O3	1.270	0.33	0.33	0.33	0.33	Y	0.258	35.46	
ZnO	1.245					Zn			
ZrO2	1.351	0.34	0.34	0.35	0.34	Zr	0.254	34.85	
		100.00	100.00	100.00	100.00				

Test Seg5

Test Segment 5						
Feed Mass (lb)	38					
Glass Product (lb)	33.9					
Baghouse Solids (g)	172.8					
Feed						
ESF-1 Feed Composition						
	Conversion	Actual	Normalized		Actual Wt%	Total g
	Factor	Feed Oxide	Feed Oxide		Feed Element	Element
Ag2O	1.074	0.107	0.120	Ag	0.100	17.22
Al2O3	1.890	8.350	9.373	Al	4.419	761.67
B2O3	3.220			B		
BaO	1.116	0.189	0.213	Ba	0.170	29.23
BeO	2.775			Be		
Bi2O3	1.115			Bi		
CaO	1.399	23.144	25.981	Ca	16.541	2851.09
CdO	1.142	0.114	0.128	Cd	0.100	17.17
CeO2	1.228			Ce		
Co2O3	1.407			Co		
Cr2O3	1.462	0.145	0.163	Cr	0.099	17.15
CuO	1.252			Cu		
Dy2O3	1.148			Dy		
Eu2O3	1.158			Eu		
Fe2O3	1.430	3.253	3.652	Fe	2.275	392.19
K2O	1.205	1.993	2.238	K	1.655	285.24
La2O3	1.173	0.005	0.006	La	0.005	0.81
Li2O	2.153			Li		
MgO	1.659	1.832	2.057	Mg	1.105	190.44
MnO	1.582	0.073	0.082	Mn	0.046	7.98
MoO3	1.500			Mo		
Na2O	1.348	0.916	1.028	Na	0.680	117.15
Nd2O3	1.166	0.392	0.440	Nd	0.336	57.97
NiO	1.273	0.126	0.141	Ni	0.099	17.04
P2O5	2.291			P		
PbO	1.078	0.108	0.121	Pb	0.100	17.20
SO3	2.497			S		
SiO2	2.139	47.204	52.991	Si	22.067	3803.60
SnO2	1.270			Sn		
SrO	1.183	0.042	0.047	Sr	0.036	6.15
TeO2	1.251			Te		
TiO2	1.668	0.470	0.527	Ti	0.281	48.52
VO2	1.628			V		
Y2O3	1.270	0.305	0.343	Y	0.240	41.42
ZnO	1.245			Zn		
ZrO2	1.351	0.310	0.348	Zr	0.229	39.52
LOI		10.921				
Total		100.000	100.000			

Test Seg5

Glass Product									
	Conversion	Glass Product Wt % Oxide				Actual Wt%	Total g		
	Factor	ESF-1-32	ESF-1-33	ESF-1-34	Average	Feed Element	Element		
Ag2O	1.074	0.05	0.04	0.05	0.04	Ag	0.042	6.43	
Al2O3	1.890	10.22	10.16	10.34	10.24	Al	5.419	832.05	
B2O3	3.220					B			
BaO	1.116	0.20	0.20	0.20	0.20	Ba	0.181	27.79	
BeO	2.775					Be			
Bi2O3	1.115					Bi			
CaO	1.399	24.90	24.78	25.20	24.96	Ca	17.838	2738.96	
CdO	1.142	0.02	0.02	0.02	0.02	Cd	0.016	2.46	
CeO2	1.228					Ce			
Co2O3	1.407					Co			
Cr2O3	1.462	0.56	0.58	0.59	0.57	Cr	0.392	60.23	
CuO	1.252					Cu			
Dy2O3	1.148					Dy			
Eu2O3	1.158					Eu			
Fe2O3	1.430	4.88	5.03	5.05	4.99	Fe	3.491	535.98	
K2O	1.205	3.86	3.49	2.35	3.24	K	2.686	412.40	
La2O3	1.173					La			
Li2O	2.153					Li			
MgO	1.659	2.13	2.09	2.10	2.11	Mg	1.273	195.44	
MnO	1.582	0.11	0.11	0.11	0.11	Mn	0.068	10.47	
MoO3	1.500					Mo			
Na2O	1.348	1.29	1.22	1.24	1.25	Na	0.930	142.76	
Nd2O3	1.166	0.46	0.45	0.44	0.45	Nd	0.384	58.99	
NiO	1.273	0.08	0.08	0.08	0.08	Ni	0.062	9.59	
P2O5	2.291					P			
PbO	1.078					Pb			
SO3	2.497					S			
SiO2	2.139	50.01	50.51	50.97	50.50	Si	23.606	3624.58	
SnO2	1.270					Sn			
SrO	1.183	0.04	0.04	0.04	0.04	Sr	0.036	5.60	
TeO2	1.251					Te			
TiO2	1.668	0.51	0.51	0.52	0.52	Ti	0.310	47.61	
VO2	1.628					V			
Y2O3	1.270	0.33	0.33	0.34	0.34	Y	0.264	40.54	
ZnO	1.245					Zn			
ZrO2	1.351	0.33	0.35	0.35	0.34	Zr	0.254	39.02	
		100.00	100.00	100.00	100.00				

Distribution

**No. of
Copies**

**No. of
Copies**

OFFSITE

K. P. Carney
Argonne National Laboratory - West
Analytical Laboratory
P.O. Box 2528
Idaho Falls, ID 83403

Lockheed Martin Idaho Technologies
Company
Mixed Waste Focus Area
2525 North Fremont
Idaho Falls, ID 83415-3875
ATTN: M. J. Connolly
W. D. St. Michel
D. Gombert

N. M. Askew
Savannah River Technology Center
Mixed Waste Focus Area
Chemical Technology Group
Savannah River Site
Aiken, SC 29808

L. J. Johnson, T9-059
Pantex Plant
P.O. Box 30020
Amarillo, TX 79120-0020

J. S. Yokum, 11-14
Pantex Plant
P.O. Box 30020
Amarillo, TX 79120-0020

K. Wittle
Electro-Pyrolysis, Inc.
996 Old Eagle School Road
Suite 1118
Wayne, PA 19087

M. S. Blau
Los Alamos National Laboratory
P.O. Box 1663
Los Alamos, NM 87545

ONSITE

4 DOE Richland Operations Office

T. L. Aldridge	K8-50
E. B. Dagan	S7-55
J. P. Neath	K8-50
J. J. Waring	S7-55

22 Pacific Northwest National Laboratory

R. E. Allen	K8-14
W. F. Bonner (2)	K9-14
J. L. Buelt	K2-14
J. M. Davis	K6-28
R. W. Goles (15)	K6-24
J. M. Perez	K6-24
G. A. Whyatt	K6-24